UNIVERSITÀ DEGLI STUDI DI ROMA
TOR VERGATA

FACOLTÀ DI SCIENZE MATEMATICHE, FISICHE E NATURALI
Dipartimento di Fisica

XX Ciclo del Corso di Dottorato

Computer Simulations of Biomolecules: the case of the N-terminal PrP Cu binding site

Francesco Guerrieri

Docenti Guida

Dr. *Velia Minicozzi*

Prof. *Silvia Morante*

Coordinatore del Corso di Dottorato

Prof. *Piergiorgio Picozza*

In prion research, as in many other areas of scientific investigation, a single hypothesis is all too often championed at the expense of a reasoned approach which requires entertaining a series of complex arguments until one or more can be discarded on the basis of experimental data.

S. B. Prusiner

Contents

Chapter 1

Introduction

Quantum theory provides an incredibly deep and complete description of reality. While at the highest energy scales a coherent theory is still missing, we have found in Quantum Electrodynamics and in its non relativistic form, Quantum Mechanics, two exceedingly useful theories, with a range of applicability wide enough to account, at least in theory, for every chemical phenomenon, thus lying at the heart of our comprehension of practically all of the events that form our life.

Such an enormous set of different reactions, processes and events is obviously very far from being *solvable* by writing a few equations: as an example of the difficulty of this project, it can be cited the vast theoretical effort which is going on just to prove the existence in the theory of a bound state corresponding to a proton, in the same sense that one can prove, by solving the Schrödinger equation, that a Hydrogenoid atom admits bound states for its electron whose energies give rise to the observed experimental spectra.

So, although chemistry, biochemistry and life itself are, in principle, contained in, and *predictable* through, Quantum Mechanics, the truth is that

any tiny step towards the comprehension and the explanation of a given physical process requires much research and work.

Physics is an experimental science, in that it tries to reconcile its theories with the results of experiments (which, in turn, have been carefully planned with the aim of testing hypotheses). When one theory is believed to be trustable enough, one can hope to extract predictions from it, or to discover the reason behind a given observed behaviour.

Our understanding of the theory has reached such a level, while at the same time the mathematical techniques and the technological innovations have provided such an amount of computing power, that it is becoming possible to devise numerical, so called *in silico*,

experiments for the study of large enough number of atoms. The careful interpretation of these *in silico* experiments is beginning to provide some useful results in an ever increasing range of fields.

In some cases, *e.g.* periodic or quasi-periodic crystals where the inherently symmetrical nature of the problem implies a slightly easier task, precise results have been obtained and continue to be improved, thus being one of the great success of the physical sciences. Furthermore, they provide an environment where new ideas and techniques can be tested, before trying more complex cases.

At the other side of the spectrum, in terms of complexity and lack of symmetry, lies biochemistry. Here the reactions of interest involve many species of atoms, and often require the presence of a solvent, of catalysts, of special external conditions (temperature and pH to name only the two most relevant). This is to be contrasted with the relative simplicity of a (quasi) periodic crystal where the unitary cell contains only few atoms, of few species, and solvent effects are often negligible.

This notwithstanding, the potential for a quantitative, atomistic comprehension and prediction of biochemical reaction is so large that many different approaches have been devised, each one with its own advantages and disadvantages.

Among these, the Molecular Dynamics approach stands forth because it is the direct implementation of a typical Gedankenexperiment: one has *simply* to select the atoms one is interested in, let their positions evolve over time and register what is happening.

Although not rigorous, this way of thinking has its own merits: it certainly is not quantum mechanically correct, but it is an useful approximation, which holds in a large variety of cases, and is close to chemistry, providing a support to it. The problem is that the actual implementation of this seemingly straightforward approach is not *simple*.

There are two main reasons for this complexity:

1. The first is conceptual, and can be defined as a *modeling problem*: picking up the molecules one is interested in is much more simply said than done. In fact, one needs to define a proper abstract model of the real problem under study, simple enough to be treatable but which still share with the real problem the crucial features. This is the same kind of issue which every experiment has to face, but in a Molecular Dynamics experiment the freedom that the researchers have is so complete (since it is up to them to choose what and how to *simulate*) that there is always the risk of missing something. In a laboratory experiment one cannot turn off all the rest of the physics, while in a numerical simulation the only interactions available will be those actually calculated.

2. The second is both technical and conceptual at the same time, and can

be defined as a *simulation problem*: assuming that one has been able to find the correct equations of motion[1] one still has to integrate them. This task is beyond any analytical solution and is practically impossible even with the help of computers. Furthermore, any numerical solution is subject to practical limitations, namely the rounding errors[2] and the memory, space and time requirements[3].

Having stated the problematic issues, it can be said that various satisfying solutions have been proposed and can be applied with the due care.

These two problems, viewed both as general issues, of a theoretical nature, and as practical issues, related to a given particular experiment, are tackled by means of experience.

The scientific community currently enjoys the fruits of decades of experimenting with computer simulations, during which many algorithms have been tested and compared with the experimental data. Today, we have reached a good understanding of the range of affidability of the various available techniques, which are continuously tested and adopted by many groups all over the world. This is due to the widespread availability of powerful enough computing resources, and to the well diffused practice of releasing the software codes under open source licenses. This may seem irrelevant, but is instead crucial for it gives to every group the means to reproduce and double check any scientific result. Furthermore, it means that there is

[1] The two main approaches, classical (in the presence of the Coulombian interaction and of refined force fields) and quantum mechanical will be discussed shortly.

[2] These are inevitable, since one can only represent a real number within a given approxkimation.

[3] Clearly each step of the computation must be represented by a state of the computer, which must have enough RAM memory to contain it, enough disk space to persistently store its results and enough computing power to process it. These are highly non trivial issues, particularly relevant given the 32-bit architecture still widespread in common computers.

no need to *reinvent the wheel* by starting from scratch: one can build over the work made available by the other groups, profiting from their previous experience, which is a key element in the scientific process.

When it comes to planning a particular computer experiment, experience plays again a role, as in any other kind of experiment. The number of molecules which have to be actually simulated, the boundary conditions, if any, and all the other kind of parameters are determined by a trial-and-error procedure, starting from some educated guess and refining it with the experience acquired. This is made possible by the relative inexpensiveness of a computer experiment: although the cpu-time of a cluster of computers can be a scarce resource, it is usually much less costly than a laboratory experiment.

There are two main alternative kinds of Molecular Dynamics approach. The first is the so called *classical* one. Its main features are:

1. Only the atoms are simulated, and not the electrons.

2. Atoms are subjected to a variety of forces, variously modeled in such a way to reproduce exact results, or experimental data.

3. The interactions among the atoms are thus not restricted to be *fundamental* in any sense: they can be represented by *springs* linking two atoms together, or can represent dipolar or quadrupolar interactions. The charge on the atoms is determined by empirical, ad-hoc means.

4. This leads to the concept of different *species* of the same atom: this is required because the Oxygen in a water molecule is different from a Carboxylic Oxygen: thus when specifying the input for the simulation, one must in general explicitly state to what kind of molecule a given atom belongs to.

5. This is roughly equivalent to fixing for the whole duration of the simulation the oxidation state of an atom and its chemical bonds.

While this can seem a crude approximation, it is without doubt a successful one. These simplifications avoid the need of solving the many body Schrödinger equation for the electrons and the ions, and allow for the simulation of a large number of atoms, and following their trajectories for times in the range from the ns to the μs. There is a large number of excellent software packages for classical Molecular Dynamics, including Gromacs[GROMACS, 2007], NAMD[NAMD, 2003], Charmm[CHARMM] and Amber[AMBER].

The intrinsic limitations of a classical Molecular Dynamics simulation is that all the effects must be accounted for in the parametrization of the force field. Namely, once that a given chemical bonding structure has been assigned, it remains fixed along the trajectory. This excludes, or severely limits, the possibility of observing interactions dominated by quantum effects, such as those where the shape and properties of the electronic orbitals play a dominant role.

The natural solution to this would be to remove the approximation, and to solve the complete quantum problem. This naive approach, although in principle exact, is not feasible, being computationally too burdensome. It turns out that the Born-Oppenheimer approximation is the right tool: the quantum treatment can be limited to the electrons, and the atoms are considered immersed in a force field due to their Coulomb interactions and to the interaction in the electrostatic field generated by the electrons.

So, if the Born-Oppenheimer approximation holds true, for every time step of the trajectory one would have to solve the many body Schrödinger equation (with or without the relativistic corrections) to determine the forces acting on the atoms. With the knowledge of these forces, the atoms could be

made to evolve, and so on. This approach is still too time-consuming. Solving the many body Schrödinger equation means self-consistently diagonalizing the interaction Hamiltonian, which is an $N_k \times N_k$ matrix for a system with N_k plane waves. It is apparent that for a large molecule, solvated in water, the number of plane waves required to describe the many electrons wave function can be quite large.

A great step forward to reduce the time needed for a simulation, retaining an acceptable treatment of the quantum effects has been made by Car and Parrinello [Car and Parrinello, 1985], who have proposed to introduce an adiabatic approximation. Namely, it is not needed to solve the Schrödinger equation at each time step but, ensuring that the electronic wave function is in its ground state, it suffices that the wave function remain *close enough* to the ground state (to the so-called Born-Oppenheimer surface). This simplification avoids the need to diagonalize the Hamiltonian at each time step, and so allows a quantum mechanical treatment (although approximated). This is the so called *ab initio* approach to Molecular Dynamics.

The merits of an *ab initio* approach are many, the first and foremost being that the force field experienced from the atoms comes from first principles and is not built ad hoc, so that any interaction which can happen is allowed to. The drawback is that the computation is so much heavier than in the classical case, that this approach is restricted to systems with a relatively small number of atoms (including the solvent) and that the trajectories can be followed for times which range is of the order of the picoseconds.

Hybrid approaches, which retain a quantum treatment for a part of the system while treating classically the rest, and the solvent, have been proposed and tried. Among these, it can be cited the QM/MM approach. Much information on this interesting development can be found in [U. Rothlisberger, 2007].

An explanation of these approaches lies outside the scope of the present work. In short, they try to keep the best of two worlds, retaining a quantum accuracy in a particularly significative region while allowing for a large number of atoms to be taken into accounts. The issues arising from the need to match the quantum mechanical part of the system with the classical one are, however, highly non-trivial.

In any case, even a classical Molecular Dynamics simulation is too burdensome for a single computer. So, the common approach is to set up a parallel simulation, subdividing the work load among the nodes of a computer cluster.

The suitability of computer clusters to this kind of program is an important issue. A PC cluster consists of a set of more or less ordinary cpu and banks of RAM memory, which exchange data across a network. It is extremely cheaper than other, more specialized hardware solutions, and as such it is a widespread solution. The performance of the network, of the parallel programming environment and of the intrinsic parallelizability of the algorithms are clearly crucial elements for the success of the task.

The work presented in this thesis is an application of the *ab initio* Molecular Dynamics approach to a biological system. However, it has been my aim to show not only the specific results obtained with respect to the biological problem, but also to put in evidence some features of the field of the computer simulations which can be generically relevant.
This has been done with the idea that one of the roles of the physical sciences, and particularly of the physicists in the modern society is to provide reliable, robust and efficient tools of prediction, be it in the field of drug design, of the growing field of the nanostructures, or in the elucidation of chemical reactions.

Under a larger point of view, many tools developed in the context of Molecular Dynamics could be extended to be valuable in fields as diverse as Genetics, Climatology, Fluidodynamics[4] and Information Theory, thus proving their effectiveness and utility well beyond the original intentions and hopes of their creators. Furthermore, many of these tools are bright and fascinating ideas or applications, thus proving to be an intellectually challenging field of study and research.

The biological system which has been studied is the so called octarepeat of the Prion Protein, namely its interactions with the Copper ions. The interest in this particular problem comes from the pathological relevance of the Prion Protein in the development of a peculiar class of diseases in the mammalians, the Transmissible Spongiform Encephalopaties. Along the years, several experiments have suggested that the interaction with Copper ions might be a crucial feature of the Prion Protein. Copper ions have an an incomplete *3-d* shell, and as such are very good candidates to require an accurate quantistic treatment.

For these reasons, a Quantum Mechanical Molecular Dynamics approach has been thought of as particularly fitting, with the double aim of clarifying the interactions of the Prion Protein with Copper and of establishing the feasibility of such an approach to subsequent studies on other systems.

The plan of the thesis is the following:

- Chapter 2 exposes the biological problem, starting with a general introduction to the field of prion research, which is of great relevance in modern biology, then focusing on the particular domain of the Prion

[4]Which has been the first active field of research in the numerical simulations field.

Protein which will be the subject of the work. The experimental data which have constituted the starting point of the present research are presented and discussed.

- Chapter 3 describes the theory and the practice of the Molecular Dynamics simulations. After an introduction to the Density Functional Theory approach, the main theoretical result, the Car Parrinello Lagrangian, is introduced. Then, a crucial simplification of the Car Parrinello approach is introduced and discussed, that of the *pseudopotentials* and in particular of the Vanderbilt's Ultrasoft pseudopotentials. Finally, the parallel implementation of the algorithms is presented. The parallel approach is strongly needed, since the memory requirements of even the simplest calculations are beyond the possibility of a single computer, not to mention the exceedingly large amount of time which would be required if only a single processor were to be used for the simulations.

- Chapter 4 describes the common protocol adapted for carrying out the simulations.

- Chapter 5 contains the original results of the work. It contains a description of the various simulations performed, and their analysis.

- Chapter 6 contains the general conclusions and a summary of the original results of the work.

A detailed description of sections and subsections is provided at the beginning of each chapter.

The original results presented in this work have been published [Furlan et al., 2007b, Furlan et al., 2006, Furlan et al., 2007a] and presented at several Workshops and Congresses, *e.g.* [ABR, 2006].

The results and the experience acquired with this work have strengthened the idea that such an approach can lead to fruitful results on many other interesting problems, always at the crucial intersection of Physics, Chemistry, Biology and Medicine. The attention of many groups all over the world, including the Biophysics Group of the University of Rome Tor Vergata, has already found a particularly good candidate, and precisely the β-Amyloid Protein and its interaction with Zinc and Copper, which has a strong relevance for the Alzheimer Disease.

It seems reasonable that in the future more and more research problems will benefit from contributions of the Physicists' *computer-simulations community*, with a direct impact on the understanding, and the cure, of an increasing number of diseases; and the diffusion of the conceptual and technical progresses will have an influence on several other fields outside of Biology and Medicine. This would be an important contribution to the whole of the society.

Acknowledgments

I am sincerely pleased to thank my thesis advisors, Professor Silvia Morante and Doctor Velia Minicozzi. The fruitful discussions that I have had with them along these years have greatly helped me to develop my scientific approach, and it is a pleasure for me to express my gratitude for having always shared with me their ideas and suggestions, and, above all, their friendship. Thank you!

I acknowledge my debt of gratitute towards Professor Gian Carlo Rossi, who allowed me to switch from theoretical physics to the world of computer simulations, and whose office room has been always open for me.

All of them, Silvia, Velia and Gian Carlo, are from the Physics Depart-

ment of the University of Tor Vergata, and are founding members of the Biophysics Group of the Department.

The original research contained in this work has been carried on together with them and with Dr Sara Furlan, Dr Giovanni La Penna (both ISMAC - CNR). Thank you for your hard work and for all the time you have spent with me, sharing with me your experience.

I gratefully acknowledge the financial support of an INFN fellowship.

The computations described in this work have been performed at the Fermi cluster at E. Fermi Research Center in Rome (many thanks to Dr Roberto Ammendola and Dr Nazario Tantalo), the BEN cluster at ECT* in Trento (Dr Andrea Nobile and Dr Luigi Scorzato), the CERM cluster in Firenze and the CINECA cluster in Bologna.
As it is discussed in the text, simulations have been performed using the ESPRESSO package (`www.pwscf.org`). In particular, Prof Paolo Giannozzi has always been ready to resolve my doubts on many simulation issues.
Other software packages particularly useful have been: the Atlas and the GotoBLAS numerical libraries, VMD, gnuplot, VEGA. Elaborations have been performed with in-house perl and python scripts.

I would like to express my deep gratitude to Professor Kensuke Yoshida for accepting me as a student, for encouraging me to continue my studies in a Ph.D. program, and for all the good advices and support he has always given to me. It is also a pleasure to expressly thank two Professors who have always found time, literally hours and hours, for explanations and discussions: Prof Massimo Testa and Prof Gianni Jona–Lasinio. They have greatly shaped and influenced my views.

I thank the Department of Physics of the University of Rome 'Tor Vergata', where I have attended many courses, so many seminars and have had

the chance to interact with many bright scientists. I have spent there a lot of my time and it has become a sort of a second home to me.

I thank my friends who have supported me along many years: Federico (who has started *many* important things), Daniele and all the friends known during the study years and in the *stanza Dottorandi*.

I thank the (enlarged) *Circolo Pickwick* with whose members I shared so many hours which remain, and always will, in my memories.

It is a pleasure to thank my friends Luca, Matteo, Vladimiro, Luca, Daniele and Ivan for their support and encouragement, during the last months of the Ph.D.

I am grateful to my family, for all the love they gave to me. It is true that all I have comes from them.

I dedicate my work to Simona. She has always loved and trusted me.

Chapter 2

The Prion Protein

2.1 Introduction

In this chapter a summary of the clinical and biochemical motivations for the study of the prion protein will be given. At the end of the chapter, Sec. 2.5 outlines in detail the purposes of the present work.

The interest raised in the scientific world by the discovery of transmissible diseases mediated by a pathogen completely different from the already known ones (*e.g.* viruses and bacteria) prompted a great amount of research, which led to the formulation of a so called *Prion hypotheses*, namely that the Prion protein, a constituent of all normal mammals and avian cells [Prusiner, 1998] [Millhauser, 2007], undergoes some modification which gives rise to a pathological state, without involvement of genetic material.

The structure of the chapter will be as follows:
in section 2.2 a medical introduction will be outlined, describing the pathologies related to the Prion protein and their discovery; then, in section 2.2.2 some clinical and biochemical experiments will be described to clarify the

chemistry of the prion protein. Since both the physiological and pathogenical role of PrP have not been completely understood yet, many suggestions from experimental analysis will be presented.
A particular attention will be devoted to a characteristic hallmark of PrP, *i.e.* the *octarepeat* (see section 2.4) whose study constitutes the main subject of the present work.

Given the multidisciplinar nature of the subject, which lies in part beyond the usual area of expertise of a physicist, simple explanations of some medical aspect, needed to better appreciate the reasonings exposed, will be provided. As a reference text for histological notions the classical textbook [Adamo et al., 2002] has been adopted.

2.2 Transmissible Spongiform Encephalopaties

Transmissible Spongiform Encephalopaties (TSEs) comprise a group of fatal infectious neurodegenerative diseases which affect several animal species (for instance, mammalians).

The following table lists the names of these diseases and their predominant host.

Disease	Host
Creutzfeldt-Jakob (CJD)	Humans
(in various forms, see later)	
Kuru	Fore people
Gerstmann-Sträussler-Scheinker syndrome (GSS)	Humans
Fatal Familial Insomnia (FFI)	Humans
Scrapie	Sheep
Visna	Sheep
Bovine Spongiform Encephalopathy (BSE)	Cattle
Chronic Wasting Disease (CWD)	Mule deer, elk
Transmissible Mink Encephalopathy (TME)	Mink
Feline Spongiform Encephalopathy (FSE)	Feline
Exotic Ungulate Encephalopathy	Greater Kudu, Nyala and Onyx

The *Fore* people, living in New Guinea, were reported to practice ritual antropophagia until recent times and suffered from an epidemy of Kuru (a Fore word meaning *"shaking death"*) which extended well into the XX century, reaching its maximum incidence in the 70's. The study of this disease has proven to be insightful for the further understanding of the TSEs in general.

While it is now accepted that these diseases are related, the identification of a common link has been particularly complex, and its subtler aspects are still matter of debate. Actually, in all of these cases, a complete understanding of both the transmission mechanism and of the disease insurgence is still lacking.

Furthermore, from an epidemiological view point, it is important to stress that the possibility of transmission of a disease characteristic of a given animal species to another one (*e.g.* contamination of humans through as-

sumption of bovine–derived infectious substance, via food) presents many unclear aspects.

All of these diseases are characterized by *spongiform degeneration*[1] and *astrocytic gliosis*[2] of the Central Nervous System (which comprises the brain and the spinal cord). This invariably leads to death.
Strikingly, for a disease process which is invariably fatal, there is no febrile response, no immune system response, nor all the other common reactions shown by an organism which comes into contact with a pathogen. This observation has been crucial for the perception of being in the presence of a novel infectious mechanism [Prusiner, 1998].

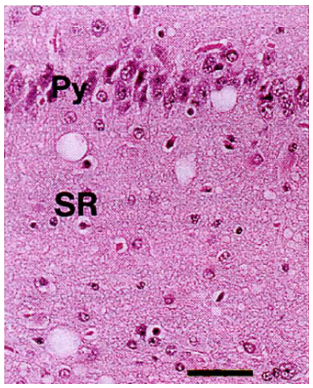

Figure 2.1: Neuropathologic changes in Swiss mice brain following inoculation with scrapie prions. Spongiform degeneration, with the presence of vacuoles of diameter in the range of 10 to 30 μm, is clearly visible in the left and upper parts of this hematoxylin and eosin stain of a serial section of the hippocampus. The bar represents 50 μm. The photomicrograph has been prepared by Stephen J. DeArmond and is taken from [Prusiner, 1998].

[1] Spongiform degeneration, or brain vacuolation, is the formation of fluid-filled holes in the otherwise compact brain tissue.

[2] Also termed *astrogliosis*, it is the process of proliferation and branching of glial cells, structural non-neuronal cells in the brain, in response to various types of brain damage.

2.2.1 Creutzfeldt-Jakob Disease (CJD)

In animals, the most common TSE is scrapie, which has been known for centuries. In the last decade BSE has gained much attention because of the possible relevance for human safety. In particular, because of the epidemic of BSE, clinical surveillance of the most common occurring TSE in humans, CJD, was established in several countries[3].
CJD can appear in three main forms:

1. *sporadic*, in the 85% of cases,
2. *familial*, due to hereditary factors, in the 10% of the cases,
3. *iatrogenic*, *i.e.* due to an exposure to an infective sample in the course of a medical operation, *e.g.* in the case of a medical doctor contracting the disease from a patient, or by assuming infected medical products.
4. A novel form, called *variant CJD*, (vCJD) was reported in 1996 [Will et al., 1996].

The main characteristics of the sporadic form of CJD are, see [Collinge and Rossor, 1996]:

- Uniform annual incidence of about one case per million;
- Mean onset age of 65 years;
- Rapidly progressive dementia with myoclonus (rapid muscular contractions);
- Characteristic pseudoperiodic sharp complexes of peaks in the electroencephalogram;
- Cerebellar ataxia (non-coordination of movements);

[3] In Europe one can cite the United Kingdom, France, Germany, Italy and the Netherlands.

- Cortical blindness (*i.e.* blindness due to cerebral damage);
- Pyramidal and extrapyramidal signs (paralysis, anomalous muscular tone and rigidity);
- Development of the disease via a kinetic mutism (phonation is made impossible by defects at a central nervous system level);
- Death within 3-4 months;
- Accumulation of plaques in the brain (typical of kuru) only in a small minority of cases (5% of total cases).

Since 1991 it has been shown that sporadic and iatrogenic CJD occur mainly in individual homozygous for a specific genetic mutation, a polymorphism at codon 129 of the PRNP gene, which codifies for the Prion Protein [Palmer et al., 1991, Collinge et al., 1991].

In contrast to these characteristics, the vCJD can affect young individuals (average age of 27 years) and has a relatively longer decourse (14 months). Interestingly in the first scientific report on the vCJD [Will et al., 1996] it is noted that using the diagnostic criteria established for sporadic CJD, none of the vCJD cases would have been identified as a CJD case.
The low average onset age is the most surprising difference: until 1995, only four cases were known of sporadic CJD in teenagers.
Other relevant aspects in the clinico-pathological picture are [Soto, 2004]:

- Behavioral and psychiatric disturbances (anxiety, depression, apathy, withdrawal and delusions);
- Persistent painful sensory symptoms;

- Early ataxia;
- Although the EEG is abnormal, the typical features observed in sporadic CJD are absent;
- Extensive plaque formation in all the cases.

All of these signs are strongly reminiscent of kuru. Since its initial discovery, vCDJ has been associated with consumption of BSE infected food, see [Will et al., 1996, Collinge and Rossor, 1996]. Unambiguous prove of this link is, however, still missing [Soto, 2004].

The GSS syndrome is a hereditary condition with slightly different histopathological features, characterized by progressive cerebellar signs, followed by mental deterioration and a slower progression to death than that of CJD. The age of the subjects at insurgence is similar to that of iatrogenic CJD.

FFI is characterized by the loss of the ability to sleep at ages varying between 40 and 60, along with the occurrence of dream–like episodes. The disease progressively affects the autonomic and motor systems, and is invariably fatal within 6–18 months. Its nature of a prion disease has been established by the study of an Italian family [Lugaresi et al., 1986]. The histological signs are different from the other prion diseases (spongiform degeneration is missing) [Aguzzi and Weissmann, 1996].

2.2.2 Study of the infectious agent

The discovery of the source of CJD and of all the other TSEs has been complex and still presents some uncertainty. Nonetheless, to the present day, TSEs rank among the best understood of the neurodegenerative disorders, [Collinge and Rossor, 1996] and many studies, including the present one, are

prompted by the aim of improving the understanding of the remaining unclear points.

At the beginning of the XX century, it was not understood that CJD could be an infectious disease and only familial forms were thought of. The discovery that apes inoculated with brain extracts from CJD patients would develop the disease was crucial in clarifying that some sort of pathogen was the cause of the disease.

The nature of this pathogen was far from clear, since, as stated above in 2.2, the responses typical of a organism in the presence of a pathogen were missing.

A first systematization was the proposal of the concept of *slow virus*, with particular reference to scrapie and visna in sheeps and to kuru in humans, whose infective nature was recognized in the second half of the XX century.

The most surprising feature of the pathogen, and, with hindsight, the most clear indication of its nature, is the resistance to inactivation by exposition to UV or to ionizing radiation, which would be lethal to a pathogen containing nucleic acids, such as bacteria, which are prokaryotes with their own genetic material; viruses, whose genetic material is enclosed in a protective proteic coat (the capside); viroids which don't have a capside.

At the same time (and thanks to the development, due to Stanley B. Prusiner[4], of accurate titration methods by which it was possible to purify and quantify the amount of infective agent in a given sample), it has been determined that scrapie infectivity can be reduced by procedures which hydrolyze or modify proteins. These observations can be interpreted by postulating that a particular, purifiable, proteic macromolecule was the pathogen for scrapie and CJD.

[4]Recipient of the Nobel Prize for Physiology and Medicine in 1997.

Following a proposal by S. B. Prusiner, this pathogen was defined a *prion*[5], which can be defined as a *proteinaceous infectious particle that lacks nucleic acid.*

According to the data obtained by a large amount of researchers, it can be almost definitively concluded that prions are composed entirely by a protein, the prion protein (PrP), although the possible relevance of non-genetic-material-containing ligands or of other, species specific, smaller proteins (so called Protein X) cannot still be ruled out.

Purification of samples extracted from the brains of deceased individuals has shown that the main component of the prion is a protein called PrP^{Sc} (from Scrapie Prion Protein). In particular, it has been shown that PrP^{Sc} and infectivity co-purify[6] and that the concentration of the protein is proportional to the infectivity titre, see [Bolton et al., 1982, Gabizon et al., 1988]. To confirm this, it has been shown that highly purified preparation of PrP^{Sc} retain infectivity.

Following the discovery that infective diseases can be mediated by a proteic pathogen, PrP^{Sc} , it is necessary to understand the origin of this proteic material.

It turns out that the aminoacid sequence of PrP^{Sc} is contained in the genome of all the species which can develop a TSE (actually, in all the mammalians), it is sequenced by a single gene, and that the corresponding expressed protein, called Cellular Prion Protein (PrP^{C}), is commonly synthesized in the brains of uninfected animals[7] [Basler et al., 1986].

This immediately suggests that the different behaviour of PrP in healthy and infected brains is due to post-translational events, since from a genetic view-

[5] The name prion is a portmanteau from *proteinaceous* and *infectious*.

[6] That is, if PrP^{Sc} is purified from a solution, correspondingly the solution is no longer infective.

[7] The early experiments were conducted on Syrian Hamster.

point the infective PrP^{Sc} is identical to the physiologically expressed PrP^{C} . Accepting this explains in a simple way the missing immune response: actually, the organism is not exposed to any not-self pathogen.

Further confirmations are given by the finding that mice whose expression of the relevant gene had been suppressed, *knockout mice* , were resistant to mouse-adapted scrapie and did not propagate infectivity [Büeler et al., 1993, Sailer et al., 1994].

2.2.3 Biochemical properties of the Prion Protein

The most important fact about the Prion Protein is that PrP^{C} and PrP^{Sc} are two different isomers of the same protein. They share the same chemical properties but have different biochemical behaviour, due to marked structural changes in the secondary and tertiary structure.

Even if the direct consequences of this are pathologic, it is important to remark the conceptual leaps prompted by this discovery: in contrast to pathogens with a nucleic acid genome, prions can encode their properties (eventually strain specific) in their tertiary structure. This idea has important ramifications: we can begin to say that the primary structure of a protein is not the *only* determinant of its tertiary structure, and that information can be stored, for long periods of time, via a non-genetic transmission of phenotypes. See [Bussard, 2005] for an interesting review, focusing on so-called yeast-prions.

All of the TSEs discussed in the above sections are now referred to as *prion diseases*. In fact, the characteristic sign of the prion diseases is the accumulation of neurotoxic plaques in brain, which leads to neuron apoptosis[8]. These plaques are fibrils composed of the misfolded form of the prion pro-

[8] Apoptosis is the process of programmed cell death.

tein, PrP^{Sc}

2.3 General Properties of PRP

2.3.1 Characteristic Features

The cellular human prion protein, PrP^{C} , is expressed, under normal and physiological conditions, by cells of the central nervous system, brain, heart, lungs and lymphoid system. Lower expression levels can be found in other tissues such as muscles, and very small traces can be found in blood[9].

The expressed protein is a 254 amino acids long glycoprotein[10]. Mature PrP^{C} undergoes two post-translation modifications: an N-terminal signal peptide comprised by the first 22 residues is removed, and so are the last 23 C-terminal residues, upon the addition of a *C-terminally* linked glycosyl phosphatidylinositol (GPI) anchor[11]. It is interesting to note that not all the PrP^{C} undergoes this GPI anchoring, thus leaving a, relatively small, fraction of PrP^{C} freely floating in the cytosol of the cell.

PrP^{C} is N-glycosylated. Only two Cysteines are present in the mature form, linked together by a disulfide bond.

Nuclear Magnetic Resonance studies on recombinant human PrP^{C} have shown that the C-terminal region, starting from residue 125, adopts a globular fold that is largely helical but with a small two strand β-sheet [Zahn et al., 2000].

[9] It has been proposed that these small traces in blood samples can be relevant for the early detection of disease, with significant medical consequences. See [Soto, 2004] for references.

[10] This is the lenght of the human PrP^{C} . Other species can have slightly different lenghts, typically corresponding to the presence of repeated insertions in the N-terminal region.

[11] The GPI is a glycolipid, thus characterized by a hydrophobic nature, able to bind to the plasma membrane. A large number of plasma membrane proteins undergo this modification. [Alberts et al., 2002].

Similar conclusions are drawn for hamster and mouse PrP^C [Riek et al., 1996, Riek et al., 1997, James et al., 1997].

The structure of PrP^{Sc} is much less, if at all, known, given the experimental difficulty of obtaining high-resolution data for an aggregating protein. Recent electronic crystallographic results seem to show that residues 89-175 refold into a β helix [Govaerts et al., 2004], [Wille et al., 2002].

The N-terminal region of PrP^C , up to residue 110, is unstructured and highly flexible in solution [Donne et al., 1997]. A characteristic hallmark of this region is the so-called *octarepeat domain* composed of tandem repeats of the fundamental eight-residue sequence PHGGGWGQ. Since the octarepeat is the main focus of this work, it will be discussed in greater details in what follows.

Circular Dichroism analysis reveal that PrP^C has a largely alpha-helical structure, whereas the pathogenic PrP^{Sc} isoform is rich in beta-pleated sheets

It has been suggested that the infectious, pathogenic agent of the transmissible spongiform encephalopathies is a protease-resistant, insoluble form of the PrP protein that is derived post-translationally from the normal, protease-sensitive PrP protein

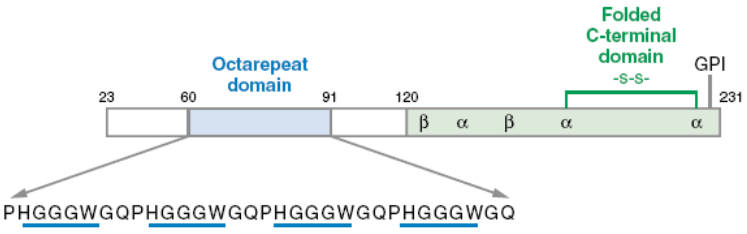

Figure 2.2: This is an useful sketch of the main sequence features of the PrP. The picture has been taken from [Millhauser, 2007]

There is increasing evidence that PrP functions as a copper transporter.[12]

[12]The process by which a carrier protein transfers a solute molecule across the lipid

The physiological function of PrP is unknown, but a series of proposals has been made. Among these, one remarkable feature is the interaction with metals and in particular with copper[13]. The prion protein binds copper in vivo, and the interaction between PrP^C and Cu requires the presence of the N-terminal octarepeat domain [Brown et al., 1997]. It is a fundamental problem to determine if this copper interaction is physiologically significant. See section 2.4 for an analysis of the topic.

Several lines of research have cleared that PrP^C is a neuroprotectant, that is, it is involved in maintaining the integrity of neurons. By comparing the nerve cells of ordinary (wild-type) mice with those of knockouts it has been found that the former are much more resistant to the deleterious oxidative effects mediated by copper or reactive oxygen species, and that this resistance requires the presence of the octarepeat domain [Brown et al., 1998]. Furthermore, PrP knockout mice present widespread tissue damage upon aging, mainly through protein and lipid oxidation [Klamt et al., 2001]. On the other hand, it has been reported that multiple insertions of octarepeat, up to 9 copies, occurring as a hereditary trait, have been linked with the insurgence of familial forms of neurological degeneration [Yanagihara et al., 2002]. One important idea, fostered by Brown et al. [Brown et al., 1997], is that PrP^C has a role of neuronal Superoxide Dismutase (SOD)[14]. This would account

bilayer resembles an enzyme–substrate reaction. Each type of carrier protein has one or more specific binding sites for its solute, and the transport is made possible by reversible conformational changes that expose the solute–binding site first on one side of the membrane and then on the other. See [Alberts et al., 2002] for a detailed discussion.

[13]One can note that other neurological diseases like Alzheimer's, Parkinson's and Wilson's are linked with metals, and that the function of the proteins responsible for their insurgence is still unknown. Another common pattern of these disease is the formation of amyloid fibrils.

[14]SOD is a copper containing enzyme which catalyzes the reduction of superoxide, O_2^- to peroxide. This is important because superoxide is a particularly stable radical which is able to exert significant oxidative damage to the cells. Once it has been reduced to peroxide, it can be efficiently handled by many other protective mechanisms. The reduction of the superoxide is balanced for by the simultaneous oxidation of the copper ions from Cu(I) to Cu(II).

for the neuro-protective role and explain the reason for the conservation of the octarepeat. Unfortunately, this idea cannot be completely accepted, given many doubts on the effective affinity of PrP^C for Cu and, most importantly, to the fact that other studies have failed to show a SOD activity [Hutter et al., 2003], [Jones et al., 2005b].

A different proposal associates PrP^C endocytosis[15] with the concentration of copper. In fact, it has been reported by Pauly et al. [Pauly and Harris, 1998] that the addition of Cu^{2+} results in an acceleration of the internalization of PrP^C from the cell surface to the interior.

It is remarkable that PrP^C is concentrated at presynaptic membranes where there is a high copper localization and flux [Hartter and Barnea, 1988]. The exchange of copper could be related to the neurotransmitter activity.

Peptides from prion proteins, such as the central fragment from amino acid 106 to 126 (PrP[106-126]), form ion channels permeable to physiological ions, and in particular to Cu^{2+} . Channels form in planar lipid bilayers at concentrations greater than 20μM. Heterogeneous channels of various conductances are observed for a single peptide, perhaps reflecting different oligomeric states of the channel-forming peptide in the membrane [TCDB].

PrP[106-126] is a protease resistant, neurotoxic, heterogeneous channel former. It may exist in at least two oligomeric β-sheet forms. One of its oligomeric forms is a Cu^{2+} -sensitive fast-cation channel. It has been suggested that it binds Cu^{2+} to M109 and H111 (that is, to the Methionine amino acid at position 109 and to the Histidine at position 111 in the primary structure) in the mouth of the channel and the formation of these neurotoxic channels has been proposed to underlie the toxicity associated with the prion diseases [Kourie et al., 2003].

[15] Endocytosis is the process of delivering macromolecules from the exterior to the interior of an eucaryotic cell.

An interesting application of the QM/MM hybrid method to the non-octarepeat Cu binding site can be found in [Colombo et al., 2007].

All of these hypotheses share a common trait: the relevance of the interaction of PrP^C with the copper ions. The nature of this interaction is debated, but a first, crucial, step lies in clarifying the affinity of PrP^C with copper and possibly with other ions. A further step is to identify exactly which part of the PrP^C plays which role in this interaction.[Walter et al., 2006]

2.3.2 PrP affinity for Copper

The determination of PrP affinity for Copper is a difficult issue. In fact, even if it is clear that PrP selectively binds Cu^{2+} [Stöckel et al., 1998, Millhauser, 2004, Millhauser, 2007], while other bivalent ions, such as Ni^{2+}, Zn^{2+} and Mn^{2+} are bound with much lower affinity [Jackson et al., 2001] (but see also [Jones et al., 2005a]), the actual relevance in vivo of this interaction is difficult to determine.

This is relevant to define the physiological role of PrP: an enzymatic activity would be characterized by a higher affinity, while a buffering or sensing activity would be consistent with a lower affinity.

It is difficult to determine the affinity without affecting the measurements, which has led different groups to report wildly different affinities. The latest, and apparently more uncontroversial findings are reported in [Walter et al., 2006], where, using several different techniques (such as Circular Dichroism, Fluorescence and EPR) it is concluded that the affinity ranges from approximately 0.1 nm at low Cu^{2+} occupancy to 10 μM at high Cu^{2+} occupancy. Furthermore, these data indicate *negative*, rather than the previously suggested *positive* cooperativity.

The formation of Copper complexes is enhanced by the formation of five or six membered chelate rings, because of the higher thermodynamic

stability, see Fig. 2.3.2. When an imidazole is involved in the binding motif, this fact selects the deprotonation of the N-1 imidazole nitrogen rather than the the N-3. Particularly stable complexes are those where more than one 5 or 6 membered chelate ring is formed. See [Sigel and Martin, 1981, Gaggelli et al., 2006] for review.

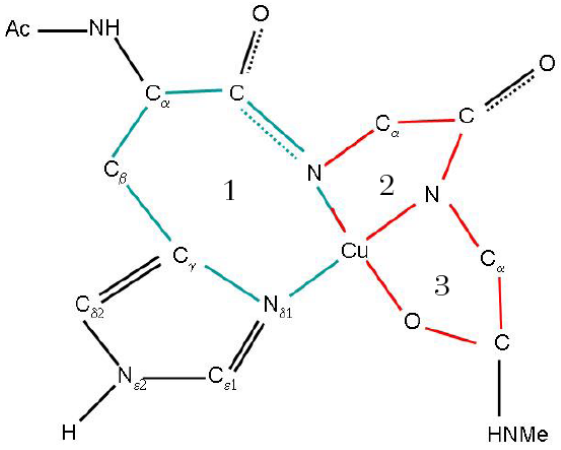

Figure 2.3: This is a planar view of the crystallographic structure of the oligopeptide Cu-HGGGW. HGGGW is a sequence repeated many times in the PrP, see Sec. 2.4. The numbers denote the three chelate rings which are formed when Cu is complexed in this way, which is expected to be thermodynamically favored. The picture is taken from [Furlan et al., 2007b].

2.4 The Octarepeat

As it has been said in section, 2.3.1, a hallmark of the prion proteins is the presence in the N-terminal region of tandem repeats of a sequence of eight a.a., the so-called *octarepeat*: PHGGGWGQ.[16]

Most species, including humans, have four or five repeat segments. It is found that the octarepeat domain is among the most highly conserved regions of the prion protein, which hints at its relevance for the physiological role of the PrP [Wopfner et al., 1999].

It has been proved that the octarepeat is a binding site for metals: thus every prion protein has at least 4 binding sites. The position of other known binding sites, in the C-terminal region, is still debated.

The high flexibility of the N-terminal region is a direct cause for its lack of definite tertiary structure, thus making very difficult to determine precise quantitative information. To overcome this difficulty, many different techniques have been adopted for the analysis of the octarepeat region: Circular Dichroism (CD), Electron Paramagnetic Resonance spectroscopy (EPR), NMR spectroscopy, X-ray Absorption Spectroscopy (XAS), mass spectrometry, Raman spectroscopy, infrared spectroscopy, voltammetry, fluorescence spectroscopy.

The crystal structure of the oligopeptide HGGGW bound with copper, Cu-HGGGW, has been obtained by Burns *et al.*[Burns et al., 2002].

The crystal of the oligopeptide was obtained by capping the two terminus, applying respectively a carboxy-metil group, CO-CH_3 at the N-terminus and a NH_2 group at the C-terminus. This has the effect to simulate a peptidic bond while rendering each terminus chemically inert.

[16] P = Proline, H = Histidine, G = Glycine, W = Tryptophan, Q = Glutamine. This is the standard one-letter notation for amino acids.

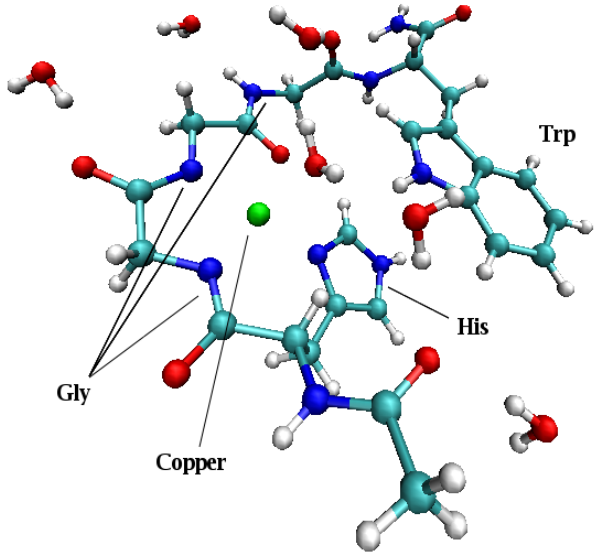

Figure 2.4: This is the crystallographic structure of the oligopeptide Cu-HGGGW. The copper ion is indicated in green, oxygens are red, nitrogens are dark blue, carbons light blue and hydrogens are white. Nearby water molecules are also drawn. The picture has been generated from pdb data (personal communication to Prof. S. Morante) with the help of the VMD program.

As it can be seen in the structure of Fig. 2.4, three Nitrogen and one Oxygen are involved in the copper coordination. Namely the copper is penta-coordinate with four equatorial ligands in a square-planar arrangement plus an additional water molecule. Coordination includes an imidazole nitrogen ligand, two *deprotonated amides* from the next two glycines and a carbonyl oxygen from the second glycine. The axial water ligand is stabilized, through hydrogen bonding, by the presence of the trypthophan indole.

From this simple description it would seem that the basic binding unit of the octarepeat region should be HGG, as the third Gly does not play a direct rôle in the coordination and the trypthophan only stabilizes a very volatile water molecule.

The coordination with the deprotonated amides of the backbone is very interesting. Usually the interaction between proteins and metal ions happens through the side-chains groups: the presence of an interaction with the backbone atoms is unusual, although not unique.

In fact, although the imidazole ring of the His has usually a high affinity for Copper, other binding sites appear in the literature where there is interaction with the deprotonated amide nitrogens. The coordination with the backbone amides is facilitated at high pH. See [Gaggelli et al., 2006] for a review.

Experimental data are available which propose the possibility of other coordination modes. In particular the analysis of XAS data [Morante et al., 2004] suggests both intramolecular and intermolecular Cu binding to the prion protein, and some of the proposed configurations show the Cu^{2+} ion directly bound to two His residues, consistently with an inter-repeat binding mode.

EPR data [Chattopadhyay et al., 2005] are consistent with the above described crystal when Cu^{2+} is present at high concentrations. This can be

interpreted in this way: if there are enough copper ions to saturate every octarepeat (actually, every penta-peptide HGGGW), the coordination will involve the imidazole Nitrogen of the Histidine and two amide Nitrogens from deprotonated Glycines [Chattopadhyay et al., 2005, Millhauser, 2007]. Millhauser's group proposed, with the solved crystal structure, a coordination with the two Glycines immediately following the Histidine, while Raman spectroscopy [Miura et al., 2005] seems to indicate that copper is instead coordinated with the second and the third Glycines following the His.

The complete Prion Protein structure is sketched in Figure 2.4.

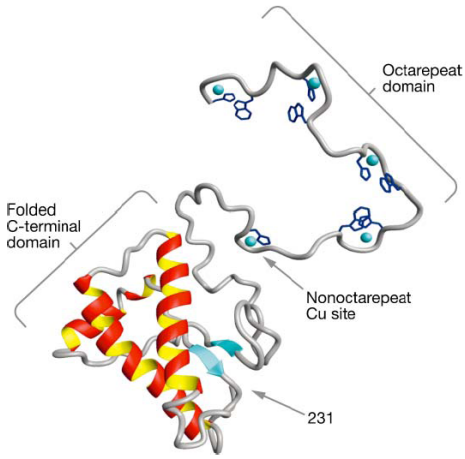

Figure 2.5: This is the hypothetical structure of the complete PrP with all of the available octarepeat sites saturated. Note the four octarepeats domain coordinated as in the crystal of Cu[HGGGW] and the presence of a non octarepeat site at intermediate length of the protein, which could be the one coinciding with the H111, discussed in section 2.3.1, [Kourie et al., 2003]. The picture has been taken from [Millhauser, 2007].

At sub-stoichiometric copper concentrations, different coordination modes have also been described. Following EPR terminology, [Chattopadhyay et al., 2005, Millhauser, 2007], three main kinds of Cu interactions can be distinguished from their component in the EPR spectra:

1. Component 1 is the Cu[HGGGW] coordination mode just discussed, typical of fully Cu^{2+} -occupied octarepeat complexes;

2. Component 2 is an intermediate state, to be found at decreasing Cu^{2+} concentration, with a different coordination than that of the crystal;

3. Component 3 is the dominant mode at low Cu^{2+} concentration, and is characterized by a single Cu^{2+} ion which coordinates multiple His side chains.

As it is to be expected, being an intermediate state, the description of Component 2 is not clear-cut. As reported above, multiple His coordination is suggested by several papers, [Morante et al., 2004, Millhauser, 2007], but it is also suggested that the His can act as a bidentate ligand, coordinating Cu^{2+} via the usual imidazole nitrogen and another atom [Chattopadhyay et al., 2005].

It is interesting to note that the backbone amides nitrogens are crucial for the presence of Component 1, and that the study of Component 2 is facilitated by rendering them chemically inert[17], see [Walter et al., 2006].

2.5 Aim of the present work

The aim of the present work is to study and clarify the interaction of Copper with the octarepeat. Since it is believed that only the five central amino acids, HGGGW, of each octarepeat for which crystallographic data are available, are actually involved in Cu coordination, the study will be focused on this portion.

The method that will be adopted is the *ab initio* Car–Parrinello approach, that is considered particularly suitable for this problem since one doesn't

[17] This is obtained by substituting the ordinary Glycine with a Sarcosine, that is an N-metil Gly, where the amidic Hydrogen is replaced by a CH_3 group.

want to impose by hand the chemical bonds between the Copper and the amino acids, as would be necessary to do in the classical Molecular Dynamics approach, if the actual coordination must be studied.

Due to the presence in the system of Cu^{2+} ions with an incomplete shell ($[Ar]3d^9$), and the presence of the Oxygens, Nitrogens and Carbons the use of the so-called ultra-soft pseudo-potentials, described in Sec. 3.8, is strongly suggested.

However, the system shown in 2.4 is composed by 70 atoms, excluding water molecules. This is already a size so large to exceed the power of a single computer. Given the availability of Linux-based PC-clusters, as discussed in the Introduction, chapter 1, it has been natural to subdivide the burden of the computations with a parallel approach.

Given this analysis, it has been decided to adopt the ESPRESSO package, [Baroni et al.], which is a set of program for *ab initio* computations with support for parallel Car–Parrinello simulations using ultra-soft pseudopotentials.

Following the introduction and the analysis illustrated in this chapter, the actual questions posed in this work are:

1. Definition of the minimal binding unit, and in particular, of the relevance of the Trp;
2. Study of the deprotonation mechanism of the amide nitrogens;
3. Study of the interaction with the solvent (water molecules);
4. Study of the interaction between multiple copies.

Chapter 3

Theoretical Methods

3.1 Introduction

In describing the electronic states of an atom, it is natural to cross a distinction between chemically *active* valence states and chemically *inert* core states. This idea dates back to the very early years of chemistry, and its validity is evident when the regularities of the periodic table of elements are considered. When more complex systems, like crystals or molecules, are studied, the distinction is still useful and applicable, but a great care is required. The whole notion of electrons filling up orbitals needs to be reconsidered because the self interaction due to Coulomb repulsion changes the Hilbert space of the states, and the n-electrons wave function is not simply a product of n one-electron wave functions. This is taken into account by Density Functional Theory (DFT).

Section 3.2 discusses the main results of DFT, namely the Hohenberg-Kohn theorem, section 3.2.1, and the Kohn-Sham equations 3.2.2. Section 3.3 clarifies the meaning of the Eigenvalues in the framework of DFT. Section 3.4 extends the results of the previous sections to the case of a spin depen-

dent functional. Section 3.5 discusses the properties which must be satisfied by a physical Exchange Correlation functional, including some scaling limits and exact conditions. Sections 3.6, 3.7 and 3.8 describe the Pseudopotential approach, which is a crucial approximation to reduce the computational burden of the DFT calculations while retaining the desidered accuracy. Finally, Section 3.9 describes the actual implementation of the theory.

3.2 The main theorems

Consider a system of N non-relativistic electrons with Hamiltonian

$$H = T + U + V, \tag{3.2.1}$$

where

$$\begin{aligned} T &= -\frac{1}{2}\sum_{i}^{1,N} \nabla_i^2 \Psi^\star \Psi \\ U &= \frac{1}{2}\sum_{i\neq j} \Psi^\star(r_i)\Psi^\star(r_j)\frac{1}{|r_i - r_j|}\Psi(r_i)\Psi(r_j) \\ V &= \sum_{i}^{1,N} v(r_i)\Psi^\star\Psi. \end{aligned} \tag{3.2.2}$$

The external potential $v(r_i)$ acting on the i-th electron can be any sufficientrly well behaving function of r, not necessarily the Coulomb potential due to a puntiform nucleus.

The electron density

$$n(\mathbf{r}) \equiv \Psi_0^\star(\mathbf{r})\Psi_0(r) \tag{3.2.3}$$

will play a dominant role in what follows.

The following results constitute the core of the so called Density Functional Theory.

3.2.1 The Hohenberg-Kohn theorem

The starting point of DFT is the Hohenberg-Kohn (HK) theorem [Hohenberg and Kohn, 1964] which states that the ground state density of an electronic system uniquely determines the Hamiltonian of the system, and thus any physical quantity relative to it (from the simplest, like the number of electrons which is clearly given by the spatial integral of the density, to the more complex like the energy spectrum and the scattering properties).

The classical demonstration of HK is by contradiction. Consider two N particle systems, with two different potentials, $V_1(\mathbf{r})$ and $V_2(\mathbf{r})$ and consequently two different ground states, Ψ_1 and Ψ_2, with energies E_1 and E_2. Assume that the ground state is not degenerate. Now suppose that the two potentials give rise to the same density $n(\mathbf{r})$. This will lead to a contradiction.

In fact, by the Rayleigh-Ritz variational principle one finds

$$E_1 = \langle\Psi_1|T+U+V_1|\Psi_1\rangle < \langle\Psi_2|T+U+V_1|\Psi_2\rangle, \tag{3.2.4}$$

because $|\Psi_2\rangle$ is not the right ground state. The inequivalence is strict because we have assumed non degeneracy.

Now, adding and subtracting V_2 in the r.h.s. of (3.2.4) one obtains:

$$\begin{aligned} E_1 &< \langle\Psi_2|T+U+V_2|\Psi_2\rangle + \langle\Psi_2|V_1-V_2|\Psi_2\rangle = \\ &= E_2 + \int d\mathbf{r}(V_1-V_2)n(\mathbf{r}). \end{aligned} \tag{3.2.5}$$

Now by exchanging the indices 1 and 2 in (3.2.4):

$$E_2 < E_1 + \int d\mathbf{r}(V_2 - V_1)n(\mathbf{r}). \tag{3.2.6}$$

Adding together (3.2.5) and (3.2.6) there is a cancellation since the densities were equal, and one has a contradiction:

$$E_1 + E_2 < E_1 + E_2. \tag{3.2.7}$$

Thus two potentials which differ for more than a constant cannot give rise to the same ground state density, and so a one-to-one correspondence between ground state density and potential is established: $n(\mathbf{r})$ is obviously a functional of $V(\mathbf{r})$ but it was not obvious for the converse to be true. This is the content of the Hohenberg-Kohn theorem.

From the HK theorem it follows the existence of a functional $F[n(\mathbf{r})]$, universal in the sense that its definition does not refer to any external potential but only to the kinetic and self-energy of the electron system:

$$F[n(\mathbf{r})] = \langle \Psi | T + U | \Psi \rangle. \tag{3.2.8}$$

It is now natural to define, for a given, arbitrary external potential V', the functional

$$E_{V'}[n] = F[n] + \int d\mathbf{r} n(\mathbf{r})V'(\mathbf{r}). \tag{3.2.9}$$

If $n(\mathbf{r})$ is the right ground state density corresponding to V', be it n', it follows by definition that $E'_V[n']$ is the ground state energy of the system.

From this, a minimum principle follows:

$$E_V[n] = F[n] + \int d\mathbf{r} n(\mathbf{r})V(\mathbf{r}) \tag{3.2.10}$$

is minimized by the unique density corresponding to the external potential V, provided that the minimum is searched among the densities corresponding to a fixed number of electrons,

$$\int d\mathbf{r} n(\mathbf{r}) = N. \tag{3.2.11}$$

Given a ground state density and the single wavefunction which gives rise to it, the potential is explicitly obtained by the inversion of the differential operator (namely, the Schrödinger operator):

$$V(\mathbf{r}) = -\frac{1}{2}\sum_{i=1}^{N}\frac{\nabla_i^2\Psi}{\Psi} + \frac{1}{2}\sum_{i\neq j}\frac{1}{|\mathbf{r}_i - \mathbf{r}_j|}, \tag{3.2.12}$$

which determines the potential up to a constant. This assumes that the ground state is nodeless so that this is a well defined operation.

The HK theorem arises the problem of so called V-representability. A density $n(\mathbf{r})$ is V-representable if it is associated with an anti-symmetric ground state wave function of a certain Hamiltonian H with a certain external potential V. But it is not *a priori* evident that an arbitrary density distribution can be realized by some external potential, and this could raise troubles when adopting the variational principle[1].

This difficulty has been solved by Levy [Levy, 1979], relaxing at the same time the request of non-degeneracy. The basic step is to pass to N-representable densities, which are most simply those that can be obtained by an antisymmetric wave function. It follows that the class of V-representable densities is comprised into the class of the N-representable ones. Levy proposes an universal functional, $Q[n]$, defined for N-representable densi-

[1] See the original HK paper, [Hohenberg and Kohn, 1964], and footnote 35 in [Gunnarsson and Lundqvist, 1976].

ties, which is equal to the F functional of HK when the density is also V-representable.

The definition of $Q[n]$ is

$$Q[n] = \min_{\Psi \to n} \langle \Psi | T + U | \Psi \rangle, \tag{3.2.13}$$

where the minimum is searched among all the wavefunction which give the density n.

From the definition and the Rayleigh- Ritz principle, the following generalizations of (3.2.9) and (3.2.10) hold:

$$E_{\rm gs} \leq Q[n] + \int d\mathbf{r} n(\mathbf{r}) V(\mathbf{r}) \tag{3.2.14}$$

$$E_{\rm gs} = Q[n_{\rm gs}] + \int d\mathbf{r} n_{\rm gs}(\mathbf{r}) V(\mathbf{r}), \tag{3.2.15}$$

where $E_{\rm gs}$ and $n_{\rm gs}$ are the ground state energy and density corresponding to the Hamiltonian characterized by V. These equations are not affected by the possible ground state degeneracy.

3.2.2 Kohn Sham equations

The importance of the density arises from the fact that the total energy of the system depends upon effects external to the system itself (and thus not universal) only *via* the integral of the product of the density and of the external potential.

Two problems affect this result: namely that the conditions for a density n to be an acceptable ground state are not *a priori* evident, and most importantly, that the functional F is unknown.

Since the HK theorem provides a minimum principle, it is natural to derive Euler-Lagrange equations for the density. These equations would

be useless if they directly involved the $F[n]$ functional, because its exact form is unknown. Actually, it is possible to take exactly into account some major contributions, limiting the unknown effects to reasonably small terms. This approach is due to Kohn and Sham (KS) [Kohn and Sham, 1965] and provides the basis for a large part of the current quantum chemistry research, and for the present work in particular.

The following Ansatz for the F functional is posed:

$$F[n(\mathbf{r})] = T_s[n(\mathbf{r})] + \frac{1}{2}\int \frac{n(\mathbf{r})n(\mathbf{r}')}{|\mathbf{r}-\mathbf{r}'|} + E_{xc}[n(\mathbf{r})], \tag{3.2.16}$$

where T_s is the kinetic energy of a *non interacting* system[2] and E_{xc}, the exchange-correlation (xc) functional, is the unknown contribution which accounts for the difference between the physical Kinetic and Potential energy operators and the *non interacting* ones[3].

In particular, the xc functional is defined to be:

$$E_{xc}[n(\mathbf{r})] = T[n(\mathbf{r})] - T_s[n(\mathbf{r})] + \langle V_{e-e}\rangle - \frac{1}{2}\int \frac{n(\mathbf{r})n(\mathbf{r}')}{|\mathbf{r}-\mathbf{r}'|} \tag{3.2.17}$$

where $T[n(\mathbf{r})]$ is the kinetic energy operator of the interacting system, and $\langle V_{e-e}\rangle$ is the electron-electron contribution.

We impose that the density is normalized to N electrons, $\int d\mathbf{r} n(r) = N$ with a Lagrange multiplier and obtain the Kohn-Sham equations upon varying E_V (see eq. (3.2.9) and (3.2.16)) w.r.t. $n(\mathbf{r})$,

[2] The subscript s stands for *single particle* .

[3] The assumption that the physical density can be realized by a product of non interacting wave functions must be made.

$$\int \delta n(\mathbf{r})\{V_s(\mathbf{r}) + \frac{\delta T_s[n]}{\delta n(\mathbf{r})}\}d\mathbf{r} = \quad (3.2.18)$$

$$\int \delta n(\mathbf{r})d\mathbf{r} = 0, \quad (3.2.19)$$

where

$$V_s = V(\mathbf{r}) + \int d\mathbf{r}' \frac{n(\mathbf{r}')}{|\mathbf{r} - \mathbf{r}'|} + \frac{\delta E_{xc}}{n(\mathbf{r})} \quad (3.2.20)$$

Eq. (3.2.18) are the equations that one would get for a system of non self interacting electrons in a potential V_s, thus leading to Schrödinger like equations

$$\{-\frac{1}{2}\nabla^2 + V_s\}\psi_i = \epsilon_i\psi_i. \quad (3.2.21)$$

The ground state energy will then be, from (3.2.9),

$$\sum_{i=1}^{n} \epsilon_i - \frac{1}{2}\int \frac{n(\mathbf{r})n(\mathbf{r}')}{|\mathbf{r} - \mathbf{r}'|} d\mathbf{r}d\mathbf{r}' - \int \frac{\delta E_{xc}}{n(\mathbf{r})} + E_{xc}[n], \quad (3.2.22)$$

where $n(\mathbf{r})$ is the self consistent density, $n(\mathbf{r}) = \sum_i |\psi_i|^2$.

It is possible to sum up the KS approach saying that it consists in mapping the system of interacting electrons onto an auxiliary system of non interacting ones which give rise *to the same density*, and this map is realized through the introduction of an unknown term in the potential for the non-interacting particles, which has the role of a chemical potential.

These single particle wave functions of the fictitious non interacting system correspond to the the intuitive mental picture of electrons in atomic orbitals, but have the nice property to be in a well defined and unique correspondence with any actual interacting system wave functions.

From (3.2.22) it is clear that the individual Eigenvalues ϵ_i must not be

thought as the energies of the orbitals. Their meaning will be clarified in 3.3. The physical meaning of the Eigenfunctions ψ_i is to give rise to the correct self consistent density.

There are a few key points which is worth stressing:

1. The usefulness of this approach is that the exact non-interacting kinetic energy is a large contribution to the total kinetic energy[4] and the Hartree term accounts for the largest part of the electron-electron interaction. Thus it follows that a major part of the effects of exchange and correlation are exactly computed, and the xc functional is *a priori* small.

2. The exchange-correlation functional is amenable to approximations whose validity extends to a wide range of different physical systems.

3. Although the exchange-correlation functional gives only a minor contribution to the total energy of the neutral system, it is nevertheless crucial for the formation of bonds, being often of the same order of magnitude of the chemical bonding energy. Thus, any approach which discarded it altogether, would obtain a model where atoms formed only very weak chemical bonds, if at all. Good approximation of it are thus needed if realistic systems have to be studied.

4. It appears from eq. (3.2.12) that the potential V_s felt by the non interacting particles is in practice only known as a function of $\mathbf{r}$ and not as a functional of $n(\mathbf{r})$. It is typical that the theory is formulated in terms of the density but actual computations are carried out in terms of non interacting wave functions $\phi(\mathbf{r})$.

[4] Thus resolving one of the issues with previous, older, approaches, such as the Thomas-Fermi one.

5. The Hamiltonian, and in particular the external potential, must admit a ground state.

6. The implicit assumption of spatial finiteness of the system has subtle consequences. In the case of infinite systems, such as infinite crystals or, more related to the present work, in the case of periodic boundary conditions, some physical properties such as polarizability can defy a too naïve application of the DFT[5]

3.3 The meaning of the Eigenvalues

The meaning of the Eigenvalues of the Hamiltonian operator $H = T(\mathbf{p}) + V(\mathbf{r})$ in the usual Schrödinger equation is very clear: they are the energy spectrum of the system, and the energy of a single particle in the potential V will belong to the set of the Eigenvalues of H.

The picture becomes different in the case of many particles, already in the Hartree-Fock approximation. The crucial modification is that the Hamiltonian is now self consistent w.r.t. to the orbitals. Thus it follows that the total energy is not the sum of the individual Eigenvalues, because the mutual interaction among the electrons is counted twice. If we imagine to remove an electron from an N-electron system, and assume that the self consistent orbitals are left unchanged, we see that the difference between the energy E_N of the former system and E_{N-1} of the latter is equal to the Eigenvalue corresponding to the orbital of the removed electron. Thus we can think of a Hartree Fock self consistent Eigenvalue as the ionization energy

[5]Although in the rest of the work we will not be concerned with it, given that we're giving a short survey of DFT it's interesting to note that a coherent comprehension of such a basic quantity as polarizability of a crystal in the framework of DFT, has been only relatively recently attained. See [Martin and Ortiz, 1997] and references therein for a clear description of the issue.

of the corresponding orbital. This is the content of Koopmans' theorem [Koopmans, 1934], see [Bransden and Joachain, 2001] pag. 328-330.

In the contest of DFT the meaning of the Eigenvalues can be made more precise, [Janak, 1978]. In fact, Koopmans' theorem assumes that the orbitals of the ionized system are unchanged, which is clearly an approximation, the less tenable the more the extracted electron is deep. Moreover, one has not a quantitative estimate of the error being made.

In order to make the procedure more accurate the first step is to generalize DFT by introducing occupation numbers n_i, thus defining a charge density

$$\rho(\mathbf{r}, \{n_i\}) = \sum_i n_i \left|\psi_i(\mathbf{r})\right|^2 \tag{3.3.1}$$

where the ψ_i are the self consistent solutions of KS equations (3.2.18) with this generalized density. It is important to note that the parameters n_i are not restricted to be integer values.

In the same fashion, a generalized kinetic operator $\tilde{T}$ is defined:

$$\tilde{T} = \sum_i n_i t_i, \tag{3.3.2}$$

where

$$t_i = \int \psi_i^\star(-\nabla^2)\psi_i = \epsilon_i - \int \psi_i^\star(V_H + v_{xc})\psi_i, \tag{3.3.3}$$

where ϵ_i is the eigenvalue corresponding to ψ_i, and V_H, v_{xc} are the Hartree and exchange correlation contributions to the energy.

For a given set $\{n_i\}$, the generalized operator

$$\tilde{E} \equiv \tilde{T} + U[\rho] + E_{xc}[\rho], \tag{3.3.4}$$

where $U[\rho]$ is the classical Coulomb energy operator and E_{xc} is the exchange-

correlation functional, will be made stationary by self consistently solving the corresponding generalized KS equation.

$\tilde{E}$ is useful when one wants to study the relationship between the ground state energies of N and N+1 particles systems, by continuously increasing the occupation number of the lowest unoccupied state of the N particle system.

To show this relationship it is only needed to take the derivative of $[\tilde{E}]$ w.r.t. a given n_i, by allowing relaxation (thus correcting the deficiency in Koopmans' theorem that assumed that the orbitals were left unchanged):

$$\begin{aligned}\frac{\partial \tilde{E}}{\partial n_i} &= t_i + \sum_j n_j \frac{\partial t_j}{\partial n_i} \\ &+ \int (V_H + v_{xc})(|\psi_i|^2 + \sum_j n_j \frac{\partial |\psi_j|^2}{\partial n_i} = \\ &= \epsilon_i + \sum_j n_j (\int \frac{\partial \psi_j^\star}{\partial n_i}(-\nabla^2 + V_H + v_{xc})\psi_j + \text{c.c.}) \qquad (3.3.5)\end{aligned}$$

Using (3.3.3), the term in parentheses equals

$$\sum_j n_j \epsilon_j \frac{\partial}{\partial n_i} \int |\psi_j|^2 ,$$

which is zero because the wavefunctions are normalized.

Thus Janak's result follows:

$$\frac{\partial \tilde{E}}{\partial n_i} = \epsilon_i. \qquad (3.3.6)$$

As noted by Janak, this slightly extends the domain of DFT beyond the ground state, to obtain some properties of excited states. It connects the ground states of N and N+1 particle systems by introducing n electrons, $(0 \leq n \leq 1)$ in the lowest unoccupied level. Since $\tilde{E}$ equals the true total

energies when $n = 0$ and $n = 1$, one has exactly:

$$E_{N+1} - E_N = \int_0^1 \epsilon_i(n) dn, \tag{3.3.7}$$

thus obtaining the ionization energy of the system.

Although the exact meaning of the eigenvalues is different, it is a rather common practice to use them to directly estimate excitation energies. This is usually believed to give an at least qualitatively correct picture, even if it is well known that with the simplest approximation of the XC functional, electronic gaps are often underestimated (see, *e.g.* , [Baroni et al., 2001], pag. 519).

3.4 Spin Density Functional Theory

Spin is a crucial characteristic of electrons, but it is not easy to study it in the usual formulation of DFT. A simple generalization of the original HK formulation of the functionals can prove to be useful.

The first step is to consider the spin indices α of the one-electron operators $\psi_\alpha(\mathbf{r})$. Consequently the charge density $n(\mathbf{r})$, must be replaced by the density matrix $\rho_{\alpha\beta}$ which is given, with standard notation, by:

$$\rho_{\alpha\beta}(\mathbf{r}) = \langle \Psi | \psi^\dagger_\beta(\mathbf{r}) \psi_\alpha(\mathbf{r}) | \Psi \rangle. \tag{3.4.1}$$

Now all the HK and KS results can be reformulated in terms of a spin dependent external potentials and KS potentials. In particular, the potential V_{ext} must be replaced by a spin dependent potential $\mathrm{V}^{\alpha\beta}_{ext}(\mathbf{r})$.

It follows [von Barth and Hedin, 1972] that all ground-state properties are functionals of the density matrix $\rho_{\alpha\beta}$, and the energy E is stationary

with respect to variations to it provided that

$$\sum_{\alpha} \int d\mathbf{r} \rho_{\alpha\alpha} = N \tag{3.4.2}$$

holds.

Within this framework the effective spin-dependent exchange-correlation potential in the single particle equations is given by

$$V_{xc}^{\alpha\beta} = \frac{\delta E_{xc}}{\delta \rho_{\alpha\beta}(\mathbf{r})} \tag{3.4.3}$$

3.5 Exchange Correlation Functional

In the framework of DFT the Exchange-Correlation energy E_{xc} is defined as the difference between the exact energy and other contributions that may be evaluate exactly.

Let Φ be the KS wavefunction (non self interacting) of an N particle system.
The exchange energy functional is defined as

$$E_x[n] \equiv \langle \Phi[n] | V_{e-e} | \Phi[n] \rangle - U[n]. \tag{3.5.1}$$

This is the usual definition of the exchange term in the Hartree-Fock theory, see ([Bransden and Joachain, 2001], sec. 7.4, pg. 324).

From the KS Ansatz, (3.2.16), all the contribution to the F functional, (3.2.8) that one explicitly knows about are expressed in terms of the density directly, or indirectly from the non interacting wave functions.
The correlation effects, then, express the difference between computing the physical quantities in terms of the interacting wave functions and the non

interacting ones. The correlation functional is defined as:

$$E_c[n] \equiv F[n] - T_s[n] - U[n] - E_x[n]. \tag{3.5.2}$$

From (3.2.8) it is possible to further subdivide the correlation energy in two parts, the contributions to the kinetic and to the potential energy:

$$E_c[n] = T_c[n] + U_c[n] \tag{3.5.3}$$

$$T_c[n] = T[n] - T_s[n] \tag{3.5.4}$$

$$U_c[n] = V_{e-e}[n] - U[n] - E_x[n]. \tag{3.5.5}$$

The two terms are of the same order of magnitude, $T_c \sim -U_c/2$ [Burke and friends].

Within the KS theory, the problem of studying a many body system is reformulated to that of finding the Exchange Correlation Functional, which appears in the KS equations, (3.2.18) but whose explicit form is unknown. Were it exactly known, in fact, would mean that any many body system would be exactly tractable.

Lacking the knowledge of the exact functional, it has been clear since the very first work, [Hohenberg and Kohn, 1964], that good approximations of it were needed.
If the density of the real physical system is slowly varying in space, the xc functional can be expanded as

$$E_{xc}[n] = \int \epsilon_{xc}(n(\mathbf{r}))n(\mathbf{r})d\mathbf{r} + \int \epsilon_{xc}^2(n(\mathbf{r}))\left|\nabla n(\mathbf{r})\right|^2 d\mathbf{r} + \ldots \tag{3.5.6}$$

To clarify the relationship between the the interacting system, which is the real object of interest, and the corresponding noninteracting system, which experiences the Exchange-Correlation functional, it is interesting to

model the interaction as

$$\lambda V_{ee} = \frac{\lambda}{|\mathbf{r} - \mathbf{r}'|} \tag{3.5.7}$$

and let the coupling constant λ vary from 0 to the full interaction (which can be set to 1 in the relevant unities). The exposition follows the review [Jones and Gunnarsson, 1989].

Consider an external potential V_λ such that the ground state of the Hamiltonian

$$H_\lambda = -\frac{1}{2}\nabla^2 + V_{\text{ext}}(\mathbf{r}) + V_\lambda + \lambda V_{ee} \tag{3.5.8}$$

has density $n(\mathbf{r})$ for all λ. The exchange-correlation energy is then exactly given in term of an integral over λ [Gunnarsson and Lundqvist, 1976]:

$$E_{xc} = \frac{1}{2}\int d\mathbf{r} n(\mathbf{r}) \int d\mathbf{r}' \frac{1}{|\mathbf{r} - \mathbf{r}'|} n_{xc}(\mathbf{r}, \mathbf{r}' - \mathbf{r}), \tag{3.5.9}$$

where the exchange correlation hole n_{xc} is given by

$$n_{xc} \equiv n(\mathbf{r}') \int_0^1 d\lambda [g(\mathbf{r}, \mathbf{r}', \lambda) - 1] \tag{3.5.10}$$

and g is the pair correlation function of the system with density $n(\mathbf{r})$ and the Coulomb interaction λV_{ee}. The exchange-correlation hole accounts for the repulsion among electrons, that is how much the presence of an electron in $\mathbf{r}$ reduces the probability of finding one at $\mathbf{r}'$. Thus from (3.5.9) the exchange-correlation energy can be seen as the energy of the interaction between an electron and its exchange-correlation hole.

Since $g(\mathbf{r}, \mathbf{r}', \lambda) \to 1$ as $|\mathbf{r} - \mathbf{r}'| \to \infty$, the exchange-correlation contributions can be seen as the consequences of short-range effects of the Coulomb interaction. Furthermore, given the isotropic nature of V_{ee}, it is easy to

rewrite (3.5.9) as

$$E_{xc} = \frac{1}{2}\int d\mathbf{r} n(\mathbf{r}) \int_0^\infty dR R^2 \frac{1}{R} \int d\Omega n_{xc}(\mathbf{r}, \mathbf{r}' - \mathbf{r}), \tag{3.5.11}$$

where it appears that only the spherical average of n_{xc} contributes. This means that exact values for E_{xc} can be obtained even if the description of the nonspherical parts of n_{xc} are not very accurate.

Moreover, given the fact that the exchange-correlation hole is constrained by a sum rule - whose physical meaning is that it contains a single electron -

$$\int d\mathbf{r}' n_{xc}(\mathbf{r}, \mathbf{r} - \mathbf{r}') = -1,$$

it follows that n_{xc} can be thought of as a normalized weight factor, and so

$$E_{xc} = -\frac{1}{2}\int d\mathbf{r} n(\mathbf{r}) \langle \frac{1}{R} \rangle_{\mathbf{r}}, \tag{3.5.12}$$

with $\langle 1/R \rangle_{\mathbf{r}} = -\int d\mathbf{r} n_{xc}(\mathbf{r}, R)/|R|$. This again shows that the exchange-correlation energy actually depends only weakly from the details of n_{xc}.

Some exact conditions which must be satisfied by the functional are discussed in the following section.

3.5.1 Exact conditions and scaling Limits

The simplest condition which must be fulfilled by an energy functional is *size consistency*: if the system can be thought of as composed by two separated parts, A and B with energy E_A and E_B respectively, the energy of the total system must be $E_{A+B} = E_A + E_B$.

Consider how an N-electron wavefunction, $\Psi(\mathbf{r}_1, \ldots, \mathbf{r}_N)$ behaves under

an uniform scaling of the coordinates by a factor $\gamma > 0$:

$$\Psi_\gamma(\mathbf{r}_1, \ldots, \mathbf{r}_N) = \gamma^{3N/2}\Psi(\gamma\mathbf{r}_1, \ldots, \gamma\mathbf{r}_N) \tag{3.5.13}$$

where the scaled function is indicated with a subscript. The constant is determined by imposing that in the scaled coordinate system the (scalar) number of electrons doesn't vary. The scaled density will then be n_γ, and a basic question is if the Hohenberg-Kohn relationship is preserved, that is if $\Psi[n_\gamma] = \Psi_\gamma[n]$. Since the Kohn Sham kinetic energy scales quadratically, $T_s[\Psi_\gamma] = \gamma^2 T_s[\Psi]$, if Ψ minimizes T_s, the scaled wave function Ψ_γ will also minimize T_s, yielding the scaled density n_γ.

The Lieb-Oxford bound is an inequality which states that the exchange correlation functional must be greater than LDA exchange functional times a finite constant:

$$E_{xc}[n] \geq C_{LO} E_X^{LDA}, \tag{3.5.14}$$

where $C_{LO} \leq 2.273$.

3.5.2 Local Density Approximation

The first approximation is the so called *Local Density Approximation*, LDA, again due to Hohenberg and Kohn. It amounts to keeping only the first term in the r.h.s. of (3.5.6), approximating the xc functional as a simple integral over a *function* of the density:

$$E_{xc}^{LDA} = \int \epsilon_{xc}(n(\mathbf{r}))n(\mathbf{r})d\mathbf{r}. \tag{3.5.15}$$

This is termed local because the integrand depends locally on $\mathbf{r}$.

Since the expansion (3.5.6) holds for slowly varying density, it is obvious to

take as a reference system the case of a homogeneous electron gas. This means that the function $\epsilon_{xc}(n)$ in (3.5.15) must be the exchange-correlation energy per particle of a uniform *interacting* electron gas of density n.

In the early works, it was always required for the density of the real system to be slowly varying. Surprisingly this simple approximation is useful in a wide range of applications, well beyond what was thought at the beginning. A very clear discussion of this issue can be found in the lectures by Burke [Burke and friends].

3.5.3 Generalized Gradient Approximation

A very useful and widely adopted approximation to the Exchange-Correlation Functional is due to Perdew, Burke and Ernzerhof (PBE) [Perdew et al., 1996]. It is a Generalized Gradient Approximation, meaning that it keeps the first two terms in the expansion (3.5.6):

$$E_{xc}[n\uparrow, n\downarrow] = \int d\mathbf{r} n(\mathbf{r})\epsilon_{xc}(n\uparrow, n\downarrow) + f(n\uparrow, n\downarrow, \nabla n\uparrow, \nabla n\downarrow). \quad (3.5.16)$$

This has the effect to improve energy computations, typically favoring density inhomogeneity more than the Local Spin Density (LSD) approximation (which is the extension of LDA which takes into account the spin).

While the exchange-correlation energy for an uniform electron gas ϵ_{xc} is well established, the choice for f is less clear-cut. An explicit analytic form is useful and fruitful both for explicit computations and for a better understanding.

A first feature that seems natural to impose is to satisfy the largest possible number of exact conditions. This has been the approach followed by Perdew and Wang, [Perdew and Wang, 1991].

Actually, the PBE approach takes a different point of view: instead of imposing all the known exact conditions, only those already satisfied by the LSD approximation and by the numerical GGA approximation derived from sum rules on the exchange-correlation hole[6].

This brings two main advantages:

1. The imposed conditions are the most energetically significant, while at the same time ensuring that the uniform electron gas response is correctly described.

2. The resulting analytic function is simple and parameter-free.

The computations described in the present work are all performed with the PBE exchange functional.

The reason behind the shortcomings of the earlier approaches is that the form (3.5.16) is too restrictive to reproduce all the exact conditions, while being well suited to reproduce only the subset chosen by PBE.

The GGA expression for the correlation energy is parametrized with the Ansatz:

$$E_C[n\uparrow, n\downarrow] = \int d\mathbf{r} n \left(\epsilon_C^{unif}(r_s,\zeta) + H(r_s,\zeta,t)\right), \tag{3.5.17}$$

where r_s is the local Seitz radius,

$$\frac{4\pi n r_s^3}{3} = \frac{3\pi^2 n}{k_F^3} = 1,$$

$$\zeta = \frac{n\uparrow - n\downarrow}{n\uparrow + n\downarrow}$$

[6] See (3.5.10).

is the relative spin polarization,

$$t = \frac{|\nabla(n)|}{2\phi k_s n}$$

is a dimensionless density gradient, where $\phi(\zeta) = \frac{(1+\zeta)^{2/3}+(1-\zeta)^{2/3}}{2}$ is a spin scaling factor, and $k_s = \left(\frac{4k_F}{\pi a_0}\right)^{1/2}$ is the Thomas-Fermi screening wave number, and $a_0 = \hbar^2/me^2$ is the Bohr radius.

3.6 Pseudopotentials

Notwithstanding the possibilities offered by advanced techniques, both theoretical (Car–Parrinello approach) and technical (Parallel algorithm for Fast Fourier Transform and amazing increase in computational capacity in modern day computers), *ab initio* simulations naively including all the electronic states would still prove to be too inefficient and expensive. In the present contest, this is due to three main reasons, strictly related:

1. the core states have a very small spatial support around the ion core, and so their characteristic length-scale is much smaller than the length scales of the atomic bonds, which is the one we are interested in. This is a typical problem when plane waves are used.

2. the valence states, which have a smooth and monotonous behaviour in the bonding region ($\sim e^{-\alpha r}$ as $r \to \infty$), may present strong oscillations near the ion core, or there may be a non negligible interaction with inner states. This is true, in particular, for elements like C, N, O and for the transition metals (where nd orbitals are filled after $(n+1)s$ ones).

3. The contribution to total energy coming from core electrons is much

larger than that due to valence electrons, simply because of Heisenberg's principle: being localized in a small region of space surrounding the nucleus, both kinetic and potential contributions are larger than those coming from valence electrons. Thus, small relative errors in the core orbitals will deeply affect the affidability of the results.

One of the approaches that have been tried to face these difficulties is the so-called pseudopotential method [7].

Consider a single, isolated, ion. All the electrons will be subjected to the Coulomb attraction towards the nucleus, to the Hartree term and to the exchange correlation contributions. See (3.2.18) and (3.2.21) in Section 3.2.2 above.

It is meaningful, and in agreement with chemical intuition and with the discussion at the beginning of the present section, to mentally divide the electronic states of this system in two classes:

- core states, localized near the nucleus,
- valence states, which comprise all the states chemically active, involved in the formation of the bonds.

Such a distinction is chemically sound, since it has been well known for more than one century that elements with the same valence states display similar chemical properties. This is, in fact, the basis for the periodic table of the chemical elements, organized by Dmitri Mendeleev in 1869.

A pseudopotential is a mathematical construction, realized in such a way that the ground state of a Hamiltonian where the KS potential has been substituted with the pseudopotential mimics the Kohn Sham wavefunction

[7] It is by no means the only one. A very interesting all-electrons approach is due, for instance, to Blöchl, [Blöchl, 1994].

(which is thought of as the *true* one) outside a given, reasonable, core radius. Since by definition core states are localized, only valence states contribute to the KS wavefunction outside the core radius.

The initial Hamiltonian of a system composed by core and valence states is changed to a pseudo Hamiltonian for the valence electrons only.

This has a twofold effect:

1. it reduces the number of electrons since only valence electrons are explicitly present,

2. the resulting valence wave functions are much smoother than in the original system, since there is no more the need to ensure orthogonality with the core states which are no longer present;

thus addressing all the problems listed at the beginning of this section.

The pseudopotential approximation consists in writing the new Hamiltonian for the system

$$H = T + V_{\text{pseudo}}$$

where T is the kinetic energy operator and V_{pseudo} is the *pseudo potential* which takes into account the effects of the core electrons and of the nucleus. Since by construction the pseudopotential ensures a smooth wavefunction, the convergence of a plane wave expansion is greatly improved.
On the other side, it must be noted that the complexity of the calculation is transferred to the generation of the pseudopotential. The second, important, point to be noted is that, assuming that a satisfying algorithm can be found to generate accurate enough pseudopotential for the given isolated ion, it remains to be seen if such a pseudopotential is of some use for a non isolated ion.
At first, one could be worried that the pseudopotential would result to be

unusable when other states, as the presence of other nuclei and of their electrons is due to affect the KS wavefunction. While this is a legitimate issue, it has been found that *transferability* of the pseudopotentials, so that a pseudopotential computed when the nucleus is isolated can be applied when the nucleus is surrounded by other nuclei, can be ensured.

This is similar to the effective lagrangians, and potentials, derived via Renormalization-Group techniques ([Polchinski, 1984]) in Quantum Field Theory.

The first step in any renormalization procedure is to set a cut off (*e.g.* the highest wave vector $\mathbf{k}$ which one decides to reach in a Fourier expansion, which corresponds to the smallest length scale which will be physically meaningful). The contributions to the physical amplitudes coming from wave vectors larger than $\mathbf{k}$ are re-adsorbed in the redefinition (*renormalization*) of the couplings (*e.g.* masses and charges) which appear in the resulting, so-called effective, potential for the low-energy degrees of freedom.

While the form of the starting Lagrangian is usually simple, due to various constrains of symmetry and renormalizability[8], the resulting effective lagrangian will usually be much more complicated, comprising for instance non local terms[9].

This bears a strong resemblance to the pseudopotential method. Here one focus on the valence electrons only, discarding altogether the KS equations for the core orbitals, with the aim to replace the strongly oscillating potential felt by the valence electrons in the neighborhood of the core with a sort of effective potential. These oscillating short ranged contributions from the core

[8] In the Standard Model of elementary particles the only allowed terms in the Lagrangian are Lorentz invariant and transform in a well defined way under the action of three Lie Groups, $SU(3) \times SU(2) \times U(1)$.

[9] *E.g.* the Lagrangian could contain terms like $f(\mathbf{r}) = \int d\mathbf{r}' g(\mathbf{r}, \mathbf{r}')$, for some function g.

orbitals and the nucleus had a rather simple analytical expression, (3.2.18). The price to be paid for their elimination is that the resulting *pseudopotential* will have a much more complex appearance, and its form will no longer be derived from microscopic equations (like Maxwell's).

3.6.1 Pseudopotentials from first principles

Experience has shown that the use of pseudopotentials is practically equivalent to the frozen core approximation within an *all electron* approach [von Barth and Gelatt, 1980]. The pseudopotential approximation implicitly assumes that the energy functional is linear with respect to the partition of the total charge into core and valence contributions [Baroni et al., 2001].

Since the core states are only slightly affected by the environment (because of their strong spatial localization) and their contribution to chemical properties (namely to bond formation) is to alter the shape of the valence wave functions within a small region of space, to enforce mutual orthogonal between core and valence states, it can be expected that the microscopic first-principle potential can be replaced by an effective one, a *pseudo potential* which will maintain unaltered the physical properties of the relevant wave functions while being computationally much more tractable.

To obtain a pseudopotential, many different techniques have been tried, empirical or from first principles. In the first case, a simple form for the effective potential acting on the valence electrons, arising from interaction with core electrons and atomic core, was fit to the experimental data to give the correct energy spectrum. The postulated form typically exhibited a Coulombian behaviour at large radius and was more or less smoothly joined at a core radius with some simple function, *e.g.* a constant value or a form

like:

$$\begin{aligned} V &= V_0 \cos(kr) + C \text{ for } r < r_c \\ V &= -\frac{1}{r} \text{ for } r > r_c. \end{aligned} \tag{3.6.1}$$

But a more rigorous and systematic approach is needed for accurate *ab initio* computations where chemical reaction are quantitatively studied.
The correct valence charge distribution is required to study the formation of chemical bonds [Topp and Hopfield, 1973] and of all the quantum effects, such as Hydrogen bonds or the formation of coordination complexes[10].
Deriving pseudopotentials from *first principles* atomistic calculations appear to be the most efficient way to obtain reliable pseudopotentials suitable for generic systems. Many different techniques have been tried and refined along the years, starting from the orthogonalized-plane-wave (OPW) approach [Herring, 1940] to arrive at the Norm-Conserving pseudopotentials, [Hamann et al., 1979, Bachelet et al., 1982] and the Ultra-Soft pseudopotentials [Vanderbilt, 1990].

While there are infinite ways of deriving an analytic function which can be used as a pseudopotential, the physical content is expressed by the following properties:

1. The energy spectrum for the real valence eigenfunctions and the pseudo valence eigenfunctions must be the same for a given atomic configuration.

2. Real and pseudo atomic wave functions must be identical beyond a

[10] Historically, the simple pseudopotential (3.6.1) was introduced by Topp and Hopfield precisely with the aim of reproducing the correct valence charge distribution, going beyond the simple fit of the energy spectrum.

chosen *core radius* r_c.

3. The integrals from 0 to r, for $r > r_c$ of the real and pseudo charge densities, for each valence state, must be the same[11].

4. The logarithmic derivatives (with respect to r) of the real and pseudo wave functions, and of their first energy derivatives must agree for $r > r_c$.

While the reason of requiring properties 1 and 2 is clear (one wants to simplify the description of a well defined space of states, and the pseudopotential must re-create the effect of the core states and of the strong ion potential), the full meaning of the properties 3 and 4 deserves some comment.
Gauss' theorem guarantees that, if property 3 holds, the electrostatic potential produced beyond r_c by the true[12] and the pseudo wave function is the same.
If property 4 holds, the scattering properties of the full potential are reproduced, to *first order in the energy difference* by the pseudopotential.
Furthermore, these two properties are strictly related by an identity [Shaw Jr. and Harrison, 1967, Topp and Hopfield, 1973] which is of great practical relevance:

$$-\frac{1}{2}\left[(\rho R_{\epsilon,l}(\rho))^2 \frac{d}{d\epsilon}\frac{d}{d\rho}\ln R_{\epsilon,l}(\rho)\right]_{\epsilon=E,\rho=r} = \int_0^r (\rho R_{E,l})^2 \, d\rho \qquad (3.6.2)$$

where $R_{E,l}$ is the radial part of the solution of the Schrödinger equation with energy E and angular momentum l, and $r > r_c$. Proof of eq. (3.6.2) will be given in section (3.6.2).

[11] The energy may well correspond to an unbound state [Hamann, 1989], in which case the wave function will be non normalizable. This is, however, because of long range behaviour, but regularity at any finite point, in particular at the origin, is always required and so integrals over a closed interval are always finite.
[12] At least, true for the isolated atom.

3.6.2 Transferability

Transferability indicates the ability of the pseudopotentials to correctly represent the *ab initio* potential in the biggest possible range of cases, *e.g.* when chemical bonds are formed and the atom is no longer isolated.
To be of practical use, the same pseudopotential must be appropriate to obtain results which are independent of the local chemical environment of the individual atoms. This is a a highly desirable property in static computations, and an irrenounceable request in dynamic computations, such as Car Parrinello MD, because the atomic configurations are then subject to all kind of variations (electron transfers, change in occupation numbers and so on).
Furthermore a non transferable pseudopotential would be able to give the correct valence wave functions only in the case of an isolated nucleus, thus being redundant since the KS equations for the isolated nucleus have to be exactly solved to derive the pseudopotential itself.
By adopting a pseudopotential approach, we are replacing by hand a part of the (*a priori unique*, apart from the various approximation for the Exchange Correlation functional) Hamiltonian with terms of our choice. In this sense, a pseudopotential captures the *unique* characteristic properties of the interaction of the core states with the valence states, and for this reason a non transferable pseudopotential, *i.e.* a Hamiltonian which is different for different chemical environments, is a sort of contradiction in terms. This means that the existence itself of a pseudopotential is not guaranteed but, rather it remains in any case to be checked if the decomposition of the Hamiltonian which one is realizing is meaningful or not.

Transferability clearly depends on the quality of the pseudopotential (*e.g.* a local, spin independent pseudopotential will be less able to correctly rep-

resent the chemical properties of the atom than a nonlocal one) and on the chosen cutoff radius (a larger cutoff will mean that a larger part of the potential has to be approximated by the pseudopotential, thus usually increasing inaccuracies) As a matter of fact, two properties are usually related to transferability:

1. The scattering properties of the PP should be compared to those of the *ab initio* self consistent, potential in the *given reference state* which was used to compute the PP.

2. The eigenvalues of the PP and of the *ab initio* self consistent potential should match for different atomic configurations, namely for excited, or ionized, states.

One of the necessary conditions for this key physical request to be fulfilled is that (3.6.2) holds.
Equation (3.6.2) relates the charge contained inside a sphere of radius R to the scattering phase shifts of the potential which appears in the KS equation. Consider two wave functions, ϕ_1 being the solution of the KS equation with the true potential and ϕ_2 being the solution with the pseudo potential. If they give the same integrated charge (the right hand side of (3.6.2)), the linear variation w.r.t. the energy of the scattering phase shifts of the corresponding potentials will be the same. This insures that, if both the w.f. are normalized and $\phi_1 = \phi_2$ for $r > r_c$, thus giving the same integrated charge for $r > r_c$, the scattering phase shifts of the two potentials will have the same energy variations, to first order, when transferred to other systems.

3.6.3 Phase shifts

To exhibit the relationship of the left hand side of (3.6.2) to the physical properties of the potential appearing in the KS equation satisfied by ϕ, consider the non relativistic scattering of a spinless particle by a given central, real and time independent potential V. The Schrödinger equation[13] is

$$\big[-\frac{\hbar^2}{2m}\nabla^2 + V(\mathbf{r})\big]\Phi(\mathbf{r},t) = i\hbar\frac{\partial}{\partial t}\Phi \tag{3.6.3}$$

where m is the physical mass of the scattered particle. As is well known, a stationary solution of (3.6.3) is $\Phi(\mathbf{r},t) = \phi(\mathbf{r})e^{-i\frac{Et}{\hbar}}$, with ϕ satisfying the equation

$$[-\frac{\hbar^2}{2m}\nabla^2 + V(\mathbf{r})]\phi(\mathbf{r}) = E\phi(\mathbf{r}) \tag{3.6.4}$$

where $E = (\hbar^2k^2)/(2m)$, k being the conserved momentum. Define

$$U(\mathbf{r}) = \frac{2m}{\hbar^2}V(\mathbf{r}).$$

Then (3.6.4) becomes

$$[\nabla^2 + k^2 - U(\mathbf{r})]\phi(\mathbf{r}) = 0 \tag{3.6.5}$$

Because the potential is central, the Schrödinger equation is separable in spherical coordinates and the wave function ϕ can be expanded ($\mathbf{k}$ is the wave vector):

$$\phi(k,r,\theta) = \sum_{l=0}^{\infty} R_l(k,r)P_l(cos(\theta)) \tag{3.6.6}$$

where P_l are the Legendre polynomials.

Defining $u_l(k,r) = rR_l(k,r)$, it can be seen that u_l satisfies the radial

[13] KS equations are of the same form, differing only for the potential, which is not known by first principles.

Schrödinger equation

$$[\frac{d}{dr^2} - \frac{l(l+1)}{r^2} + k^2 - U(r)]u_l(k,r) = 0. \tag{3.6.7}$$

Assume that the potential $U(\mathbf{r})$ tends to zero sufficiently fast, becoming negligible for $\mathbf{r} \geq \mathbf{r}_0$. Then the radial Schrödinger equation reduces to a free particle equation, and its solution $R_l(k,r)$ is a function of the product (kr) only. It can be expressed in terms of the spherical Bessel function $j_l(kr)$ and of the spherical Neumann function $n_l(kr)$[14]

$$R_l(k,r) = B_l(k)j_l(kr) + C_l(k)n_l(kr). \tag{3.6.8}$$

The only required property of j_l and n_l is their asymptotic behaviour,

$$\begin{aligned} j_l(kr) &\sim \frac{\sin(kr - l\pi/2)}{kr} \\ n_l(kr) &\sim -\frac{\cos(kr - l\pi/2)}{kr}, \end{aligned} \tag{3.6.9}$$

as $kr \to \infty$.

From these equations it is simple to obtain the asymptotic behavior at large kr of the radial solution:

$$R_l(k,r) \sim \frac{[B_l^2 + C_l^2]^{1/2}}{kr} \sin(kr - l\pi/2 + \delta_l(k)), \tag{3.6.10}$$

where $\tan(\delta_l(k)) = -C_l(k)/B_l(k)$.

The quantities δ_l are called *phase shifts*.

[14] For the properties of these two kinds of special functions, see any standard mathematical physics textbook, like for instance [Jeffreys and Swirles, 1972].

3.6.4 Proof of the transferability criterion

If a potential gives both the atomic ground-state energy and the energies of the excited states of the same symmetry correctly, it gives the correct normalization of the wave function.

Be ψ_E and $\psi_{E+\Delta}$ the eigenfunctions, with eigenvalues E and $E+\Delta$, of the Hamiltonian $(-\frac{1}{2}\nabla^2 + V)$, with $V = V(r)$ a central potential.
Expanding them in partial waves, one gets

$$\psi_E = \sum_{l,m} a_{l,m} R_{E,l}(r) Y_{l,m}(\theta, \varphi) \tag{3.6.11}$$

and an analogous expansion for $\psi_{E+\Delta}$.
In spherical coordinates and atomic units, the Schrödinger equation is

$$\left(-\frac{1}{2}\frac{1}{r}\frac{d^2 R_{E,l}(r)}{dr^2} + (V(r) - E)\frac{1}{r} R_{E,l}(r)\right) Y_{lm}(\hat{\mathbf{r}}) - \\ -\frac{1}{2}\left(\frac{1}{\sin(\theta)}\frac{\partial}{\partial\theta}\left(\sin(\theta)\frac{\partial Y_{lm}(\hat{\mathbf{r}})}{\partial\theta}\right) + \frac{1}{\sin^2(\theta)}\frac{\partial^2 Y_{lm}(\hat{\mathbf{r}})}{\partial\phi^2}\right)\frac{1}{r^3} R_{E,l}(r) = 0. \tag{3.6.12}$$

This gives a radial equation for $R_{E,l}$:

$$-\frac{1}{2}\frac{d^2 R_{E,l}(r)}{dr^2} + \left(\frac{1}{2}\frac{l(l+1)}{r^2} + V(r)\right)(r R_{E,l}(r)) = E\,(r R_{E,l}(r))\,. \tag{3.6.13}$$

With no loss of generality we can set $R_{E,l}(r)$ to be a real function[15]. The same equation, with $E \to E+\Delta$, holds for $R_{E+\Delta,l}$.
To improve readability of the formulas, set

$$V + \frac{1}{2}\frac{l(l+1)}{r^2} \to V. \tag{3.6.14}$$

Now, multiply (3.6.13) by $R_{E+\Delta,l}$ and, vice versa, the equation for $R_{E+\Delta,l}$

[15] See for instance [Bransden and Joachain, 2001], pag. 469

by $R_{E,l}$, to obtain

$$R_{E+\Delta,l}\left(-\frac{1}{2}\frac{d}{dr^2}+V\right)R_{E,l} = ER_{E+\Delta,l}R_{E,l} \quad (3.6.15)$$

$$R_{E,l}\left(-\frac{1}{2}\frac{d}{dr^2}+V\right)R_{E+\Delta,l} = (E+\Delta,l)\,R_{E,l}R_{E+\Delta,l} \quad (3.6.16)$$

Subtract (3.6.15) from (3.6.16):

$$R_{E,l}\left(-\frac{1}{2}\frac{d}{dr^2}+V\right)R_{E+\Delta,l} - R_{E+\Delta,l}\left(-\frac{1}{2}\frac{d}{dr^2}+V\right)R_{E,l} = \Delta R_{E,l}R_{E+\Delta,l} \quad (3.6.17)$$

If V doesn't depend on energy, which is surely true for a *non-pseudo potential*[16] , there is a simplification and one gets:

$$R_{E,l}\left(-\frac{1}{2}\frac{d}{dr^2}\right)R_{E+\Delta,l} - R_{E+\Delta,l}\left(-\frac{1}{2}\frac{d}{dr^2}\right)R_{E,l} = \Delta R_{E,l}R_{E+\Delta,l} \quad (3.6.18)$$

Now integrate both sides in a spherical region around the origin, where the ion which generates the potential is sitting.

Integrating by parts:

$$-\frac{1}{2}\iiint_0^{r_c}\frac{d}{dr}\left(R_{E,l}\frac{d}{dr}R_{E+\Delta,l} - R_{E+\Delta,l}\frac{d}{dr}R_{E,l}\right) = \iiint_0^{r_c}\Delta R_{E,l}R_{E+\Delta} \quad (3.6.19)$$

Applying the divergence theorem one gets:

$$-\frac{1}{2}\iint_{r=r_c} R_{E,l}\frac{d}{dr}R_{E+\Delta,l} - R_{E+\Delta,l}\frac{d}{dr}R_{E,l} = \iiint_0^{r_c}\Delta R_{E,l}R_{E+\Delta,l} \quad (3.6.20)$$

In the limit of $\Delta \to 0$, $R_{E+\Delta}$ can be expanded, and keeping only terms up

[16] See sec. 3.6.5 for an example of a pseudopotential explicitly depending on energy.

to $O(\Delta)$ the equation becomes

$$-\frac{1}{2}\iint_{r=r_c}\Delta\left(R_{E,l}\frac{d}{dr}\frac{\partial R_{E,l}}{\partial E}-\frac{\partial R_{E,l}}{\partial E}\frac{d}{dr}R_{E,l}\right)=\iiint_0^{r_c}\Delta R_{E,l}^2 \quad (3.6.21)$$

After doing the angular integration one has:

$$-2\pi\left[R_{E,l}\frac{d}{dr}\frac{\partial R_{E,l}}{\partial E}-\frac{\partial R_{E,l}}{\partial E}\frac{d}{dr}R_{E,l}\right]_{r_c}=4\pi\int_0^{r_c}r^2R_{E,l}^2 \quad (3.6.22)$$

Rewrite the left hand side:

$$R_{E,l}\frac{d}{dr}\frac{\partial R_{E,l}}{\partial E}-\frac{\partial R_{E,l}}{\partial E}\frac{d}{dr}R_{E,l}=r^2R_{E,l}^2\frac{d}{dE}\frac{d}{dr}\ln R_{E,l}. \quad (3.6.23)$$

Thus one obtains the desired result:

$$-\frac{1}{2}r_c^2\ R_{E,l}^2\frac{d}{dE}\frac{d}{dr}\ln R_{E,l}\Big|_{r_c}=\int_0^{r_c}r^2R_{E,l}^2 \quad (3.6.24)$$

3.6.5 Phillips and Kleinman approach

It is natural to improve the convergence of the valence wave function by making it by construction orthogonal to the core states [Herring, 1940, Phillips and Kleinman, 1959]. It is interesting to briefly review this approach because of its theoretical, and historical, relevance. Consider the Schrödinger equation

$$(T+V)\,|\psi\rangle=E|\psi\rangle. \quad (3.6.25)$$

In general $|\psi\rangle$ will have an oscillating behaviour near the ion core, making a plane wave expansion difficult.

A smoother pseudo wave function can obtained by adding an appropriate

combination of core functions $|\psi_c\rangle$:

$$|\phi\rangle = |\psi\rangle + \sum_c a_c |\psi_c\rangle \tag{3.6.26}$$

where the sum runs on the core states, whose spatial support is a small region near the ion.

The pseudo wave function satisfies, by definition, a Schrödinger equation with the same eigenvalue E but the potential replaced by a pseudo potential [Austin et al., 1962]:

$$V_{ps} = V + \sum_c |\psi_c\rangle\langle F_c(\mathbf{r})|. \tag{3.6.27}$$

This representation is due to Austin, Heine and Sham (AHS). By substituting (3.6.26) into (3.6.27)

$$\begin{aligned}
(T + V_{ps})\,|\phi\rangle &= E|\phi\rangle \\
\left(T + V + \sum_c |\psi_c\rangle\langle F_c(\mathbf{r})|\right)\left(|\psi\rangle - \sum_c a_c|\psi_c\rangle\right) &= E|\phi\rangle \\
(T+V)\,|\psi\rangle - \sum_c a_c\,(T+V)\,|\psi_c\rangle + \sum_c |\psi_c\rangle\langle F_c(\mathbf{r})|\phi\rangle &= E|\phi\rangle,
\end{aligned}$$

which gives

$$E|\psi\rangle + \sum_c \left(E_c a_c + \langle F_c(\mathbf{r})|\phi\rangle\right)|\psi_c\rangle = E|\phi\rangle. \tag{3.6.28}$$

This implies that

$$\begin{aligned}
a_c E_c + \langle F_c(\mathbf{r})|\phi\rangle &= E a_c \\
a_c &= \frac{\langle F_c(\mathbf{r})|\phi\rangle}{E - E_c}.
\end{aligned} \tag{3.6.29}$$

In particular we obtain the Phillips-Kleinman [Phillips and Kleinman, 1959] pseudopotential[17] *i.e.* by setting

$$|F_c(\mathbf{r})\rangle = (E - E_c)|\psi_c\rangle$$

which gives

$$\begin{aligned} V_{PK} &= V + \sum_c (E - E_c)|\psi_c\rangle\langle\psi_c| \\ |\psi\rangle &= |\phi\rangle - \sum_c (E - E_c)\,\langle\psi_c|\psi\rangle|psi_c\rangle \end{aligned} \tag{3.6.30}$$

Note that this kind of pseudopotential depends explicitly on the energy E of the reference state, and that if the pseudo wave function is orthogonal to all core functions[18] then the pseudopotentials is equal to the true potential. Another important point is that outside the core region the normalized pseudo wave function ϕ will be proportional but not equal to the true wave function ψ, thus the correct charge density has to be reconstructed by (3.6.30).

It is important to note that, from a computational point of view, it is very convenient to recast the angular-momentum-dependent part of a pseudopotential into a sum over a few projectors [Kleinman and Bylander, 1982]. This is called the separable form of a pseudopotential.

[17] Which enjoys many interesting features, like the existence of a variational principle for the solution of the Schrödinger equation, which is not guaranteed by the more general AHS form (3.6.27) [Zwicker, 1975, Kleinman and Bylander, 1982].

[18] This is the case for many elements of the second row of the periodic table, like *e.g.* the 2p wave function of oxygen, or the 3d orbitals for transition metals.

3.7 Norm-Conserving Pseudopotentials

3.7.1 Hamann, Schlüter and Chiang

The definitive affirmation of Norm Conserving pseudopotentials is due to Hamann, Schlüter and Chiang, [Hamann et al., 1979], and to Bachelet, Hamann and Schlüter,[Bachelet et al., 1982]. The procedure that they propose is

1. An Exchange-Correlation functional is chosen. The pseudopotential will be meaningful only with this choice of functional for the simulations where it will be applied. As it could be expected, starting from the early works where local approximation were used, many different functionals have been adopted to deal with situations more and more refined.

2. An atomic configuration is chosen (*e.g.* the ground state) and an *ab initio* self-consistent computation is carried out, obtaining the self consistent potential $V(r)$ and $u_l(r)$, which is r times the valence wave function with angular momentum l, whose energy will be called ϵ_l. Only bound states, with normalizable wave functions, are considered.

3. A cutoff function $f(x)$ is chosen, with the following properties:

   - approaches to 0 as $x \to \infty$
   - cuts off at $x = 1$
   - approaches to 1 as fast as x^3 as $x \to 0$

   Possible choices for f are $f = e^{-x^4}$ or $f = e^{-x^{3.5}}$.

4. For every l a cutoff radius r_{cl} is determined, by multiplying the radius of the the outermost peak of $u_l(r)$, r_l^{outer}, times a factor less or equal

to 1.0[19]

5. A first pseudopotential V_{1l}^{ps} is formed

$$V_{1l}^{ps} = \left[1 - f\left(\frac{r}{r_{cl}}\right)\right] V(r) + c_1 f\left(\frac{r}{r_{cl}}\right). \tag{3.7.1}$$

$V_{1l}^{ps} \to V(r)$ for $r > r_{cl}$. The constant c_1 is fixed by requiring that the *nodeless* solution w_{1l} of the radial Schrödinger equation with potential V_{1l} correspond to the same eigenvalue ϵ_l of u_l. Property 1 is thus satisfied.

6. Because w_{1l} satisfies the same[20] differential equation, with the same boundary conditions, satisfied by u_l, the two functions will be equal up to a multiplicative constant γ_l,

$$\gamma_l w_{1l} \to u_l$$

when $r > r_{cl}$.

7. The final modifications to the pseudo wave function must fulfill the other properties. w_{1l} is changed to

$$w_{2l} = \gamma_l \left[w_{1l}(r) + \delta_l g_l\left(\frac{r}{r_{cl}}\right)\right], \tag{3.7.2}$$

where $g_l(x)$ cuts off at $x = 1$ and behaves as x^{l+1} near the origin. A possible choice is $g_l(x) = x^{l+1}\exp(-x^4)$. This insures a good behaviour of the pseudo wave function at the origin and so guarantees that the pseudopotential will be finite. The constant δ_l is picked to be the

[19] In [Hamann et al., 1979] it is suggested that r_{cl} be 0.5 to 1.0 times r_l^{outer}, but later experience reduced these values to the range $0.4 - 0.6$ [Hamann, 1989].

[20] Up to the cutoff $f(x)$.

smaller solution of the quadratic equation obtained by normalizing w_{2l},

$$\gamma_l^2 \int_0^\infty \left[w_{1l}(r) + \delta_l g_l \left(\frac{r}{r_{cl}} \right) \right]^2 dr = 1.$$

8. The screened pseudopotential V_{2l}^{ps} is obtained by inverting the radial Schrödinger equation which is satisfied by w_{2l} with eigenvalue ϵ_l

$$V_{2l}^{ps}(r) = \frac{1}{2} \left(\frac{1}{w_{2l}} \frac{d^2 w_{2l}(r)}{dr^2} - \frac{l(l+1)}{r^2} \right) + \epsilon_1. \qquad (3.7.3)$$

   Note that w_{2l} is nodeless and so dividing by it is a well defined operation.

9. The last step is to *unscreen* the potential, by computing and subtracting the Coulomb and the exchange correlation effects, for every l, due to the charge density of the valence pseudo wave function.

The result of this procedure, the *unscreened* pseudopotential, will replace the contributions of the ion core and of the core electrons in the *ab initio* simulations.

This approach has proven to be the most efficient scheme. Many enhancements have been introduced by several researchers. Among the many proposed improvements, the following are particularly relevant: [Bachelet et al., 1982, Vanderbilt, 1985, Hamann, 1989]

3.7.2 Rappe, Rabe, Kaxiras and Joannopoulos pseudopotentials

The work of Rappe, Rabe, Kaxiras and Joannopoulos (RRKJ), [Rappe et al., 1990] focuses on the need to improve the convergence of the total energy in a plane wave basis. They define a criterion which must be fulfilled for a pseudopo-

tential to provide optimal convergence while being appropriate for a wide class of cases, and not only for specific problems.

The key point noted by RRKJ is that the convergence of the total energy of an isolated atom, using a plane wave basis set, is as difficult a case as that of the atom in the presence of bond formation[21]. Namely, there are four cases:

1. Valence states in the generic complex and in the isolated system can be similar. In this case (*e.g.* ionic solids, noble gas solids), the classical approximation of tight binding (see [Ashcroft and Memin, 1976], chap. 10) would be useful, and by definition the convergence in the two systems is similar.

2. Valence states can be distributed nearly uniformly in the complex. In the case of a solid, the free electron approximation would be applicable. This case doesn't pose a convergence problem, because these states require much fewer plane waves than the core states.

3. Valence states could show a mixture of the two first behaviors: some states could be free-electron-like, not posing a convergence problem, while the other ones could be more concentrated, resembling the atomic states. This is the typical case of the transition metal elements. The convergence is dominated by the peaked states and is similar to that of the isolated atom.

4. Valence states could be involved in covalent bonding. The states in the complex would be very different from those in the single atom, but since the size of the bonding region is of the order of magnitude of the

[21] The original work refers to the case of single species solids, but the analysis is fruitful in a much wider class of systems.

inter-atomic distance, these states would be concentrated in a volume similar to that of the atomic states. It can be expected, then, that the convergence would be similar.

It is interesting to note that the authors checked this prediction on three case studies, involving Oxygen, Copper and Carbon atoms. The present work will be concerned with all three of these atomic species. The case of Copper is the most difficult application for a plane wave approach (see [Rappe et al., 1990], pag. 1228).

Since it can be expected that the formation of bonds does not worsen the convergence, it can be argued that improving the convergence in the isolated atom will consequently improve the convergence of the pseudo potential in all the chemical environments.

The RRKJ method consist in obtaining a kinetic energy convergence to a given level of tolerance with the smallest possible basis set. Requiring only kinetic energy convergence is an approximation justified because by scaling limits kinetic and total energy convergence are very similar[22]

Kinetic energy convergence is improved if the kinetic energy contribution due to the high Fourier components of the pseudo wave function is minimized. For a function $f(r)$, the kinetic energy content of the higher modes, $q > q_c$ is expressed by

$$-\int_0^{\infty} f^{\star}(r)\nabla^2 f(r) - \int_0^{q_c} q^2 \left|\tilde{f}(q)\right|^2 . \tag{3.7.4}$$

The first step is to choose a parameterization of the pseudowave function within the core region, $r < r_c$. As usual, the choice is free, the only requirements being that the atomic wave function be matched smoothly at

[22] If needed, this approximation could be dropped.

$r = r_c$.

The RRKJ pseudowave function is taken to be the sum of four Bessel function $j_l(qr)$,

$$F(r) = \sum_{i=1}^{4} \alpha_i j_l(q_i' r) \tag{3.7.5}$$

with the request that the logarithmic derivatives matches that of the all electron wave function at $r = r_c$.

The α_i are determined by imposing normalization and smoothness of F, F' and F'' at $r = r_c$. Four Bessel functions are needed to ensure that appropriate α_i always exist.

To improve the convergence, another function C (which stands for correction) is added to F, and the coefficients of C are varied until the kinetic energy content of the higher modes is minimized.

The definition of C is

$$C(r) = \sum_{i=1}^{N} \beta_i j_l(q_i r), \tag{3.7.6}$$

where the q_i are chosen so that the function have a node at r_c, $j_l(qr_c) = 0$, so that the function $F + C$ satisfies the same boundary conditions of F. The number N of Bessel functions in the correction and the coefficients β_i are chosen to minimize the kinetic energy content of the higher Fourier components.

The momentum cut off q_c in (3.7.4) is determined iteratively: given an initial cut off the amount of kinetic energy beyond it is minimized, then q_c is varied until the maximum tolerated kinetic energy is left in the modes higher than the cut-off.

From the final pseudo wave function $F + C$, the pseudopotential is extracted by the usual inversion of the radial equation, as in (3.7.3).

The resulting pseudowave functions do not differ much from the HSC ones, in real space, while the difference is larger in momentum space.

3.8 Ultra-Soft Pseudopotentials

Pseudopotentials which satisfy (3.6.2) are justly called *norm conserving*. However this condition can be relaxed while conserving the correct charge density necessary for self consistent *ab initio* computations[Vanderbilt, 1990]. This kind of pseudopotential is called *ultrasoft*.
The reason for this development is that the choice of the core radius r_c in the norm conserving techniques is constrained, as we have seen in section 3.7, and this means that the wave function continues, notwithstanding the pseudization procedure, to be concentrated in a small spatial region. Large plane wave cutoffs are then required, thus effectively limiting the capability of pseudopotentials to tackle many interesting cases. In particular, for many elements, such as those of the second row of the periodic table (most notably O, N, F) and for transition metals (with not completely filled 3d orbitals, such as Cu) the pseudopotential is strongly oscillating on a too short length scale, thus typically requiring a *'hard'* cut-off. Simulations of organic molecules with metallic centers prove to be a paradigmatic case where Norm Conserving pseudopotentials are at a loss.

Another interesting feature of ultrasoft pseudopotentials is the improved transferability inherent in the method.

The first steps to generate the pseudopotential are common to all other techniques, and involve solving the radial wave equation[23] at a certain defined

[23] Relativistic or not.

set of energies ϵ_i. This set is chosen to span the range of the occupied states, and the transferability of the pseudopotential can be improved by increasing the number of energies taken into account.

For definiteness, let the starting point be

$$[T + V_{AE}(r)]\,\psi_i = \epsilon_i \psi_i, \tag{3.8.1}$$

where i stands for $\{\epsilon_i lm \ldots\}$, *i.e.* all the quantum numbers needed to specify the state. V_{AE} is the All Electrons potential for the chosen reference configuration of the atom. $\psi_{\epsilon_i lm}$ is not determined self-consistently.
Although *a priori* the wave function is not normalizable we, following the usage of [Vanderbilt, 1990], introduce the ket notation and write

$$\begin{aligned} [T + V_{AE} - \epsilon_i]\,|\psi_i\rangle &= 0 \\ \langle\psi_i|\psi_i\rangle_R &= \iiint_{\rho \le R} \psi_i^\star \psi \rho^2 \sin\theta d\mathbf{r} hod\theta d\phi. \end{aligned} \tag{3.8.2}$$

Now three parameters are chosen:

1. Set r^{loc} such that V_{AE} is described by a smooth, local potential V_{loc} for all $r > r_{loc}$.

2. For every l, the pseudo wave function $|\phi_i\rangle$ will smoothly join the true all electron wave function $|\phi_i\rangle$ at $r = r_{cl}$.

3. Pick R, greater than both cutoffs, as a radius large enough that all pseudo and AE quantities agree for $r \ge R$.

Generate a pseudo wave function $|\phi_i\rangle$ corresponding to a set of energies and satisfying, besides the obvious smoothness conditions at r_{cl}, a *generalized norm conserving condition* (which will be shown to be not strictly necessary

in a later step):

$$Q_{ij} \equiv \langle\psi_i|\psi_j\rangle - \langle\phi_i|\phi_j\rangle = 0. \tag{3.8.3}$$

Now, for each $|\phi_i\rangle$, consider a wave function $|\chi_i\rangle$ which will be localized near to the core, and will play the role which, *e.g.* in the Phillips-Kleinman approach, was played by the $|\psi_c\rangle$ (see eq. (3.6.30)):

$$|\chi_i\rangle = (\epsilon_i - T - V_{loc})\,|\phi_i\rangle. \tag{3.8.4}$$

These wave functions are localized because beyond the *diagnostic* radius R, $V_{loc}(r) = V_{AE}(r)$ and $\phi_i = \psi_i$, so that (3.8.4) becomes effectively (3.8.1). Define the matrix B

$$B_{ij} = \langle\phi_i|\chi_j\rangle, \tag{3.8.5}$$

and the set of dual functions $|\beta_i\rangle$:

$$\begin{aligned} |\beta_i\rangle &= \sum_j (B^{-1})_{ji}|\chi_j\rangle \\ \langle\phi_k|\beta_i\rangle &= \sum_j {B^{-1}}_{ji}B_{kj} = \delta_{ki}. \end{aligned} \tag{3.8.6}$$

A non local pseudopotential can be defined by:

$$V_{NL} = \sum_{ij} B_{ij}|\beta_i\rangle\langle\beta_j|. \tag{3.8.7}$$

According to eqs. (3.8.5) and (3.8.7), the pseudo wave functions $|\phi_i\rangle$ will satisfy the equations

$$(T + V_{loc} + V_{NL} - \epsilon_i)\,|\phi_i\rangle = 0. \tag{3.8.8}$$

In fact, consider the action of V_{NL} on $|\phi_i\rangle$:

$$\begin{aligned} V_{NL}|\phi_i\rangle &= \sum_{kj} B_{kj}|\beta_k\rangle\langle\beta_j|\phi_i\rangle = \\ = \sum_{kj} B_{kj}|\beta_k\rangle\delta_{ji} &= \sum_{k} B_{ki}|\beta_k\rangle = \\ = \sum_{k} B_{ki} \sum_{l} {B^{-1}}_{lk}|\chi_l\rangle &= |\chi_i\rangle = \\ = (\epsilon_i - T - V_{loc})\,|\phi_i\rangle, & \end{aligned} \tag{3.8.9}$$

where the last line follows from the definition of $|\chi_i\rangle$, (3.8.4).

This proves (3.8.8), because

$$\begin{aligned} (T + V_{loc} + V_{NL} - \epsilon_i)\,|\phi_i\rangle &= \\ (T + V_{loc} - \epsilon_i)\,|\phi_i\rangle &+ (\epsilon_i - T - V_{loc})\,|\phi_i\rangle = 0. \end{aligned} \tag{3.8.10}$$

Now, it can be shown that the generalized condition of norm conservation, Q_{ij}, implies that the matrix B, and therefore the non local potential, is Hermitian[24] The demonstration is straightforward. Be $\frac{u_i(r)}{r}$ the radial wave function corresponding to $\phi_i(\mathbf{r})$:

$$B_{ij} = \int_0^R u_i^\star(r) \left(\epsilon_j + \frac{1}{2}\frac{d}{dr^2} - \frac{l(l+1)}{2r^2} - V_{loc}(r)\right) u_j(r) \tag{3.8.11}$$

$$B_{ji}^\star = \int_0^R u_j(r) \left(\epsilon_i + \frac{1}{2}\frac{d}{dr^2} - \frac{l(l+1)}{2r^2} - V_{loc}(r)\right) u_i^\star(r). \tag{3.8.12}$$

Integrating by parts and subtracting $B_{ji}^\star$ from B_{ij} one gets:

$$\begin{aligned} B_{ij} - B_{ji}^\star &= (\epsilon_j - \epsilon_i)\langle\phi_i|\phi_j\rangle_R + \\ &+ \frac{1}{2}\left(u_i^\star(R)u_j'(R) - u_i'^\star(R)u_j(R)\right). \end{aligned} \tag{3.8.13}$$

[24] In an historical perspective, note that the general AHS pseudopotential, (3.6.27), is not Hermitian.

This has reconstructed the first term of Q_{ij}. For the second term the manipulation is precisely identical with the radial wave functions v_i, v_j associated to $|\psi_i\rangle$ and $|\psi_j\rangle$ instead of u_i and u_j. In fact,

$$\int_0^R v_i^\star(r)\left(\epsilon_j + \frac{1}{2}\frac{d}{dr^2} - \frac{l(l+1)}{2r^2} - V_{AE}\right)v_j(r) = 0, \tag{3.8.14}$$

because v_j is the solution with eigenvalue ϵ_j.

Now, recall that by definition R is the radius where the true wave functions and their derivatives are matched by the pseudo wave functions and their derivatives. Thus we can subtract $\langle\psi_i|\psi_j\rangle_R$ from both sides of (3.8.13), obtaining

$$B_{ij} - B_{ji}^\star = (\epsilon_j - \epsilon_i)Q_{ij}, \tag{3.8.15}$$

which proves that, if $Q_{ij} = 0$, the matrix B is Hermitian.

Now it is evident that, by enlarging the set of $|\psi_i\rangle$ the pseudopotential will reproduce the scattering properties of the original potential over the energy range spanned by the wavefunctions, thus allowing to improve the accuracy and the transferability.

But the true improvement of the ultrasoft method[25] is that the condition Q_{ij} can be relaxed in a controlled manner.

With the following definitions

$$S = 1 + \sum_{ij} Q_{ij}|\beta_i\rangle\langle\beta_j| \tag{3.8.16}$$

$$V_{NL} = \sum_{ij} D_{ij}|\beta_i\rangle\langle\beta_j|, \tag{3.8.17}$$

where S is a *non local* overlap operator and $D_{ij} = B_{ij} + \epsilon_j Q_{ij}$.

[25] And the reason for the name.

The norm conservation condition becomes

$$\langle\phi_i|S|\phi_j\rangle_R = \langle\psi_i|\psi_j\rangle_R. \tag{3.8.18}$$

Now it is easy to prove that $|\phi_k\rangle$ satisfies a generalized eigenvalue problem:

$$(T + V_{loc} + V_{NL} - \epsilon_k S)\,|\phi_k\rangle = 0. \tag{3.8.19}$$

In fact, mirroring the demonstration of eq. (3.8.8), one has:

$$\begin{aligned} V_{NL}|\phi_k\rangle = \sum_{ij} D_{ij}|\beta_i\rangle\langle\beta_j|\phi_k\rangle \quad &= \\ = \sum_i D_{ik}|\beta_i\rangle = \sum_i (B_{ik} + \epsilon_k Q_{ik})\,|\beta_i\rangle \quad &= \\ = |\chi_k\rangle + \epsilon_k \sum_{ij} Q_{ik} B^{-1}_{ji}|\chi_j\rangle \quad &= \\ = (\epsilon_k - T - V_{loc})\,|\phi_k\rangle + \epsilon_k \sum_i Q_{ik}|\beta_i\rangle. \quad & \end{aligned} \tag{3.8.20}$$

Now compute

$$S|\phi_k\rangle = |\phi_k\rangle + \sum_{ij} Q_{ij}|\beta_i\rangle\langle\beta_j|\phi_k\rangle = |\phi_k\rangle + \sum_i Q_{ik}|\beta_i\rangle. \tag{3.8.21}$$

Replacing eqs. (3.8.20) and (3.8.21) in (3.8.19) the relation is proved.

Note that both Q and D are Hermitian operators (see eq. (3.8.15)).

Relaxation of norm conservation, $Q_{ij} \neq 0$, allows to choose a cutoff radius well beyond the outermost radial maximum[26], provided that the true and the pseudo wave function match their values, and those of their derivatives at the cutoff itself. The resulting pseudo wave function can thus be much smoother than the norm-conserving wave function, hence the name *ultrasoft*.

[26] see section 3.7 for a discussion of the cutoff to adopt

The whole procedure is similar to that of Phillips and Kleinman[27] but, as it was crucially required, this time it is possible to take into account the missing norm of the pseudo wave function, see eq. (3.8.18).
The orthonormality relations between the $|\phi_i\rangle$ are, consistently,

$$\langle\phi_k|S|\phi_i\rangle = \delta_{ki}, \tag{3.8.22}$$

and the valence charge density will be

$$n_v(\mathbf{r}) = \sum_{i,\mathbf{k}} |\phi_{n\mathbf{k}}(\mathbf{r})|^2 + \sum_{ij} \rho_{ij} Q_{ij}(\mathbf{r}), \tag{3.8.23}$$

where

$$\begin{aligned} \rho_{ij} &= \sum_{i,\mathbf{k}} \langle\beta_i|\phi_{i\mathbf{k}}\rangle\langle\phi_{i\mathbf{k}}|\beta_j\rangle \\ Q_{ij}(\mathbf{r}) &= \psi_i^\star(\mathbf{r})\psi_j(\mathbf{r}) - \phi_i^\star(\mathbf{r})\phi_j(\mathbf{r}). \end{aligned} \tag{3.8.24}$$

Note that $\int d^3r n_v(\mathbf{r}) = N$, the number of valence electron in the periodic cell.

3.9 Plane Waves

The choice of the complete set of functions for the expansion is free and different options offer different advantages and correspondingly present different problems. The most widely diffused options are plane waves, gaussian functions centered on atom positions, or wavelets. The rest of the discussion will focus on Plane Waves.

Plane waves' delocalization is both an advantage and a disadvantage.

[27] See section 3.6.5.

Valence electrons are not strongly localized around a particular atom, rather they have to be able to 'move around' to take part in bond formation. Correspondingly core electrons, which are instead sharply localized are not well described by a superposition of plane waves. Even by doing a *frozen core* approximation, which amounts to not considering the degrees of freedom associated with core electrons, the problem is not eliminated. In fact the wave functions of the valence electrons near to the core show rapid oscillations. This leads to the need for an extremely high cut-off.

The use of plane waves and of separable pseudopotentials, together with the FFT and iterative diagonalization or minimization techniques, allows a fast and efficient solution of the Kohn- Sham equations for systems containing up to hundreds of atoms in the unit cell.

A plane wave implementation is particularly transparent because no Pulay terms appear in the calculation of the energy derivatives.

3.9.1 Plane wave implementation

The most efficient and cost-effective, approach to implement the Car–Parrinello *ab initio* approach to molecular dynamics is to set up a Plane Wave calculation in a periodic system (thus typically imposing periodic boundary conditions on the unit cell), choosing a suitable Pseudopotential approach (norm conserving, RRKJ, ultrasoft or a mixture of these) and exploiting the currently routinely available hardware (Parallel Linux clusters) and software (open source Fast Fourier Transform Algorithms) facilities.

The implementation of the Car Parrinello and of the pseudopotential schemes adopted in the present work is that of the Quantum-ESPRESSO code [Baroni et al.], as described in [Giannozzi et al., 2004], which will be followed in the present section.

3.9.2 Equations of Motion

Car-Parrinello (CP) equations of motion descend from the CP Lagrangian,

$$L = \mu \sum_i d\mathbf{r} |\dot{\phi}_i|^2 + \frac{1}{2} \sum_i M_i \dot{\mathbf{R}}_I^2 - E_{\rm tot}(\{\phi_i\}, \{\mathbf{R_I}\}), \tag{3.9.1}$$

where ϕ_i are the KS orbitals, $\mathbf{R_I}$ are the coordinates of the I-th atom of mass M_I, $E_{\rm tot}$ is the total energy (comprising the pseudopotentials), μ is a fictious electron mass, whose value is chosen to ensure adiabatic separation between the electronic and the ionic degrees of freedom. The lower index i runs on all the explicitly present electron orbitals and the capital index I on all the atoms.

To derive the equations of motion, the following set of generalized constraints is imposed:

$$N_{ij} = \langle \phi_i | S | \phi_j \rangle - \delta_i j = 0, \tag{3.9.2}$$

where S is the identity operator in the norm conserving case, or the overlap operator in the ultrasoft case, see (3.8.22). Since in the present work the ultrasoft approach will be adopted, in the following S is always to be as defined in (3.8.16), here repeated for clarity:

$$S = 1 + \sum_{ij} Q_{ij} |\beta_i\rangle\langle\beta_j|. \tag{3.9.3}$$

With the introduction of the Lagrange multipliers Λ_{ij} to enforce the constraints, the Euler-Lagrange equations of motion are

$$\mu \ddot{\phi}_i = \frac{\delta E_{\rm tot}}{\delta \phi^\star} + \sum_j \Lambda_{ij} S \phi_j \tag{3.9.4}$$

$$M_I \ddot{\mathbf{R}}_I = -\frac{\partial E_{\rm tot}}{\partial \mathbf{R}_I} + \sum ij \Lambda_{ij} \langle \phi_i | \frac{\partial S}{\partial \mathbf{R}_I} | \phi_j \rangle. \tag{3.9.5}$$

It is always possible to rotate the matrix of the Lagrange multipliers into diagonal form $\Lambda_{ij} = \epsilon_i \delta_{ij}$ via a unitary transformation on the electronic orbitals.

Electron density depends on the atomic positions R_I through Q^I_{nm} and β^I_n.
Setting the quantities

$$\rho^I_{nm} = \sum_i \langle \phi_i | \beta^I_n \rangle \langle \beta^I_m | \phi_i \rangle, \tag{3.9.6}$$

$$\omega^I_{nm} = \sum_{ij} \Lambda_{ij} \langle \phi_j | \beta^I_n \rangle \langle \beta^I_m | \phi_i \rangle, \tag{3.9.7}$$

the explicit expression of the force $\mathbf{F}_I = M_I \ddot{\mathbf{R}}_I$ in (3.9.4) is

$$\begin{aligned} \mathbf{F}_I &= -\frac{\partial U}{\partial \mathbf{R}_I} - \int d\mathbf{r} \frac{\partial V^{\text{ion}}_{\text{loc}}}{\partial \mathbf{R}_I} n(\mathbf{r}) - \int d\mathbf{r} V_{\text{eff}} \sum_{nm} \frac{\partial Q^I_{nm}(\mathbf{r})}{\partial \mathbf{R}_I} \rho^I_{nm} \\ &- \sum_{nm} D^I_{nm} \frac{\rho^I_{nm}}{\partial \mathbf{R}_I} + \sum_{nm} q_{nm} \frac{\partial \omega^I_{nm}}{\partial \mathbf{R}_I}, \end{aligned} \tag{3.9.8}$$

where

$$q_{nm} = \int d\mathbf{r} Q_{nm} \tag{3.9.9}$$

are the integrated augmentation functions (see (3.8.16)),

$$V^{\text{ion}}_{\text{loc}} = \sum_I V^I_{\text{loc}}(|\mathbf{r} - \mathbf{R}_I|) \tag{3.9.10}$$

is the local part of the pseudopotential, given by a sum of atom-centered radial potentials,

$$V_{\text{eff}} = V^{\text{ion}}_{\text{loc}} + V_{\text{Hartree}} + \mu_{XC} \tag{3.9.11}$$

is a screened effective local potential and the coefficients D^I_{nm} are the screened

counterpart of the D coefficients introduced in (3.8.16),

$$D^I_{nm} = D_n m + \int d\mathbf{r} V_{\rm eff} Q^I_{nm}. \tag{3.9.12}$$

The equations of motion are discretized using the Verlet (or velocity-Verlet) algorithms (see [Frenkel and Smit, 1996], chapter 4, for a clear review).

The common rationale of these algorithms is to make a truncated (and thus discretized) Taylor expansion of the particle coordinates and velocities in terms of the coordinates, velocities and forces at earlier times. It is crucial that the resulting discrete transformation $(\{\phi_i\}, \{\mathbf{R}_I\})(t) \rightarrow (\{\phi_i\}, \{\mathbf{R}_I\})(t+\Delta t)$ is canonical[28] to ensure energy conservation.

Define a fictious-electronic-mass operator, whose matrix elements between two plane waves with momenta G and G' are

$$\Theta_{G,G'} = \max(\mu, \mu\frac{G^2}{E_c})\delta_{G,G'}, \tag{3.9.13}$$

where E_c is a cutoff of a few Ry which defines the threshold for the Fourier acceleration scheme, [Tassone et al., 1994], and determines the threshold above which the states are dominated by the kinetic energy.

[28] That is, it preserves the volume in the phase space.

In the present case, the Verlet algorithm is implemented as follows:

$$\begin{aligned}\phi_i(t+\Delta t) &= 2\phi_i(t) - \phi_i(t-\Delta t) - (\Delta t)^2\Theta^{-1}\left[\frac{\delta E_{\rm tot}}{\delta\phi_i^\star} - \right.\\ &- \left.\sum_j \Lambda_{ij}(t+\Delta t)S(t)\phi_j(t)\right] \qquad (3.9.14)\\ \mathbf{R}_I(t+\Delta t) &= 2\mathbf{R}_I(t) - \mathbf{R}_I(t-\Delta t) - \frac{\Delta t^2}{M_I}\left[\frac{\partial E_{\rm tot}}{\partial \mathbf{R}_I} - \right.\\ &- \left.\sum_{ij}\Lambda_{ij}(t+\Delta t)\langle\phi_i(t)|\frac{\partial S(t)}{\partial \mathbf{R}_I}|\phi_j(t)\rangle\right], \qquad (3.9.15)\end{aligned}$$

where Δt is the time step and $S(t)$ is the overlap operator evaluated at time t.

The orthonormality constraints are imposed at each time step,

$$\langle\phi_i(t+\Delta t)|S(t+\Delta t)|\phi_j(t+\Delta t)\rangle = \delta_{ij}. \qquad (3.9.16)$$

Set

$$\bar{\phi}_i = 2\phi_i(t) - \phi_i(t-\Delta t) - (\delta T)^2\Theta^{-1}\frac{\delta E_{\rm tot}}{\delta\phi_i^\star},$$

and define the matrices:

$$\begin{aligned}A_{ij} &= \langle\bar{\phi}_i|S(t+\Delta T)|p\bar{h}i_j\rangle,\\ B_{ij} &= \langle\Theta^{-1}S(t)\phi_i(t)|S(t+\Delta T)|p\bar{h}i_j\rangle,\\ C_{ij} &= \langle\Theta^{-1}S(t)\phi_i(t)|S(t+\Delta T)|\Theta^{-1}S(t)\phi_j(t)\rangle. \qquad (3.9.17)\\ & \qquad (3.9.18)\end{aligned}$$

With these definitions, eq. (3.9.16) can be transformed in the following matrix equation:

$$A + \lambda B + B^\dagger\lambda^\dagger + \lambda C\lambda^\dagger = 1, \qquad (3.9.19)$$

where the matrix λ is related to the matrix of the Lagrangian multipliers Λ via

$$\lambda = \Delta t^2 \Lambda^\star(t + \Delta t). \tag{3.9.20}$$

Note that λ is self-adjoint.

The solution of (3.9.19) is slightly complicated by the fact that (3.9.15) depends on $\mathbf{R}_I(t + \Delta t)$ via $\Lambda_{ij}(t + \Delta t)$. Thus the expression for $R_I(t + \Delta t)$ is not closed and iteration is required. In most practical applications the extrapolation of $\Lambda(t + \Delta t)$ from the values at t and $t - \Delta t$ converges very quickly, at the very first iteration.

The solution of (3.9.19) is obtained iteratively.

3.9.3 Algorithm implementation

The main idea of the algorithm, as presented in [Giannozzi et al., 2004], is to switch between the real and the reciprocal space, using the FFT, in order to perform every computation in the most advantageous space. This approach is called *dual space* technique.

In detail, let $\{\mathbf{R}\}$ be the vectors of the periodically repeated cell. The corresponding reciprocal lattice vectors $\{\mathbf{G}\}$ satisfy the relationship $\mathbf{R}_i \cdot \mathbf{G}_j = 2\pi n$, with n integer.

The KS orbitals can be expanded in a plane wave basis up to a kinetic energy cutoff E_c^{wf}:

$$\phi_{i,\mathbf{k}}(\mathbf{r}) = \frac{1}{\sqrt{\Omega}} \sum_G \phi_{i,\mathbf{k}}(\mathbf{G}) e^{-i(\mathbf{k}+\mathbf{G})\cdot\mathbf{r}}, \tag{3.9.21}$$

where Ω is the volume of the cell. The sum is extended over the $\mathbf{G}$ vectors which belong to the set G_c^{wf} defined[29] by all the vectors which satisfy the

[29] The index *wf* stands for wave function.

condition

$$\frac{|\mathbf{k}+\mathbf{G}|^2}{2} \leq E_c^{wf}. \tag{3.9.22}$$

The vector $\mathbf{k}$ is the Bloch vector of the electronic state[30].

According to the *dual space* technique, scalar products of the form $\langle\phi_i|\beta_n^I\rangle$ are evaluated in $\mathbf{G}$ space, giving:

$$\langle\phi_i|\beta_n^I\rangle = \sum_{\mathbf{G}} \phi_i^\star(\mathbf{G})\beta_n(\mathbf{G})e^{-i\mathbf{G}\cdot\mathbf{R}_l} \tag{3.9.23}$$

$$\langle\phi_i|\frac{\partial\beta_n^I}{\partial\mathbf{R}_l}\rangle = -i\sum_{G} \mathbf{G}\phi_i^\star(\mathbf{G})\beta_n(\mathbf{G})e^{-i\mathbf{G}\cdot\mathbf{R}_l}, \tag{3.9.24}$$

where the sums span G_c^{wf}.

Analogously,

$$-\nabla^2\phi_i(\mathbf{G}) = G^2\phi_i(\mathbf{G}). \tag{3.9.25}$$

By the same token, $(\nabla n)(\mathbf{G}) = -i\mathbf{G}n(\mathbf{G})$ and consequently both the exchange correlation functional, $\mu_{xc}(\mathbf{r}) = \mu_{xc}(n(\mathbf{r}), \nabla(\mathbf{r}))$, and the Hartree potential, $V_H(\mathbf{G}) \sim n(\mathbf{G})^\star/G^2$, are conveniently calculated in $\mathbf{G}$ space.

The kinetic and nonlocal Pseudopotential terms in the Hamiltonian are computed in $\mathbf{G}$ *space.*

For the same reasons, the local terms are more easily computed in real space, where the effective potential contribution $V_{\text{eff}}\phi_i(\mathbf{r})$ is diagonal. Having computed it, a Fourier transformation transforms it in a reciprocal space quantity.

FFT is set up by discretizing the $\mathbf{r}$ space cell with a uniform grid.

[30] If the simulation cell is large enough, a condition always satisfied in the case of molecules and liquids, the Brillouin zone can be sampled using only the $\mathbf{k}$= 0 ($\mathbf{G}amma$) point.

A function f of $\mathbf{r}$ becomes:

$$f(\mathbf{r}) \to f(m_1, m_2, m_3) \equiv f(\frac{m_1}{N_1}\vec{a_1}, \frac{m_2}{N_2}\vec{a_2}, \frac{m_3}{N_3}\vec{a_3}), \tag{3.9.26}$$

where $\vec{a_i}$ are the lattice basis vectors and the indexes m_i run from 0 to $N_i - 1$. The FFT maps a discrete periodic function in real space into a discrete periodic function in reciprocal space:

$$f(m_1, m_2, m_3) \to \tilde{f}(n_1, n_2, n_3), \tag{3.9.27}$$

where the n_i are the appropriate coefficients in the basis $\{\vec{b_i}\}$ of the reciprocal lattice. The n_i are ≥ 0, which can be enforced by a suitable shifting of multiple integers of the N_i if needed.
The FFT dimensions N_1, N_2, N_3 must be large enough to include all the non-negligible Fourier components of the functions to be transformed: ideally all the Fourier components corresponding to momenta higher than $N_i/2$ should vanish. The set of indices n_i spans the so-called *FFT grid*.

Since the soft part[31] of the charge density $n_{\text{soft}}(\mathbf{r}) = \sum_j |\phi_j|^2$ can be expressed as

$$n_{\text{soft}}(\mathbf{G}) = \sum_{\mathbf{G}' \in G_c^{wf}} \sum_j \phi^\star(\mathbf{G} - \mathbf{G}')\phi(\mathbf{G}'), \tag{3.9.28}$$

the cutoff for n_{soft} must be $E_c^{soft} = 4E_c^{wf}$, since the maximum momentum will be the double of the maximum momentum in ϕ and the dependence of the cutoff on the momenta is quadratic (see (3.9.22)).
The set of vectors satisfying $G^2/2$ will be denoted by G_c^{soft}.

[31] In the case of Norm Conserving pseudopotential, this is the complete contribution to the charge density.

In the case of Ultra Soft PP, the expression for the density is

$$n(\mathbf{G}) = n_{\text{soft}} + \sum_{i,n,m,I} Q^I_{mn}(\mathbf{G})\langle\phi_i|\beta^I_n\rangle\langle\beta^I_m|\phi_i\rangle. \tag{3.9.29}$$

The augmentation term requires a higher cutoff than E_c^{soft}, and a denser set of $\mathbf{G}$ vectors. Be $\mathbf{G}_c^{dens}$ the set of vectors needed to expand the augmentation part, up to a cutoff E_c^{dens} which is of the order of two to three times E_c^{soft}.

It is inconvenient to use a FFT grid with such a dense cutoff, since this would greatly increase the computational burden. A natural solution is to introduce two different FFT grids:

1. a coarser grid (in $\mathbf{r}$ space) for the KS orbitals and the soft part of the charge density. The grid dimensions N_1, N_2, N_3 are large enough for the cutoff E_c^{soft};

2. a denser grid (in åspace, too) for the total charge density and consequently for the exchange-correlation and the Hartree terms. The dimensions of the grid are $M_i \geq N_i$, large enough for the cutoff E_c^{dens}.

The different physical quantities, requiring different cutoffs, are then transformed back and forth from the real space to the suitable reciprocal lattice. For each time step only a few dense-grid FFT are performed, while the number of necessary coarse-grid FFT is much larger, proportional to the number of KS states. This is the so-called *dual grid* approach.

It is possible to further improve the performance of the algorithm by considering the strong spatial localization of the augmentation functions Q_{nm}. An *augmentation box* is centered at the point of the dense grid which is closer to the position $\mathbf{R}_I$ of any atom I described by an US PP. The box will thus

follow the atom during its time evolution.

The box must be large enough to completely contain the augmentation charge, but in any case its volume is a small fraction of that of the unit cell, containing only a small portion of the dense grid in real space.

The advantage of such a reduction is that the number of **G**vectors required to reach the desired cutoff in the augmentation box is smaller by a factor equal to the ratio of the volumes of the augmentation box and of the unit cell.

3.9.4 Parallel implementation

An efficient strategy for the parallelization of PW computations is to distribute the FFT grid points in real and reciprocal space across the processors. The FFT algorithm must be capable of performing three-dimensional FFT on data shared across different processors with good load balancing. The FFT algorithm adopted in the present work is the FFTW [Frigo and Johnson, 2005].

The real space FFT grid is subdivided in a number of slices equal to the number of processors, cut along planes orthogonal to user-defined crystallographic direction, labeled by 1, 2, 3. Let 3 be the chosen direction, with N_3 planes, and let N_p be the number of processors.

The number of planes for each processor will then be N_3/N_p, and the p-th processor will contain planes with m_3 values such that

$$(p-1)\frac{N_3}{N_p} \leq m_3 < p\frac{N_3}{N_p}.$$

It is apparent that the best load balancing is obtained when N_p is a divisor of N_3. The algorithm is ill-posed if the number of processors exceeds the number of planes N_3.

Chapter 4

Systems and Computational Details

4.1 Introduction

This chapter contains the description of the protocol developed for the simulation of small biological systems, focusing in particular on the octarepeat. The rationale behind the choices made and a discussion of the possible alternatives and improvements are presented.

This is required because in the field of numerical simulations it is not possible to adopt a solution *once and for all*: any case has its own peculiarities which require specific solutions.

A simulation protocol is by its very nature a work in progress, continuously undergoing a refinement and revision process.
For these reasons, a detailed explanation of the ideas tested, both rejected and accepted, can be useful as a reference point for further simulations.

The outline of the chapter is the following: Section 4.2 contains a description of the systems studied;

section 4.3 contains the description of the protocol, that will be analysed and discussed in section 4.4 together with its possible improvements.

4.2 Technical description of the systems

The number of atoms and electrons of the whole octarepeat sequence is too large for a Car–Parrinello simulation, even in the absence of the solvent. Furthermore, there are no clear available crystallographic data for the complete octarepeat, but only for its subset, the oligopeptide HGGGW. Moreover, as it has been discussed in Chapter 2, there are growing evidences that this is the region actually involved in copper coordination, and so the natural choice of not including the remaining three amino acids has been made.

For every system under study, Car–Parrinello MD simulations have been carried out with the Quantum-ESPRESSO package [Baroni et al.]. We have used Vanderbilt's ultrasoft pseudopotentials [Vanderbilt, 1990] and the PBE exchange-correlation functional, because they appeared to offer the best compromise between computational efficiency and number of free parameters, particularly in the presence of Cu ions. Periodic boundary conditions have been imposed on the super-cell, with a minimum separation of 5 and 8 Å between replica, for uncharged and charged systems, respectively. The energy cutoff was of 25 Ry, while the hard cutoff for the augmented charge density was of 250 Ry. We have conducted spin restricted simulations of all the systems described in the following chapter, while spin unrestricted simulation have been performed, as a check, on

- the monomer Cu(HGGG), with S=1/2,
- the dimer $[Cu(HGGG)]_2$, with S=1.

In all the systems we have studied the peptides are neutralized at the C-

and N-termini in the standard way by adding the CH_3-NH- and CH_3-CO- groups, respectively.

4.3 Description of the protocol

The general protocol developed for the simulations consisted of the following sequential steps:

1. Choice of the initial configuration: atomic positions and total charge of the system.

2. Electronic energy minimization with fixed atomic positions.

3. Total energy minimization as a function of both atomic and electronic degrees of freedom, in order to attain the equilibrium geometry of the full system.

4. Two preliminary sequential molecular dynamics simulations of 0.25 ps each at atomic temperatures of 100 and 200 K, with a single Nosé-Hoover thermostat [Nosé, 1984] coupled to the atomic degrees of freedom.

5. A final CPMD simulation of about 2 ps at atomic temperature of 300 K, using the same thermostat as in step 4 above.

4.4 Analysis of the protocol

The initial configuration, step 1,must be chosen in accordance with the hypotheses that one wants to test. For example a typical question could be to determine the coordination sphere of a relevant atom (in the case of the

octarepeat, the focus is on the Cu^{2+} ion). Since the trajectory will be observed only for a short physical time, the choice of the starting configuration can introduce a bias which must be kept into account, and whose influence must be reduced as much as possible.

The most natural choice is usually that of using the crystallographic data, if they exist and are accurate enough. This ensures, at least, that the starting configuration is physically acceptable.

But it can happen that the experimental data are not complete or unclear, and not sufficient to determine the validity of a given set of hypotheses. This is a direct consequence of the fact that crystallographic data are obtained in conditions very far from the physiological ones. On the other hand spectroscopical techniques which do not require such strong deviations from the physiological conditions (e.g. NMR) do not usually give data detailed enough.

These are the cases where the need for a numerical simulation is most needed, in fact if the data were already so complete that we already knew everything about the system, the simulation would only constitute an exercise. In practice, experience shows that real world systems are so complex that experimental data are never so complete to render simulations useless: they can at least provide some insight on the systems' behaviour[1].

In some of the simulations, classical random walks where used to generate initial configurations, according to the strategy of [La Penna et al., 2004].

The starting point of this Monte Carlo approach have been the classical models of the the $(PHGGGWGQ)_4$ chain constructed employing the Amber force-field [AMBER]. Each one of the Nδ1 atoms of the His in the first

[1] A striking example of this is given by the enormous amount of studies devoted to liquid water, whose chemical composition is deceptively simple and surely simpler than that of a protein.

and second repeat was bonded to a Cu ion with a spring and the two Gly residues next to these two His residues were deprotonated. A charge equal to -1 was added to each of the two N atoms of the Gly residues. The charge of the Cu^{+2} ion was partially spread on each of the bonded His. This was accomplished by removing the Hδ1 atom from the protonated His in the Amber force-field. The Hδ1 atom was replaced by Cu and one extra unit of charge was added to the Cu atom. The resulting His residue including Cu has a net charge +2, while Cu has a partial charge +1.4. The N amide atoms of Gly^{-} were not explicitly bonded with springs to Cu, but Cu and N(Gly^{-}) remained close to each other because of the strong electrostatic interactions. The van der Waals radius of Cu was chosen to be as large as 1.71 Å in order to prevent Cu and amide deprotonated N to get too close to each other. The approximated form of the force-field just described to model the Cu environment has the only purpose of constructing reasonable initial configurations for *ab initio* molecular dynamics.

The starting point for generating random (Monte Carlo) trajectories was the all-*trans* configuration of the ϕ and ψ backbone dihedral angles. A Monte Carlo trajectory was generated by suggesting new configurations through random assignments of ϕ and ψ dihedral angles and then accepting or rejecting the proposed moves according to the Metropolis test. The temperature in the Metropolis test was randomly chosen in the range 0-10000 K. Only the Pro residues were kept fixed in the $\phi = 0/\psi = \pi$ configuration. Using this procedure a random walk through reasonable configurations is obtained, thus avoiding sampling configurations with a much too high energy [La Penna et al., 2004].

During the random walk the distance between Cu and N(Gly^{-}) was rarely larger than the contact distance because of the strong electrostatic attraction

between the two charged atoms. Viceversa, the carbonyl oxygen was often found far from the closest Cu ion. Among the large set of configurations that were obtained, one with large Cu-O(Gly^-) distance was chosen as the initial configuration for the successive CPMD simulation, in order to be able to study in detail the dynamics of such a distance.

Starting from the random classical trajectory of the $(PHGGGWGQ)_4$ chain, one initial configuration for the $Cu(HG^-G^-G)$ system was obtained by cutting out from the whole chain all the atoms of the P, W, G, Q residues except for those belonging to the HGGG sequence and appropriately adjusting the N- and C-termini, with neutralizing caps.

Similarly, one configuration with Cu-Cu distance of 4.37 Å was chosen as the starting point for the CPMD simulation of the $[Cu(HG^-G^-G)]_2$ system.

Step 2 is needed to find the electronic ground state for the initial atomic configuration, a necessary condition for the applicability of the DFT approach.

Step 3 consists in an energy minimization procedure, carried out with a Steepest Descent algorithm, and is needed to reduce eventual repulsions between the atoms which could break the molecule.

Step 4 (thermalization) is necessary to slowly approach room temperature, avoiding that temperature oscillations affect in an uncontrolled way the features of the electronic ground state. In a few cases, $Cu(HG^-G^-GW)+H_2O$ and Cu(HGGG) in water, the simulations were performed at T =150 and 50 K, respectively, only. This was enough to relax the systems to the nearest local energy minimum. The velocity-Verlet algorithm [Frenkel and Smit, 1996] for integrating the equation of motion was used with a time step of 0.12 fs. The calculations were performed on Linux clusters using 8-16 processors, depending on the size of the molecular system.

Step 5 is actually indistinguishable from Step 4, if not for the fact that it is carried at room temperature.

Ab initio molecular dynamics simulations of the Car-Parrinello type are computationally extremely demanding, both in terms of CPU time and memory.

As a benchmark, the time required for a 0.12 fs step for the system Cu[$HG^{-}G^{-}G$] +41 H_2O was of 25 s on a Linux-cluster with 16 Intel/Xeon 2.8 GHz CPUs.

As a matter of fact, experience shows that solvated systems are two times more expensive than the same systems in the absence of solvent. Moreover, the box size is a very important variable, which is to be expected since as the box side increases, so does the number of plane waves required to expand the wave functions.

Among the ways to reduce the bias due to the choice of the starting configuration, which is the aim of step 3, it is possible to adopt a preliminary classical Molecular Dynamics simulation. While being not *ab initio* , it could effectively reduce the risk of having chosen a physically improbable configuration.

With regard to minimization, it has been found and applied in the more recent simulations that the adoption of a damped ionic dynamics is particularly successfull and therefore recommended. The latest implementation of the protocol involves at least 2000 steps of damped molecular dynamics after each of the thermalizations at intermediate temperatures, step 4.

The algorithm of the Steepest Descent is not necessarily the fastest choice to achieve energy minimization. A natural candidate would be the Conjugate Gradient. Unfortunately, at the present time the ESPRESSO package didn't allow for its use, and since the Steepest Descent velocity of convergence was

acceptable ($O(10^3)$ steps, which usually amounted to $O(10)$ hours or less), this has not been worked upon.

Chapter 5

Results

5.1 Introduction

This chapter contains the detailed description and analysis of all the structures studied. The protocol applied has been discussed in chapter 4.

In the following, the amino acids are denoted by their place in the sequence starting from the His: that is, considering the sequence HGGGW, we have His_1, Gly_2, Gly_3, Gly_4, Trp_5.
The equatorial coordination found in the crystal ([Burns et al., 2002] and see chapter 2), of the 3N1Otype, is with the Nitrogen ϵ of His_1, the deprotonated amide Nitrogens of the Gly_2 and Gly_3, the amide carbonyl Oxygen of Gly_3. The axially bound water molecule, instead, is kept in position by a hydrogen bond to the Hε1 of the Trp_5 indole ring.

5.2 Simulations of the penta-peptide HGGGW

In this section are presented the results of the simulations on the complex Cu[HGGGW], both in vacuum and in a box of 64 water molecules.

5.2.1 Cu(HG$^-$G$^-$GW)(wat)

This system allows the study of the relevance of the presence of the Trp residue and a single water molecule for the nature of the Cu coordination in the crystallographic Cu(HG$^-$G$^-$GW)(wat) complex [Burns et al., 2002].

The trajectory at 150 K for this complex with initially a water molecule present in the fifth site of the square pyramidal coordination of Cu, shows that water does not remain axially bonded to Cu. The Cu-O(wat) distance becomes larger than 5.46 Å right after thermalization at 300 K is attained(data not shown). In fact, while the Cu(3N 1O) planar coordination is maintained throughout the whole trajectory, the hydrogen bonded water (Nϵ1(Trp)$-$Hϵ1(Trp)$\cdots$O(wat)) does not remain close to Cu. In Fig. 5.1A the configuration of the system after 0.3 ps of CPMD simulation at 300 K, is displayed which shows that the Cu-O(wat) and Hϵ1(Trp)-O(wat) distances are 7.77 Å and 4.02 Å, respectively.

The history of the system indicates that the hydrogen-bonded water follows the Trp side chain in its wandering around, displaying no propensity for a chemical axial Cu-O(wat) bond, in broad consistence with previous DFT calculations accounting for the presence of both axial water and Trp [Franzini et al., 2003].

The presence of water in the fifth coordination site seen in the crystal structure, can be partially ascribed to crystal packing. Indeed, the simulation of the Cu(HG$^-$G$^-$GW)(wat) system in the cell mimicking the isolated system was compared with the simulation in the triclinic crystal unit cell. The latter simulation shows that the Cu-O(wat) distance increases more slowly than in the former case. Again, at T =150 K, even if Trp is constrained by the packing forces, the water molecule moves away from Cu: after 0.85 ps the Cu-O(wat) distance is 3.80 Å and the distance Hϵ1(Trp)-O(wat) is 2.13 Å

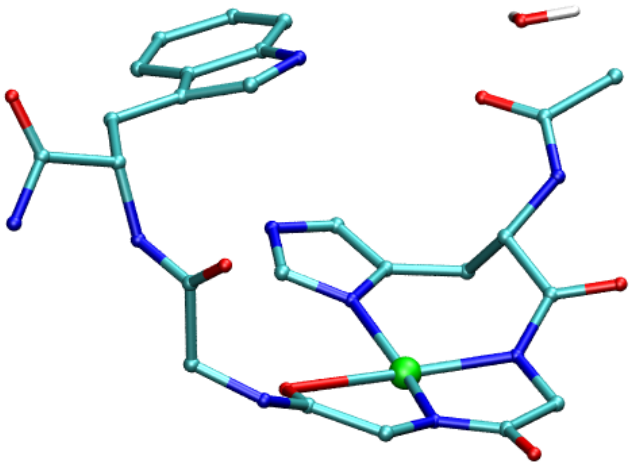

(A)

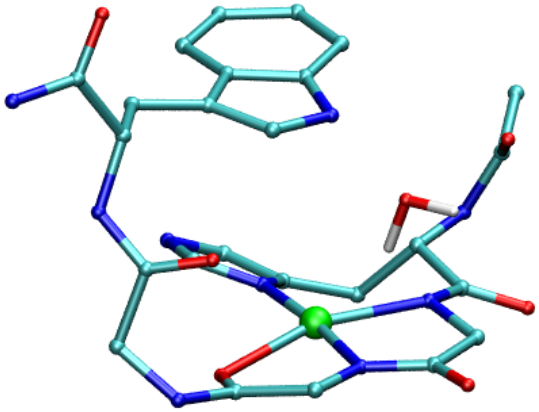

(B)

Figure 5.1: Structure of Cu(HG$^-$G$^-$GW)(wat) in the orthorhombic cell with $a = 15.1$ Å, $b = 17.3$ Å, $c = 15.8$ Å, at T =150 K, at time $t = 0.3$ ps (panel A) and in the triclinic cell with $a = 8.4$ Å, $b = 9.0$ Å, $c = 10.3$ Å, $\alpha = 82.8°$, $\beta = 79.7°$, $\gamma = 62.3°$, at $t = 0.85$ ps (panel B). Hydrogen atoms are not displayed, except for the water molecule.

(see figure 5.1B). This shows that the hydrogen-bond between water and Trp, even in the presence of positional constraints imposed on Trp by the crystal packing forces, are not sufficient to keep the water molecule at a bonding distance from Cu.

5.2.2 Cu(HG$^-$G$^-$GW)(wat) +64(H_2O)

The nature of the chemical bond between Cu and a water molecule as well as the docking of a water molecule through a hydrogen bond network in the axial position, can be of a dynamical nature: the Cu-bonded water molecule can exchange with water molecules in the bulk solvent. In order to investigate this possibility, the simulation of the Cu(HG$^-$G$^-$W)(wat) crystallographic complex in a box of 64 water molecules was performed at T =300 K for 1.2 ps. The simulation cell was taken orthorhombic with dimensions 13.6 × 15.5 × 15.6 Å.

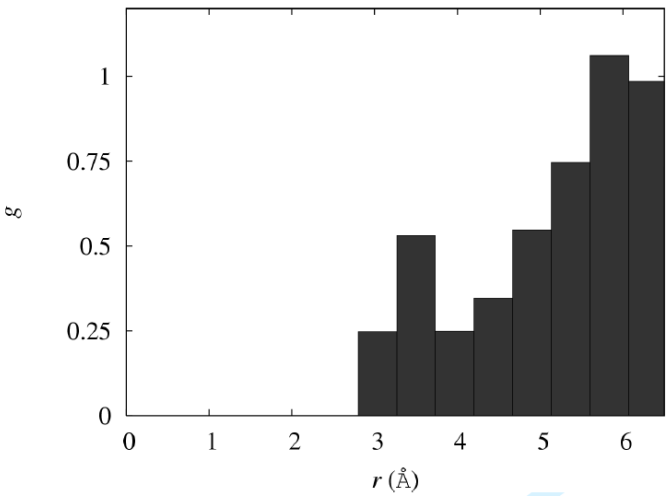

Figure 5.2: Radial distribution function, $g(r)$, for the distance between Cu and any water molecule in the solvated (64 water molecules) Cu(HG$^-$G$^-$GW)(wat) complex.

The radial distribution function of the distance between Cu and water

molecules of the system, $g(r)$, computed from the simulated trajectory, is displayed in Fig. 5.2. The vanishing of the density below 3 Å confirms the weakness of the interaction between Cu and water. The computed radial distribution function is at most compatible with a hydrogen bond between Cu and water. It is, in fact, very similar to the radial distribution function of the distance between Hϵ1(Trp) and water molecules (data not shown). As in the simulation in vacuum, the trajectory of the solvated system shows a slight expansion of the solute, with Nϵ1(Trp) moving from 4.2 Å in the crystal structure to about 5.5 Å at the end of the simulation. The Hϵ1(Trp) atom always remains hydrogen bonded to a water molecule. The square planar coordination of Cu is stable within our 1 ps simulation, with a weak Cu-O(Gly) bond, as in the simulation in vacuum.

5.3 Simulations of the tetra-peptide HGGG

5.3.1 The Cu(HG$^-$G$^-$G) monomer

Since the simulations of the Cu(HG$^-$G$^-$GW)(wat) system have shown that both the Trp residue and the axial water molecule are not involved in the Cu binding, the simplified model Cu(HG$^-$G$^-$G) has been chosen for the subsequent calculations. The same neutralizing groups used for the previous simulations have been applied at the N- and C- termini of the peptide ligand as described in 4.2.

The analysis of the time evolution of two different initial structures of the complex Cu(HG$^-$G$^-$G) at 300 K, clearly shows the stability of the Cu(3N 1O) coordination, although the Cu-O(Gly$_3$) bond, with O belonging to the carbonyl group, appears to be weaker.

In Fig. 5.3, the time history of various Cu-bond distances (panels A-D)

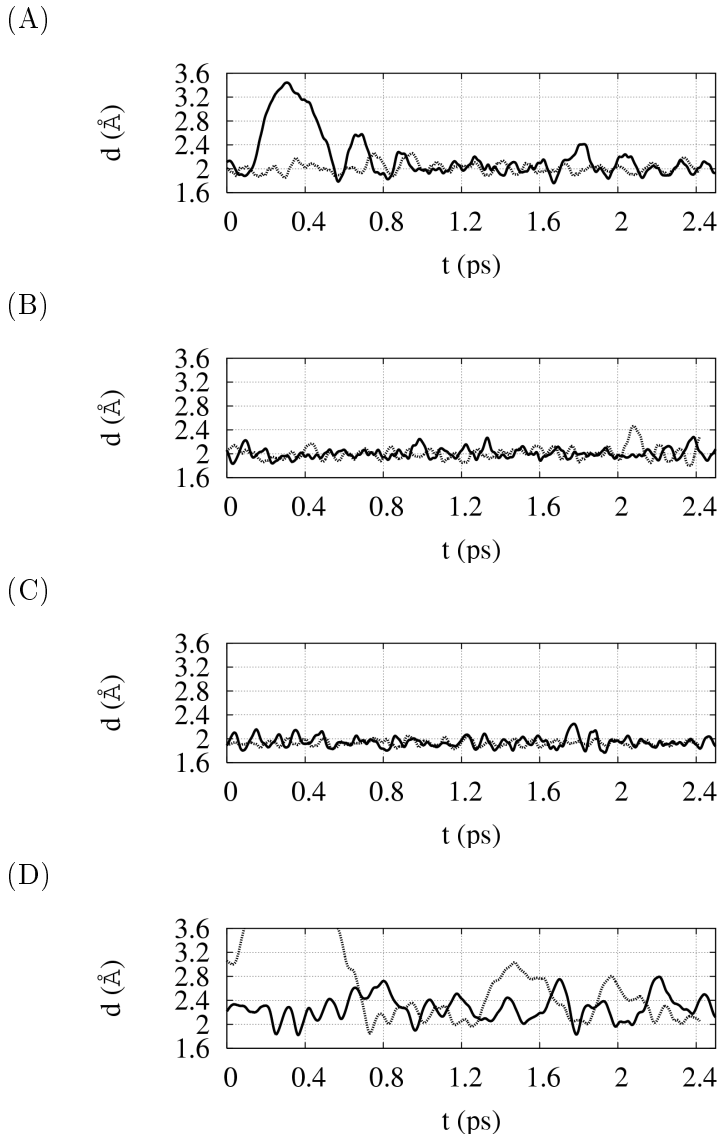

Figure 5.3: Time evolution at T =300 K of distances between Cu and ligand atoms. The trajectory started from the X-ray structure (solid line) and from one of the structures obtained through random walk generation (dotted line). Distances Nδ1(His$_1$)-Cu (panel A), N(Gly$_2$)-Cu (panel B), N(Gly$_3$)-Cu (panel C) and O(Gly$_3$)-Cu (panel D) are shown.

are reported for simulations with two different initial configurations. A first one was taken from crystallography (solid line) and a second one (dotted line) from the random set of configurations, generated according to the strategy described in Sec. 4.4. It is important to remark that the plotted data do not depend on the structural details of the initial configuration. The relative strength of the amide N-Cu bonds (panels B and C), compared to the Nδ1(His)-Cu bond (panel A), can be estimated by classically interpreting the frequencies and amplitudes of the corresponding distance oscillations. Data points show that the amide N-Cu bond oscillates with a frequency higher than that of the Nδ1-Cu bond distance, bringing us to the conclusion that the first bond is stronger than the second one. Some initial dissociation of the Nδ1-Cu (panel A, solid line) is possibly due to a distortion of the initial structure which soon relaxes.

The weakness of the Cu-O(Gly_3) bond (panel D) is clearly displayed by the wide oscillations that the distance of the latter undergoes in both trajectories. In the second trajectory (dotted line) the Cu-O(Gly_3) bond, which was not present initially, is formed after 0.7 ps. The behaviour of this bond is influenced by the mobility of the C-terminal tail of the peptide, while the N-terminal tail is kept fixed by the strong Cu-N bonds present in this region.

The relative weakness of the Cu-O(Gly_3) bond was already reported in works where the structure of the Cu(HG^-G^-GW) [Franzini et al., 2003] and Cu(HG^-G^-G) [Pushie and Rauk, 2003] complexes were determined by DFT optimization. In both DFT studies it is found that the Cu(3N) coordination is always maintained, while the carbonyl O of Gly_3 is replaced by water in the coordination sphere.

The mobility of the C-terminal portion of the HGGG peptide is moni-

tored through a number of dihedral angles. It is found that the ϕ backbone dihedral angle undergoes a *trans* to *cis* transition during the simulation that started from the crystallographic structure. It is this transition which is associated with the breaking of the Cu-O(Gly_3) bond. At 300 K the bonding energy is, in fact, of the order of magnitude of thermal fluctuations. Thus the amplitude of thermal motions of the ligand chain is sufficiently large to break the Cu-O(Gly_3) bond. One should observe that these motions are more restricted in the full octarepeat and in cases where the peptide chain is more structured. Therefore, the Cu-O(Gly) bond is expected to be more stable when the peptide chain is less mobile.

Although a stronger Cu-N bond compared to the Cu-O bond is to be expected, not much is known about the relative strength of the amide Cu-N bond with respect to that of the Cu-Nδ1(His) bond.

It is known [Sigel and Martin, 1981] that, as soon as a five-membered chelate ring is formed, the Cu^{+2} ion is capable of replacing the amide proton of Gly at neutral pH and deprotonation of the Gly amide N group occurs (see also 2.3.2). In the case at hand, the available crystal structure of Cu(HGGG) indicates that there are two such rings involving the Cu atom (see Fig. 5.1B). Thus, simulations of the Cu(HGGG) system with protonated amide N of Gly_2 and Gly_3 and in the presence of 41 explicit water molecules have been performed, in order to measure the propensity of the Gly amide groups to exchange protons with surrounding water molecules when the amide group interacts with Cu.

In Fig. 5.4 the time evolution of the H-N distance in Gly_3 measured at T =50 K in solvated Cu(HGGG) is displayed. The total energy (dashed line in fig. 5.4) clearly decreases at about 0.9 ps, displaying the formation of a bond between H(Gly_3) and O(wat). The displacement of the Hydrogen from

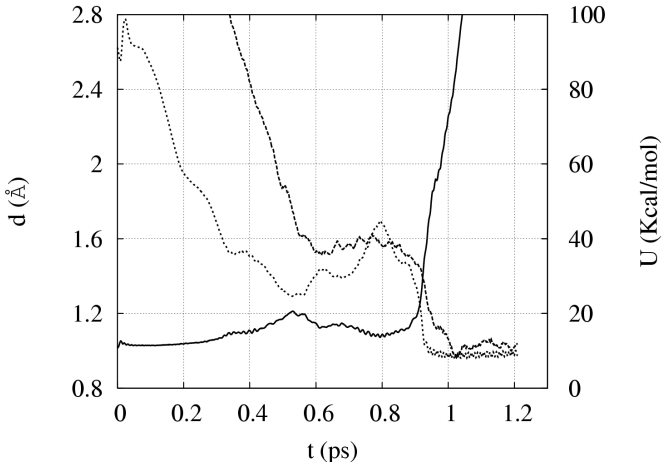

Figure 5.4: Time evolution of H(Gly_3)-N(Gly_3) (solid line) and H(Gly_3) - O(wat) distances (dotted line) in the simulation of the Cu(HGGG) system at T =50 K in water solvent. The y-axes on the r.h.s. measures the total energy (dashed line) of the system.

N to a nearby water molecule is clearly displayed by the large increase of the distance between H and N bond, and by the corresponding formation of an H-O bond occurring, as explained above, at about 0.9 ps (Fig. 5.5).

The results of these simulations are in agreement with previous DFT calculations [Pushie and Rauk, 2003]. In fact, in the picture proposed in that work the reaction in water

$$LH_2 + Cu^{+2} \rightleftharpoons CuL + 2H^+ \tag{5.3.1}$$

where L stands for (CH_3-CO)-His-Gly^--Gly^--Gly-(NH-CH_3) and LH_2 for (CH_3-CO)-His-Gly-Gly-Gly-(NH-CH_3), occurs through the following steps

$$LH_2 + Cu^{+2} \rightarrow Cu(LH_2)^{+2} \tag{5.3.2}$$

$$Cu(LH_2)^{+2} \rightarrow Cu(LH)^+ + H^+ \tag{5.3.3}$$

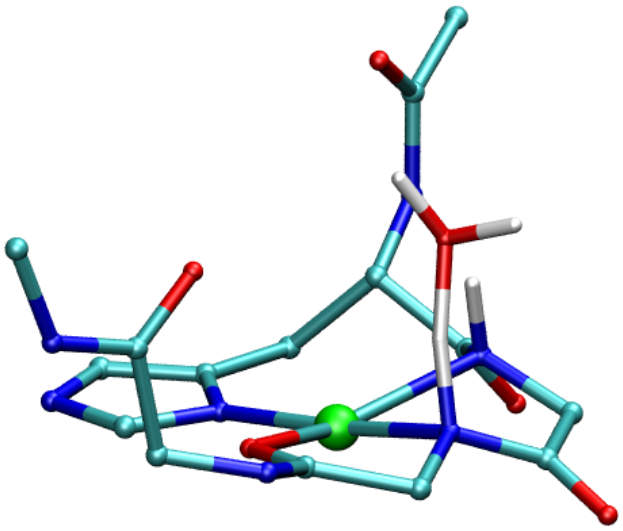

Figure 5.5: A sketch of the structure of the Cu(HGGG) system obtained from the simulation of Fig. 5.4 at $t = 0.9$ ps (*i.e.* when the Gly_3 residue is deprotonated by a water molecule). Only H of Gly_2, of Gly_3 and of the nearby water molecule are displayed.

$$Cu(LH)^+ \rightarrow CuL + H^+ \tag{5.3.4}$$

In the reaction (5.3.1) first the complex Cu(HGGG) is formed with protonated Gly residues (Eq. 5.3.2). Then the Cu ion assists the deprotonation of the second Gly residue via a *trans* effect as observed in DFT calculations (Eq. 5.3.3). Finally (Eq. 5.3.4), the first Gly residue is deprotonated with the formation of a five-member ring in the chelate complex. The simulation thus confirms the existence of a thermally accessible mechanism for the step in Eq. 5.3.3.

From the calculations reported above concerning the monomeric binding site, we conclude that the square planar Cu(3N 1O) coordination is stable in water, but it is characterized by a weak bond with the Gly_3 carbonyl O. This bond can be replaced by a bond with a water O, which according to the authors of refs. [Franzini et al., 2003, Pushie and Rauk, 2003] is found to be of comparable strength. The high stability of the bond between Cu and deprotonated Gly amide N's is confirmed by our calculations.

5.3.2 The $[Cu(HG^-G^-G)]_2$ dimer, spin-restricted

The starting configuration for spin-restricted calculations of the dimeric $[Cu(HG^-G^-G)]_2$ system was extracted from a set of randomly generated configurations, obtained following the same strategy that was employed in the case of the monomeric system (see Methods' section). The initial structure was chosen to have a short Cu-Cu distance of 4.37 Å in order to study the interactions between two Cu filled binding sites when the two Cu ions are within the range of distance ($3.5 - 6.0$ Å) estimated from EPR experiments [Chattopadhyay et al., 2005].

Figures. 5.6 and 5.7 display the time evolution at 300 K of the distances between Cu and the nearby atoms possibly involved in a chemical bond

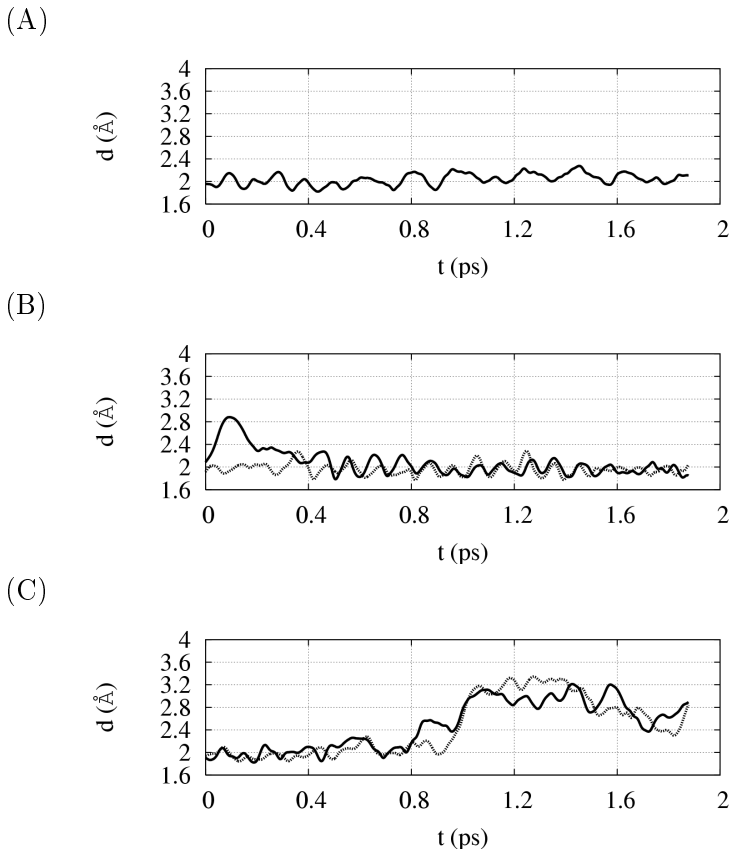

Figure 5.6: Time history at T =300 K of the Cu-X distances along the spin-restricted trajectory of the $[Cu(HG^{-}G^{-}G)]_2$ dimer, with X the atoms to which Cu was initially bonded. Solid line is for the Cu(A) site and dotted for the Cu(B) site. Plotted distances are Nδ1(His_1)-Cu (panel A), N(Gly_2/Gly_6)-Cu (panel B) and N(Gly_3/ Gly_7)-Cu (panel C). Nδ1(His_5) and Cu(B) are never bonded at T =300 K and the distance is not displayed in panel A. Residues 1-3 were initially bonded to Cu(A), residues 5-7 to Cu(B).

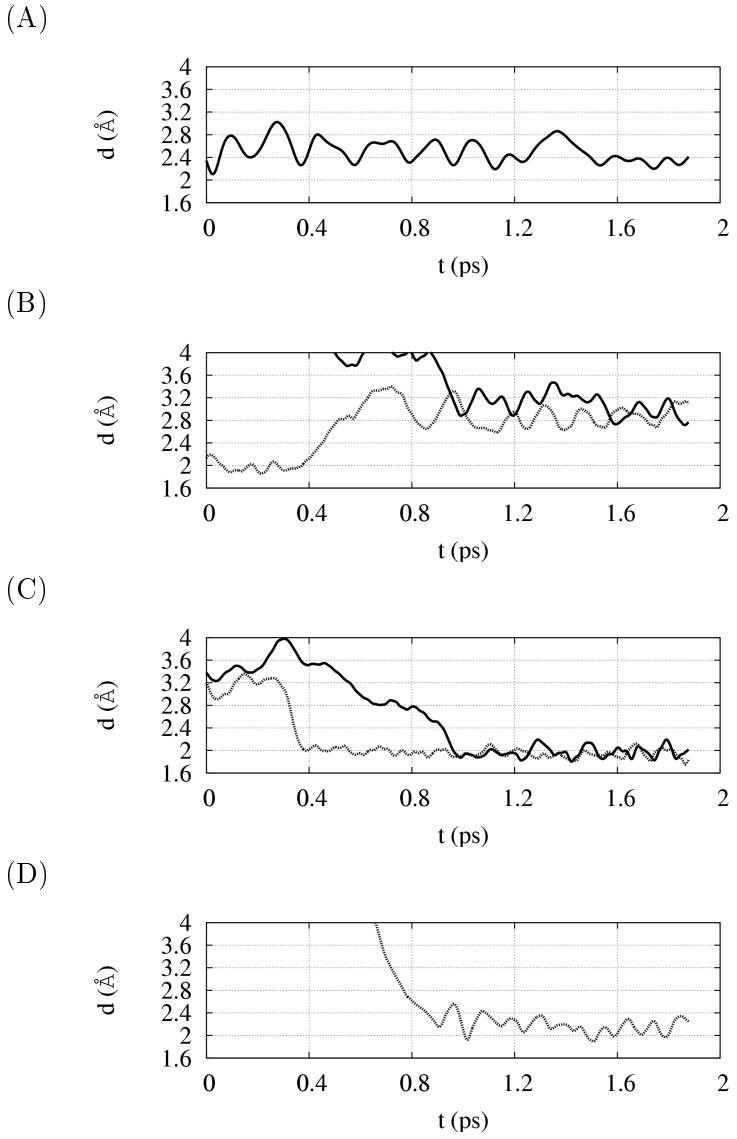

Figure 5.7: Time history of the Cu-X distances along the spin-restricted trajectory of the $[Cu(HG^{-}G^{-}G)]_2$ dimer, with X the atoms that were initially bonded to the other Cu ion. Plotted distances are Cu(A)-Cu(B) in panel A. N(Gly_6)-Cu(A) (solid line) and N(Gly_2)-Cu(B) (dotted line) in panel B. N(Gly_7)-Cu(A) (solid line) and N(Gly 3)-Cu(B) (dotted line) in panel C. O(Gly_3)-Cu(B) (dotted line) in panel D. Residues 1-3 are initially bonded to Cu(A), residues 5-7 are initially bonded to Cu(B). The Cu(A)-Cu(B) distance decreased from its initial value of 4.37 Å during thermalization (see text).

with it. Hereafter, the two Cu ions are indicated as Cu(A) and Cu(B), respectively. The amino acids initially bonded to Cu(A) are numbered as His_1, Gly_2 and Gly_3. Those initially bonded to Cu(B) are numbered as His_5, Gly_6 and Gly_7. Gly_4 and Gly_8 never interact with any Cu ion.

The nature of the coordination modes of the two Cu^{2+} ions is dynamical and the time evolution of the Cu(A)-Cu(B) distance (Fig. 5.7) deserves to be commented.

The first interesting feature is that one of the amide N of Gly_3 ($N(Gly_3)$ in the following) is exchanged between the two Cu sites. This is seen comparing panel C of Fig. 5.6 with panel C of Fig. 5.7: the distance $N(Gly_3)$-Cu(A) ($N(Gly_3)$ and Cu(A) were at a bonding distance at the beginning of the simulation) becomes larger than 2.5 Å after about 1 ps (solid line in Fig. 5.6C). At the same time, the distance N(Gly 3)-Cu(B) (solid line in Fig. 5.7C) becomes about 2 Å. Interestingly, the distances $N(Gly_7)$-Cu(A) (solid line in Fig. 5.7C) and $N(Gly_7)$-Cu(B) (dotted line in Fig. 5.6C) are both about 2 Å in the time interval $0.4 - 0.8$ ps, thus showing that $N(Gly_7)$ forms a bridge between the two Cu sites for about 0.5 ps.

Since one of the two Cu ions (Cu(A)) looses its bond with the His, to which it was bound at the beginning of the simulation, no dotted line is displayed in Fig. 5.6A. We also note that Cu(B) forms a bond with O of Gly_3 (dotted line in Fig. 5.7D), while both Cu ions loose their bonds with the initial O(Gly).

The overall structure reached after 0.86 ps is displayed in Fig. 5.8. The bonds, drawn according to the analysis of the time evolution of distances, described above, show the intricate coordination mode that gives rise to new chemical bridges between the two initially separated monomers. A distorted geometry of the ligands around each Cu center emerges. A careful analysis

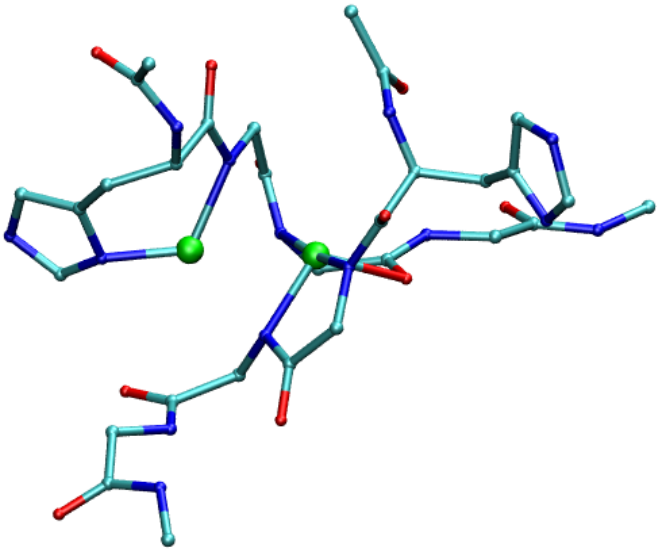

Figure 5.8: Structure of the $[Cu(HG^{-}G^{-}G)]_2$ system obtained in the spin-restricted simulation at T =300 K and at $t = 0.86$ ps. This structure is afterward used as the initial configuration for the spin-unrestricted simulation. The expectation value of the spin operator, S^2, is 2.19 in this configuration.

of Figs. 5.6 and 5.7 also shows that in this condition each Cu ion is prone to form new bonds with atoms weakly bonded with the other Cu ion. This picture suggests that each of the two Cu ions tends to coordinate at least two deprotonated amide N, while trying to fill its coordination shell with other ligands possibly available in the nearby.

For comparison, extensive simulations of the dimeric $[HGGG]_2$ system in the absence of Cu have been carried out, in a configuration where the two pairs of Gly residues (Gly_2 and 3 at site 1 and Gly_6 and 7 at site 2) are protonated. For the rest of the system the same configuration previously used was taken as a starting point.

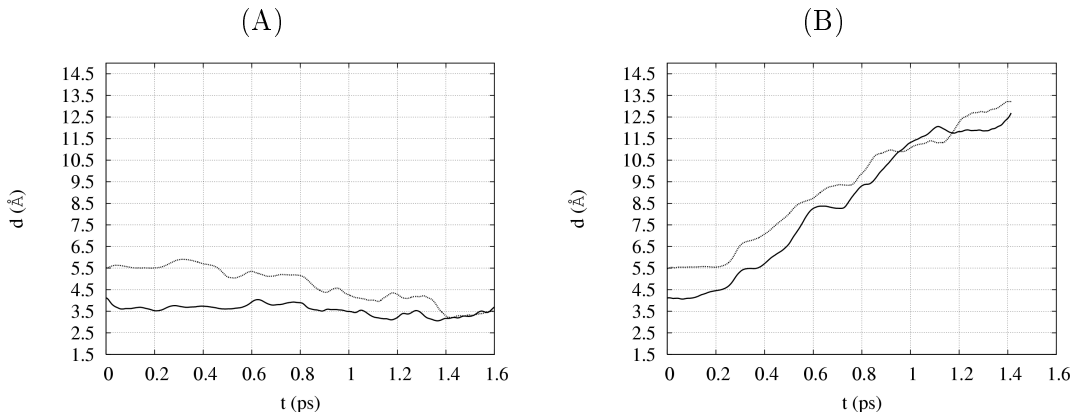

Figure 5.9: Time evolution of the $N(Gly_2)$-$N(Gly_6)$ (solid line) and $N(Gly_3)$-$N(Gly_7)$ (dotted line) distances in the simulation of the $[Cu(HG^-G^-G)]_2$ (panel A) and $[HGGG]_2$ (panel B) systems at T =300 K.

In Fig. 5.9 the time evolution of two distances that monitor the relative position of the two monomers are plotted, namely $N(Gly_2)$-$N(Gly_6)$ and $N(Gly_3)$-$N(Gly_7)$. Without Cu ions bonded to their binding sites (panel B), the two monomers move away from each other. This means that the long-range electrostatic and dispersive interactions acting between the two monomers do not suffice to keep them close together in vacuum. Even if

hydrophobic interactions in the water solvent may modify this situation, in the present model the formation of covalent bonds between Cu and ligands initially involved in bonds with the other Cu ion (see Fig. 5.7), provides the force that keeps the two filled sites at short distances (Fig 5.9A).

As for the Cu-Cu distance, it is found that it already decreased from its initial value of 4.37 Å to about 2.4 Å during thermalization. In the rest of the simulated trajectory at 300 K (Fig. 5.7, panel A) the Cu-Cu distance takes values smaller than the shortest estimate coming from EPR experiments, which is 3.5 Å [Chattopadhyay et al., 2005]. The time evolution of the Cu-Cu distance shows a tendency towards values that are typical of Cu-Cu bonds in bimetallic clusters, *i.e.* in the range of 2.1-3.0 Å [Smith, 1998].

5.3.3 The $[Cu(HG^{-}G^{-}G)]_2$ dimer, spin-unrestricted

In order to check the reliability of this conclusion and have a better quantum mechanical understanding of the Cu-Cu coordination site the dimer simulation has been repeated using spin-unrestricted CPMD simulations.

The starting configuration for this new simulation was the spin-restricted configuration obtained at 0.86 ps and discussed above. The spin configuration was chosen to have two parallel spins, in order to be in a state with $M_S = 1$. A few configurations were extracted from the MD trajectory and for all of them we found that the expectation value of the spin operator S^2 was within 10% from the expected value $S(S+1)$ =2. The spin contamination between different eigenstates of S^2 is, therefore, small [Young, 2001]. Furthermore for one of these analyzed structures, the electron energy was computed for two spin configurations: one with $M_S = 1$ (158 states with spin up and 156 states with spin down) and another one with $M_S = 0$ (157 states with spin up and 157 states with spin down). For the latter spin

configuration the expectation value of $S(S+1)$ was as large as 0.8, thus showing that this configuration is not a pure $S = 0$ state, but it is contaminated by the $S = 1$ state. We find that for the $M_S = 0$ configuration the electron energy is 21.8 kJ/mol larger than for the $M_S = 1$ configuration. These two observations (the ones concerning spin contamination and energy) show that actually the ground state for the investigated molecular geometry is that corresponding to a spin configuration with $M_S = 1$, while the other spin configuration contributes to some excited state. Even if the $S = 0$ state is admittedly not too well described by anyone of these spin configurations, the results above suggest that the $S = 0$ state has an energy larger than the one measured in the ground state.

In Figs. 5.10 and 5.11 the time evolution of the same distances plotted in Fig. 5.6 and 5.7 are displayed. The Cu-Cu distance (Fig. 5.11A) is, on average, slightly larger (2.7 Å) than in the restricted calculation (2.5 Å, see Fig. 5.7A). Even if the unrestricted calculation goes in the right direction of leading to a larger Cu-Cu distance, we are still below the lower bound given by experiments. This discrepancy is most probably due to the lack of solvent in the simulation as well as to having neglected in the model large residues, such as Pro and Trp. Clarification of this point would require further very demanding simulations. According to the accumulated experience of our research group, in fact, it has been established that in order to have a sufficiently large number of solvent molecules to adequately fill the minimal simulation box, one should add about 200 water molecules. This number comes from the requirement that a box large enough to avoid self interaction of the periodic repetitions be filled by water with density 1. Unfortunately, routinely available computer clusters, as those accessible to the group, are not able to cope with such a large system.

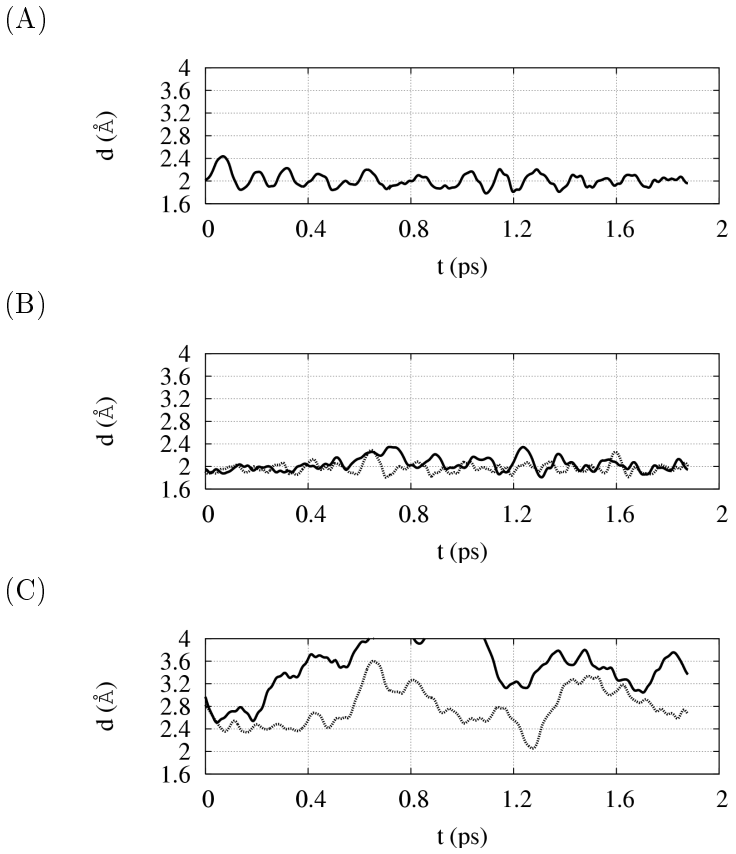

Figure 5.10: Same as for Fig. 5.6 but in the spin-unrestricted simulation.

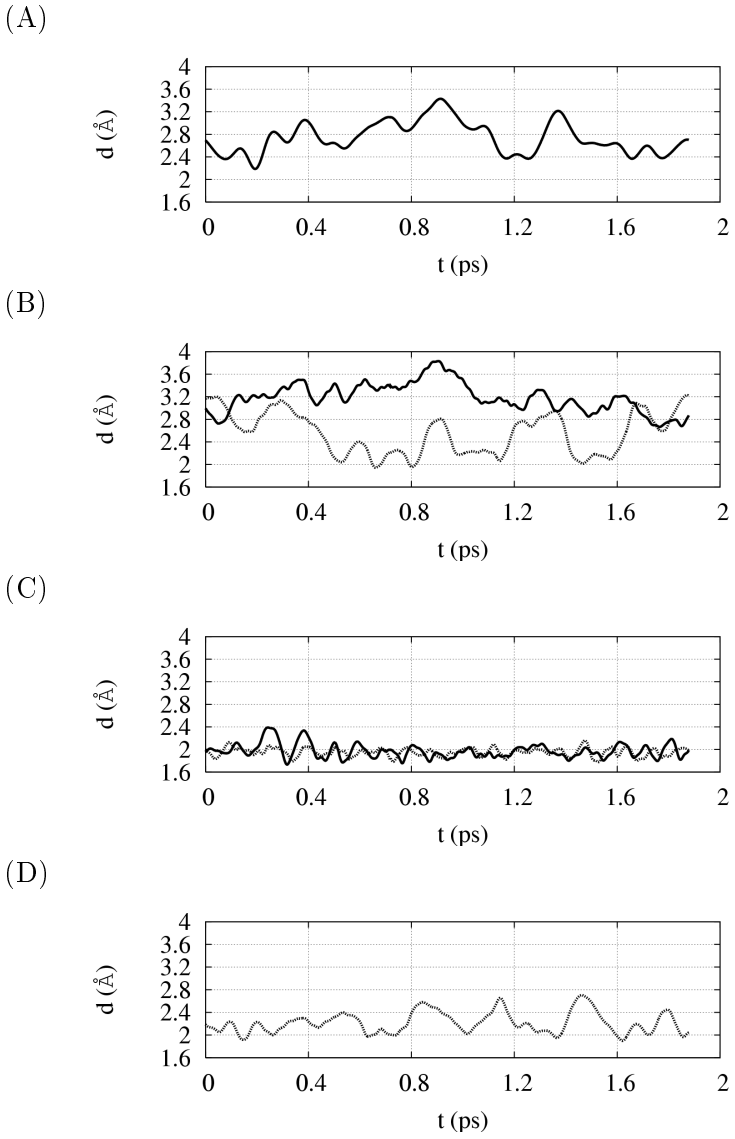

Figure 5.11: Same as for Fig. 5.7 but in the spin-unrestricted simulation.

The Cu ligands maintain their coordination with the initially bonded Cu sites, displaying a slightly smaller mobility. The only difference with respect to the spin-restricted calculation, is the tendency of the N(Gly_2) atom to form a bond with Cu(B) for about 1 ps (Fig. 5.11B). The chemical bond that is established between the two monomers still appears of a dynamical nature as a result of the exchange of N amide ligands between the two Cu sites.

From this analysis it can be concluded that the results obtained in spin-restricted simulations are, as a whole, in nice agreement with the more sophisticated (and time consuming) spin-unrestricted ones.

It must be noted that a small Cu-Cu distance, as the one reported in these dimer simulations (both spin-restricted and spin-unrestricted), may be suggestive of a strong Cu-Cu interaction. In this case the spin density for the dimer would display important differences with respect to the monomeric species with the consequence that EPR spectra would be appreciably different in the two cases. In order to investigate this question, the spin density was calculated for the monomer in the Cu(3N 1O) coordination mode and for the dimer configuration obtained from the spin-unrestricted simulation at 1.7 ps, which is the structure for which the two calculations with different spin configurations were performed and analyzed above.

In Fig. 5.12 the isosurfaces of the spin density corresponding to a value of 0.01 $Å^{-3}$ are compared for the two structures. The dimer is in the $M_S = 1$ spin configuration. In the monomer (panel A) the spin density is localized on the atomic orbitals of Cu, N and O, with the last two atoms belonging to the same peptidic linkages. No contribution from the Nδ1(His) is visible. The spin density maintains approximately the same shape in Cu(HG^-G^-G) and in both the Cu sites of $[Cu(HG^-G^-G)]_2$. This shows that the two

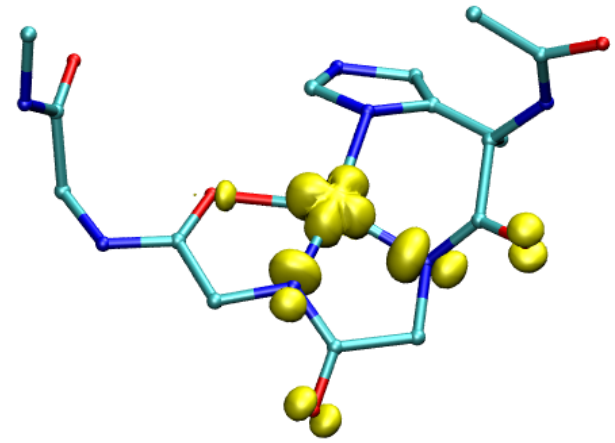

(A)

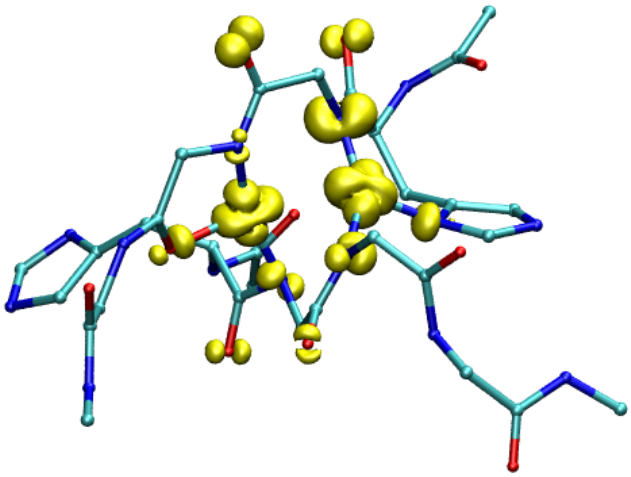

(B)

Figure 5.12: Spin density for the Cu(HG$^-$G$^-$G) monomer (panel A) and for the [Cu(HG$^-$G$^-$G)]$_2$ dimer (panel B). The isosurface corresponds to a value of 0.01 Å^{-3}.

sites in the dimer, even when the Cu-Cu distance is small, behave like two almost isolated units with S=1/2. This observation is consistent with EPR experiments, where also at full Cu occupancy, the spectrum appears to be that of a S=1/2 system.

By comparing the two panels of Fig. 5.12, the spin density when the two Cu ions are bonded to different ligands (the two Cu sites in panel B) is remarkably similar to the case of the monomer and always determined by the amidic N bonded to each Cu ion and by the O atoms both bonded to Cu and belonging to peptidic linkages with the Cu bonded nitrogens. The contribution from Nδ1(His) is very small and, therefore, the absence of a His bonding to Cu(B) does not affect the spin density.

5.4 Simulations with an additional imidazole ring

Given the various indications of several Cu coordination modes according to the relative concentration of octarepeats and Cu ions, the study of the interaction of the Cu^{2+} ion with more than one imidazole ring is particularly relevant.

Moreover, the imidazole ring (and, accordingly, the His amino acid) has a well known affinity copper; several experiments suggest the possibility of Cu^{2+} coordinating more than one His at the same time [Morante et al., 2004, Chattopadhyay et al., 2005].

To this end, a series of simulation, both in the vacuum and in the presence of water molecules have been carried out. The complex studied is the tetrapeptide Cu(HGGG) plus one imidazole ring, which is intended to model the presence of a complete Histidine coming from a different octarepeat. This simplification is required by the need to reduce the size of the system, as discussed in chapter 4.This is not expected to affect the result, since all of the coordination modes proposed from the experiments involve only the imidazole Nitrogen. The imidazole ring is capped with a metyl group to ensure chemical inertness: the brute formula of the molecule is then CH_3–C–CH–NH–CH–N.

The possible ligands of Cu will be denoted as follows:

Nϵ of the His: N(His)

Nϵ of the imidazole ring: N(ring)

N^- of the first Gly: N(Gly_1)

N^- of the second Gly: N(Gly_2)

Carbonylic O of the second Gly: O(Gly_2)

O of a water molecule: O(water)

These abbreviations make sense since these are the principal ligands rel-

evant for the study. Other atoms will be explicitly referred to when needed.

5.4.1 Cu(HG$^-$G$^-$G) + imidazole ring in the vacuum

The first simulation started from the crystallographic structure. Given the closed conformation of the Cu[HGGG] complex, it has been decided, to reduce steric hindrance, to initially place the imidazole ring in an axial position, see figure 5.13. To reduce complexity of this first simulation, it has been carried out in the vacuum.

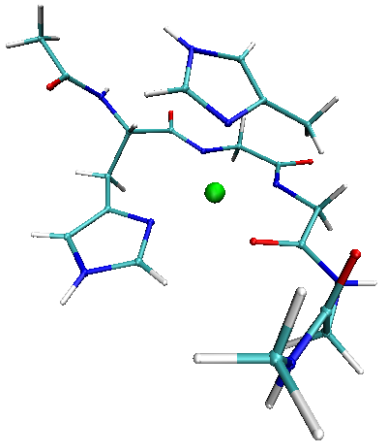

Figure 5.13: Initial configuration. The imidazole ring is in an axial position with respect to the equatorial plane determined by the crystallographic structure.

The system, composed by 61 atoms, has been followed up to 300 K but the imidazole ring has monotonously increased its distance from the Cu^{2+} ion, showing that it was never bonded. The simulation has been stopped when the imidazole ring had reached the boundary of the periodic box.

The next obvious step has been to try to place the imidazole in the equatorial plane, where it was expected that the molecular orbitals of the Cu^{2+} were available for coordination.

To achieve this result, the third and fourth Glycines have been rigidly

rotated, displacing them from the equatorial plane defined by the Cu^{2+} ion, N(His) and N(Gly_1). After the thermalization protocol described in Sec 4.3, the resulting initial configuration at 300 K is shown in Fig. 5.14. The two initially rotated Glycines are still far from the equatorial plane.

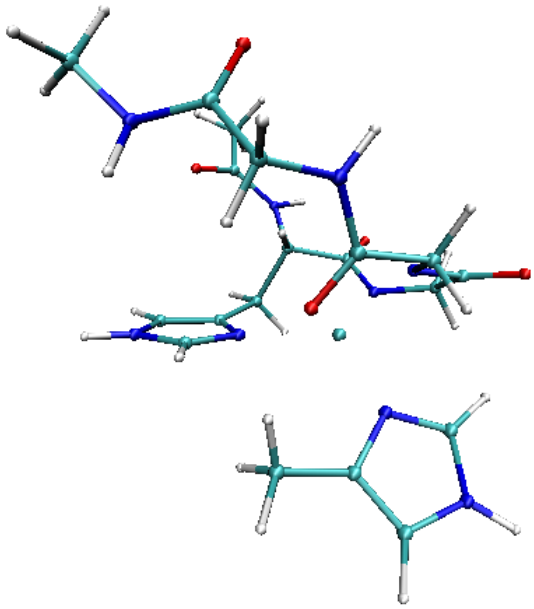

Figure 5.14: Initial configuration at 300 K.

At the start of the 300k trajectory the distance N(His)-Cu is 2.17Å while N(ring)-Cu is instead 2.11 Å. The behaviour of these distances, see fig. 5.15, is interesting, since for a large part of the simulation it appeared that the imidazole ring had displaced the Histidine. In fact, up to 1 ps, the distance Cu-N(His) increases almost monotonically, reaching up to 3.67Å. Correspondingly, the distance Cu-N(ring) oscillates around 2Å. Starting from 1 ps, the distance Cu-N(His) begins to decrease, going back down to 1.8Å at 1.8 ps, while the distance Cu-N(ring) increases without bound.

Thus, the results of these simulations show that apparently there is not a propensity for multiple His coordination, and that the Nitrogen of the His

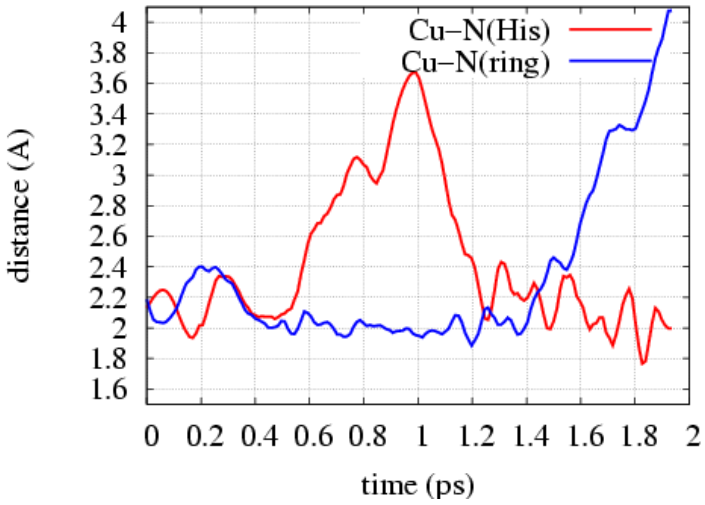

Figure 5.15: Distances between Cu^{2+} and the two Nitrogens at 300 K

can be displaced without much effort.

5.4.2 Cu(HG$^-$GG) + imidazole ring

To provide further information on the possibility of multiple His binding, it has been natural to reduce the number of available ligands, namely protonating one of the Glycines. The resulting system is thus charged.

The trajectory at 300 K has been followed for 0.8 ps. Fig. 5.16 shows the initial configuration at 300 K. From the behaviour of the distances between Cu^{2+} and the other ligands, figure 5.17, it appears that both the imidazole ring and the His remain at bonding distance. From the frequency of the distance oscillations, it appears that the bond with the N(His) (red line) is slightly stronger than that with the N(ring) (blue line), given the fact that it completes two oscillations compared with one and a half of the imidazole ring. The two distance oscillations are in opposite phases. The bond with deprotonated Gly results the strongest one, having the highest frequency.

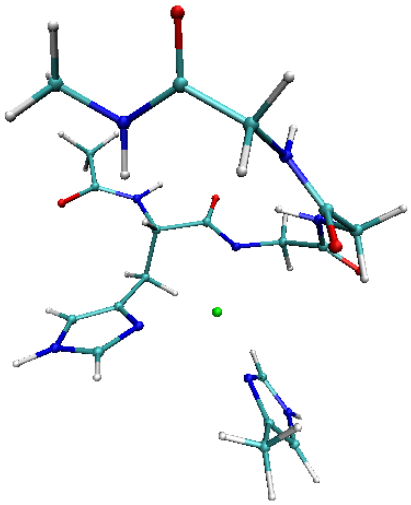

Figure 5.16: Initial configuration at 300 K

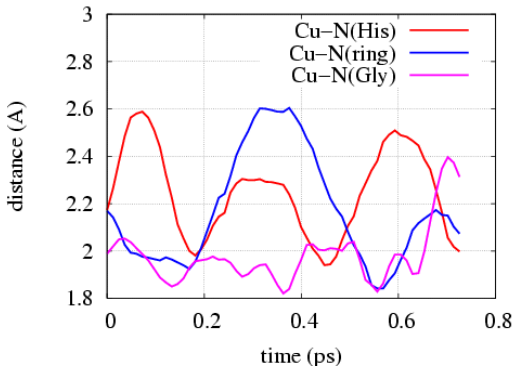

Figure 5.17: Time evolution of the distances. Note the frequency of oscillation of Cu-N(Gly), higher compared to the other two.

5.4.3 Cu(HG$^-$GG) + imidazole ring + 92(H_2O)

Given the results of the previous simulations, the system described in Sec. 5.4.2 has been studied in the presence of 92 water molecules, to provide further information on the propensity for multiple His coordination.

The single deprotonation can be thought of as the microscopic representation of an acidic pH. If the pH were strongly basic, the presence of the metal ion would favor complete deprotonation. Conversely, if the pH of the solution were acidic it would be less easy for the Cu^{2+} ion to deprotonate both Glycines.

The initial configuration of the system is the same of the previous system, Sec. 5.4.2, that is a deformation of the original crystallographic structure in such a way as to reduce the sterical hindrance. The solvent has been introduced by adding 92 water molecules, whose position was extracted by the VEGA simulation program [Pedretti et al., 2004].

Having followed our standard procedure for thermalizing the initial configuration, (Sec. 4.3) and reducing the bias, we have studied its trajectory at 300 K for 1.4 ps in real time.

In the starting configuration at 300 K, see figure 5.18, the three ligands N(His), N(ring) and N(Gly_1) are inside the coordination sphere of the Cu ion and roughly lie in a plane.

More precisely, the distance from Cu of the N(His) was of 1.96 Å while the N(ring) lied at 2.03 Å. The distance Cu-N(Gly) was of 1.98 Å.

The atoms N(HIS) - Cu - N(ring) formed an angle of 134.07°.

The four atoms N(HIS) - N(Gly) - Cu - N(ring) formed a dihedral angle ϕ of 191.9°[1], thus broadly lying on a plane.

These short distances were mantained during the whole trajectory, thus

[1]The convention adopted is that a *trans* configuration corresponds to 180°.

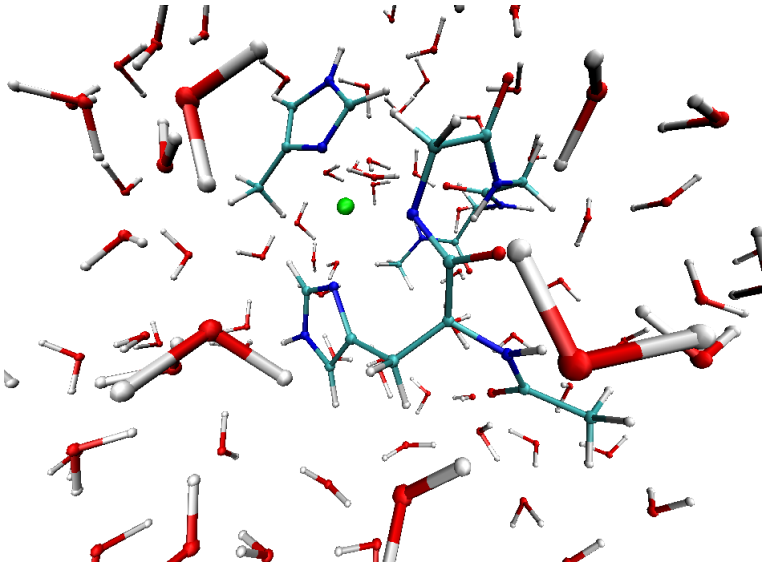

Figure 5.18: Initial configuration at 300 K. It can be seen that the Cu ion is coordinating the two imidazole rings and one deprotonated amide Nitrogen.

confirming the hypothesis that the Cu ion is coordinating all of the three atoms.

With regards to the effects of the solvent, we have observed that a specific water molecule (wat_b), which at the start of the 300 K simulation was at 5.93 Å from the Cu, constantly reduced its distance reaching a distance of 2.48Å at 0.62 ps. In correspondence with this first approach, the dihedral angle ϕ was of 189.8°, thus the water had not affected the coordination with those three atoms, which were still lying on the same plane. For this reason we don't interpret this first approach as a coordination. Having reached this minimum distance, the water molecule wat_b began to slowly and monotonously recede, reaching a largest separation of 3.00Å at 0.82 ps. At this time the dihedral angle ϕ was of 180°, which is in agreement with the fact that no other water molecule was near enough to the coordination sphere of Cu^{2+} .

Starting from 0.82 ps, the water molecule wat_b began to move towards Cu, reaching again the distance of 2.48 Å at 0.87 ps and progressing this time much nearer to the Cu, reaching a minimum distance of 1.93 Å at 0.91 ps. With the entrance of the wat_b in the coordination sphere, the effect on the other ligands was this time notable, with the dihedral angle ϕ being distorted and becoming 226.9°. We can then confidently conclude that a fourth coordination position can be occupied by the Oxygen of a water molecule, without displacing the other ligands initially present, namely N(His), N(ring) and $N(Gly_1)$.
The distance at this point were, in increasing order:

distance	[Å]
O(wat) - Cu	1.93
N(ring)- Cu	1.97
N(His) - Cu	2.13
$N(Gly_1)$ - Cu	2.39

Having reached this minimum distance, wat_b receded a bit, remaining for the rest of the trajectory within a a distance of 2.1 - 2.4 Å from the Cu. From the time evolution of the dihedral angle formed by N(His)-$N(Gly_1)$-Cu-O(water) we can see that the coordination was rather distorted from planarity, with the angle being centered around 100°.

Notwithstanding the capability of the solvent of acquiring a proton, the presence of the Cu ion was not sufficient to deprotonate the $N(Gly_2)$, whose distance from Cu at the start of the trajectory at 300 K was 3.85 Å and remained at a distance of about 4.3 Å for all the rest of the simulation.

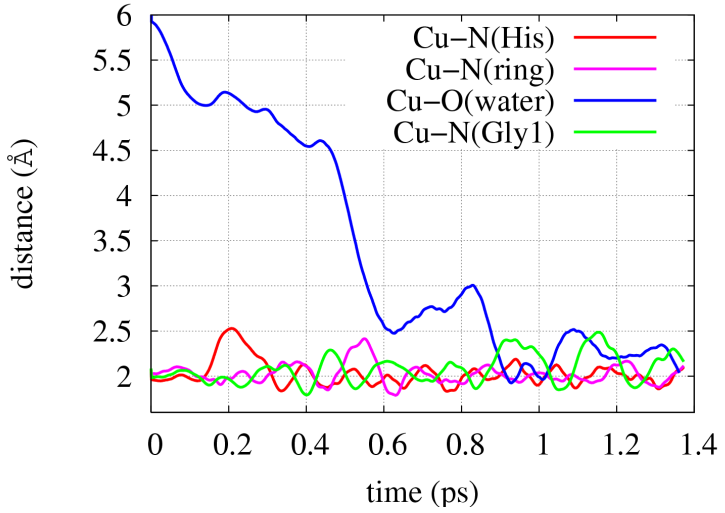

Figure 5.19: Time evolution of the distances between Cu and its ligands. It can be seen that after 0.8ps Cu is coordinating four atoms.

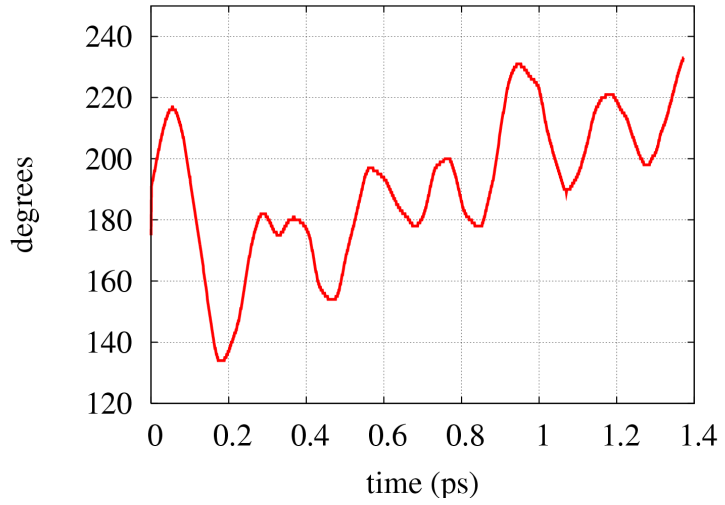

Figure 5.20: Dihedral angle formed by N(His)-N(Gly_1)-Cu-N(ring). Note that, for the first 0.8 ps, the angle remains near to $180° \pm 20°$, with the only exception of an initial fluctuation probably due to the change in the temperature of the thermostats After 0.8 ps the Cu is coordinating four ligands, including a water molecule, and the dihedral angle deviates to larger values.

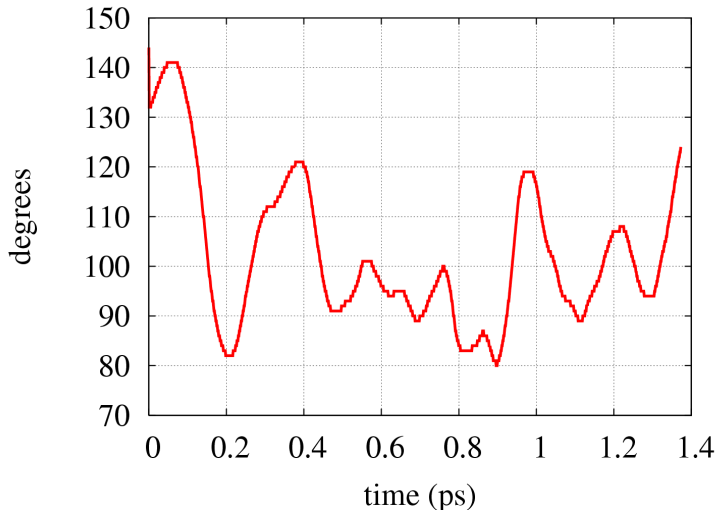

Figure 5.21: Dihedral angle formed by N(His)-N(Gly_1)-Cu-O(water).

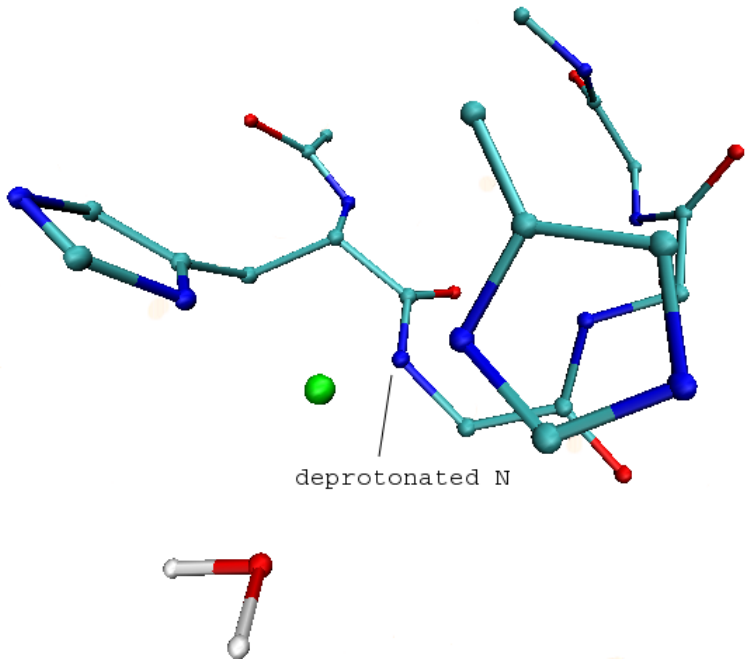

Figure 5.22: Final configuration at 300 K. Hydrogens are not shown. The only the water molecule is the one which has entered the coordination sphere of Cu^{2+} .

5.4.4 Cu(HGGG) + imidazole ring + 92(H_2O)

The only difference with respect to the system studied in the above section, Sec. 5.4.3, is the protonation of all the Glycines, including the one nearest to the His.

This implies that, unless a deprotonation occurs and a proton is donated to a water molecule in the solvent, no Glycine is able to bind Cu via its backbone Nitrogen.

The only immediately available ligands are, thus, the Nϵ of the His and of the imidazole ring, the carbonylic Oxygens from the backbone (in particular those of the Gly, which we call O(Gly_1) and O(Gly_2)), and the Oxygens of the water molecules.

Having followed our standard procedure for thermalizing the initial configuration, as described in Sec. 4.3, we have studied its trajectory at 300 K for 1.4 ps in physical time.

At the start of this 300 K trajectory, see figure 5.23, the Cu was coordinating three atoms: the distance Cu-N(His) was 1.96 Å, the distance Cu-N(ring) was 2.01 Å and the distance Cu-O(Gly_2) was 1.90 Å.

No backbone Nitrogen was coordinated. During our simulation there has not been any deprotonation due to a transfer of a proton from the backbone Nitrogen to a nearby water molecule. As it has been reported in Sec. 5.3, when discussing Fig. 5.4, this process is instead possible when the Cu ion is sufficiently near.

After 0.22 ps the distance Cu-N(His) began to grow monotonously reaching distances larger than 2.5 Å. At about 0.5 ps there were some small oscillations, never decreasing to values lower than 2.5 Å, but after that the coordination was lost and the distance Cu-N(His) increased, reaching a value of 5.08 Å at the end of the simulation.

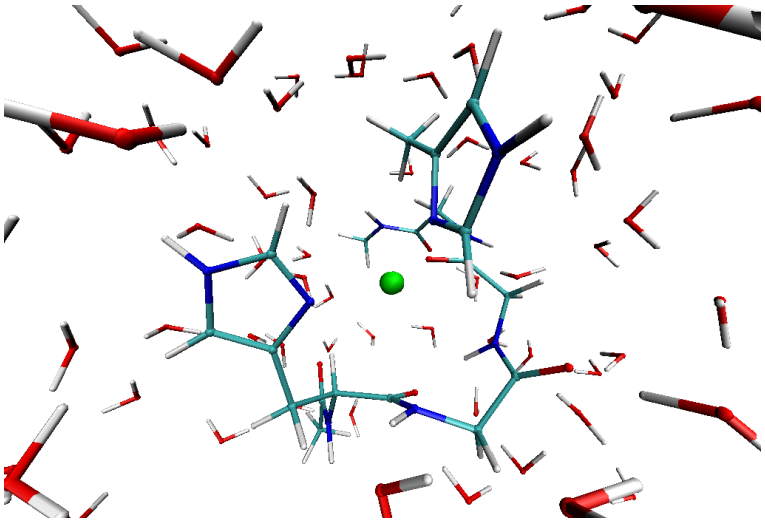

Figure 5.23: Initial configuration at 300 K. All of the Gly are protonated.

A water molecule, which at the start of the trajectory was 6.98 Å apart, approached the Cu ion and reached for the first time a distance of 2.05 Å at 0.89 ps. Then it slowly receded up to 2.75 Å at 1.01 ps. After this elongation, it again neared to the Cu ion, oscillating around a distance of 2.1 Å. We can conclude that the water was coordinated by the Cu at about 0.85 ps.

The dihedral angle defined by the initial ligands of Cu and Cu itself, namely N(His)-Cu-N(ring)-O(Gly_2), undergoes large fluctuations. One can see that, for the first part of the trajectory, the angle is loosely centered around 180°, although with a rather large excursion down to 98.5° at 0.36 ps, corresponding to the initial displacement that we have described. After about 0.6 ps, the angle was unconstrained and freely assumed every possible value in the interval [0, 360]. This was due to the fact that Cu was no longer coordinating N(His). It is suggestive that just around t=0.6 ps, the distance Cu-N(His) began to monotonously increase.

It is possible to consider another dihedral angle, formed this time by O(Gly_2)-O(water)-Cu-N(ring), since we have observed the coordination of

the water molecule. We found that, after an initial oscillatory phase when the water molecule had still not been coordinated, the dihedral is compatible with a slightly distorted planar configuration starting from 0.8 ps, in perfect agreement with the time evolution of the distance Cu-O(water).

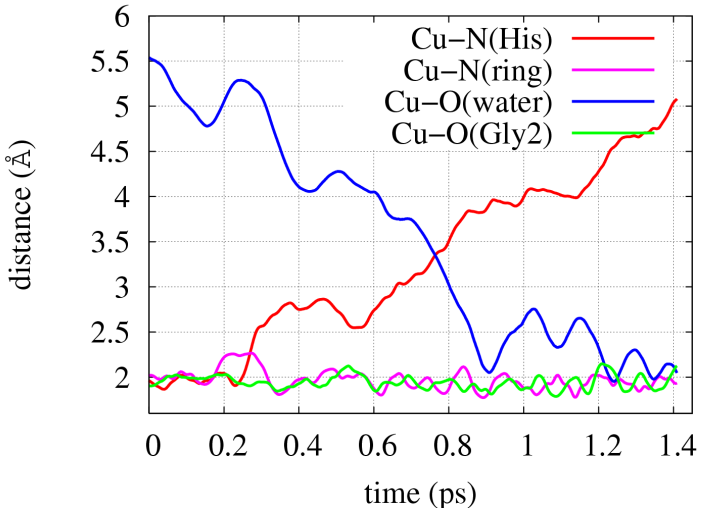

Figure 5.24: Time evolution of the distances of the ligands from Cu in the absence of deprotonated backbone Nitrogens. Note that the coordination with N(His) seems to be lost right after the first 0.2 ps, while the distance wits N(ring) is always well under 2.5 Å.

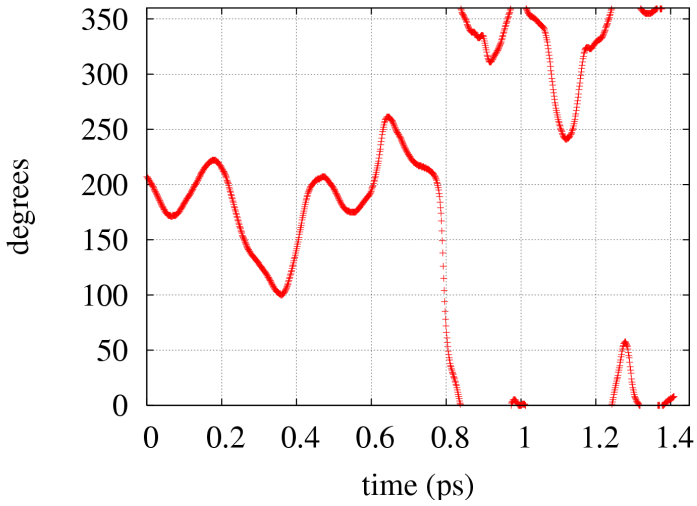

Figure 5.25: Dihedral angle formed by N(His)-Cu-N(ring)-O(Gly_2). Note that this angle is completely unconstrained since one of the atoms which defines it, the N(His), loses its coordination to the Cu and is freely rotating.

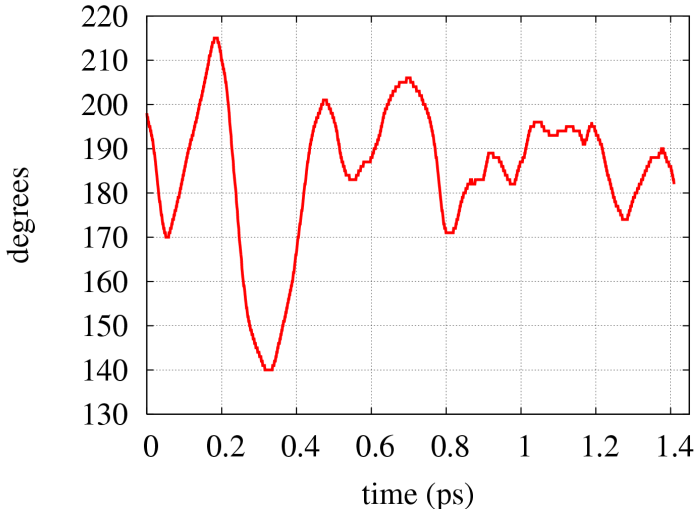

Figure 5.26: Dihedral angle formed by O(Gly_2)-O(H_2O)-Cu-N(ring). After the initial oscillatory phase the angle stabilizes itself around a value compatible with a slightly distorted planar geometry.

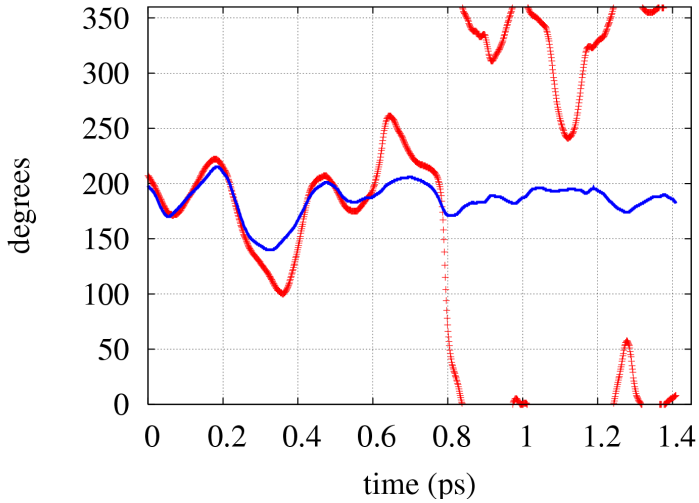

Figure 5.27: Both of the dihedral angles shown on the same scale. In red, the angle determined by O(Gly_2)-O(H_2O)-Cu-N(ring). In blue, the angle formed by O(Gly_2)-O(H_2O)-Cu-N(ring).

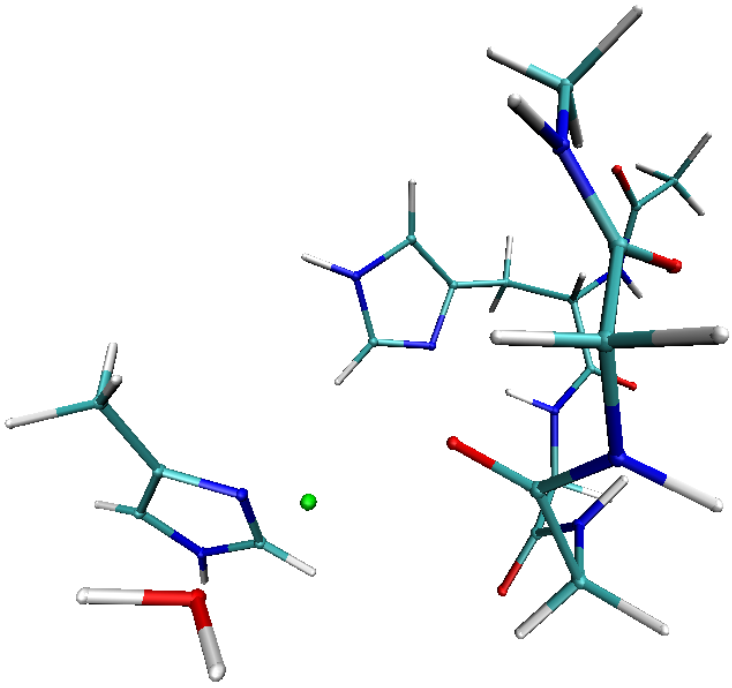

Figure 5.28: Final configuration at 300 K. All of the Gly are protonated. No water molecule is shown, except for the one which is coordinated by Cu^{2+} .

Chapter 6

Conclusions

This work has shown an application of numerical simulations to biophysics, and namely the study of the interaction of a Copper ion with a binding site found in the Prion Protein. This interaction is believed to be relevant from a biological point of view, as it has been explained in Chapter 2.

The main theoretical techniques adopted for the this study have been the Density Functional Theory, the Car–Parrinello Lagrangian and the pseudopotential approximation. These methods allow the *ab initio* study of the biological system, reducing to a minimum the number of assumptions, which is to be contrasted with the other possible approach, namely that of classical Molecular Dynamics.

With regard to the Prion Protein and to the interaction of the octarepeat with Cu^{2+} ions, a series of results has been obtained:

1. It is indeed possible to perform meaningful biophysics computations with present day hardware.

2. The proposed experimental protocol has demonstrated its validity as a starting point for this kind of investigations.

3. *Trp Relevance*: Tryptophan appears not to be directly involved in Cu coordination. The key structure appears to be a planar coordination of two amidic Nitrogens from deprotonated Glycines, a Nitrogen from the Histidine and an Oxygen from the backbone.

4. *Preference for the Amidic Nitrogens*: All the simulations show a characteristic preference for the amidic nitrogens rather than for the imidazole, both in the absence and in the presence of the solvent.

5. *pH, Gly's deprotonation*: It has been observed an acidic behaviour of the Cu^{2+}(HGGG) complex. The process of Gly deprotonation is energetically accessible. This is interesting because rather unusual.

6. *Interaction with more than one imidazole ring*: Several experiments with different starting configurations have been carried out. Since imidazole has a high affinity for Cu, it has been rather surprising to find that it is very difficult to observe more than one imidazole ring bound to Cu. This suggests that multiple His binding is more difficult than what was previously thought, and easier at low pH when Gly's are not available as ligands

7. In the presence of solvent the Cu coordination sphere can be filled by water Oxygens, which confirms that the Cu ion is well simulated, confirming that the ultra-soft pseudopotential is sufficiently faithful.

8. *Interaction between two tetrapeptides*: The formation of a dimer is possible only in the presence of Cu, by the exchange of main chain ligands. This is in line with the other observations. In the absence of Cu, no dimer formation has been observed.

It is of great relevance the fact that these results, appeared in [Furlan et al., 2006,

Furlan et al., 2007a, Furlan et al., 2007b] have been obtained with computing resources which are accessible even for a single research group. While it remains true that super-computers have an enormous computing power, they are not the only opportunity available.

This is important, because it means that a growing number of researchers, all over the world, will have access to resources powerful enough to test their hypothesis and promote new experiments.

Bibliography

[ABR, 2006] ABR (2006). Acta biophysica romana 2006. Biophysics Conference held in Rome, University of Tor Vergata, from 22 to 24 Feb 2006.

[Adamo et al., 2002] Adamo, S., Carinci, P., Molinaro, M., Siracusa, G., Stefanini, M., and Ziparo, E. (2002). *Istologia di V. Monesi*. Piccin, 5th edition. Reference histology book, in italian. See in particular chapter 16, by G. Siracusa, on *Tessuto Nervoso e Nevroglia*.

[Aguzzi and Weissmann, 1996] Aguzzi, A. and Weissmann, C. (1996). Sleepless in Bologna: transmission of fatal familial insomnia. *Trends in Microbiology*, 4(4):129–131. See also the response to this paper, by Jun Tateishi, pages 131–132 of the same issue.

[Alberts et al., 2002] Alberts, B., Johnsons, A., Lewis, J., Raff, M., Roberts, K., and Walter, P. (2002). *Molecular Biology of the Cell*. Garland Science, 4th edition.

[AMBER] AMBER. Assisted Model Building and Energy Refinement. amber.scripps.edu. Classical MD software package, small fee required for non profit organizations.

[Ashcroft and Memin, 1976] Ashcroft, N. and Memin, N. D. (1976). *Solid State Physics*. Harcourt College Publishers.

[Austin et al., 1962] Austin, B., Heine, V., and Sham, L. (1962). General Theory of Pseudopotentials. *Phys. Rev.*, 127(1):276.

[Bachelet et al., 1982] Bachelet, G. B., Hamann, D. R., and Schlüter, M. (1982). Pseudopotentials that work: From H to Pu. *Phys. Rev. B*, 26(8):4199.

[Baroni et al.] Baroni, S., Dal Corso, A., de Gironcoli, S., Giannozzi, P., Cavazzoni, C., Ballabio, G., Scandolo, S., Chiarotti, G., Focher, P., Pasquarello, A., Laasonen, K., Trave, A., Car, R., Marzari, N., and Kokalj, A. http://www.pwscf.org/.

[Baroni et al., 2001] Baroni, S., de Gironcoli, S., Dal Corso, A., and Giannozzi, P. (2001). Phonons and related crystal properties from density-functional perturbation theory. *Rev. Mod. Phys.*, 73:515.

[Basler et al., 1986] Basler, K., Oesch, B., Scott, M., Westaway, D., Wälchli, M., Groth, D. F., McKinley, M. P., Prusiner, S. B., and Weissmann, C. (1986). Scrapie and cellular PrP isoforms are encoded by the same chromosomal gene. *Cell*, 46:417–428,.

[Blöchl, 1994] Blöchl, P. E. (1994). Projector augmented-wave method. *Phys. Rev. B*, 50(24):17953–17979.

[Bolton et al., 1982] Bolton, D. C., McKinley, M. P., and Prusiner, S. B. (1982). Identification of a protein that purifies with the scrapie prion. *Science*, 218:1309–1311.

[Bransden and Joachain, 2001] Bransden, B. and Joachain, C. (2001). *Physics of Atoms and Molecules*. Longman, first edition.

[Brown et al., 1997] Brown, D. R., Qin, K., Herms, J. W., Madlung, A., Manson, J., Strome, R., Fraser, P. E., Kruck, T., von Bohlen, A., Schulz-

Schaeffer, W., Giese, A., Westaway, D., and Kretzschmar, H. (1997). The cellular prion protein binds copper *in vivo*. *Nature*, 390:684–687.

[Brown et al., 1998] Brown, D. R., Schmidt, B., and Kretzschmar, H. A. (1998). Effects of copper on survival of prion protein knockout neurons and glia. *J. Neurochem.*, 70:1686–1693.

[Büeler et al., 1993] Büeler, H., Aguzzi, A., Sailer, A., Greiner, R. A., Autenried, P., Aguet, M., and Weissmann, C. (1993). Mice devoid of PrP are resistant to scrapie. *Cell*, 73(7):1339–1347.

[Burke and friends] Burke, K. and friends. The ABC of DFT. These lectures can be found on Kieron Burke's homepage, at http://dft.rutgers.edu/dftbook.html.

[Burns et al., 2002] Burns, C., Aronoff-Spencer, E., Dunham, C., Lario, P., Avdievich, N., Antholine, W., Olmstead, M., Vrielink, A., Gerfen, G., Peisach, J., Scott, W., and Millhauser, G. (2002). Molecular Features of the Copper Binding Sites in the Octarepeat Domain of the Prion Protein. *Biochemistry*, 41(12):3991–4001.

[Bussard, 2005] Bussard, A. E. (2005). A scientific revolution? *EMBO reports*, 6(8):691–694.

[Car and Parrinello, 1985] Car, R. and Parrinello, M. (1985). Unified approach for molecular dynamics and density-functional theory. *Phys. Rev. Lett.*, 55:2471.

[CHARMM] CHARMM. Chemistry at HARvard Macromolecular Mechanics. www.charmm.org.

[Chattopadhyay et al., 2005] Chattopadhyay, M., Walter, E. D., Newell, D. J., Jackson, P. J., Aronoff-Spencer, E., Peisach, J., Gerfen, G. J., Ben-

nett, B., Antholine, W. E., and L.Millhauser, G. (2005). The octarepeat domain of the prion protein binds Cu(II) with three distinct coordination modes at pH 7.4. *J. Am. Chem. Soc.*, 127:12647–12656.

[Collinge et al., 1991] Collinge, J., Palmer, M., and Dryden, A. (1991). Genetic predisposition to iatrogenic Creutzfeldt-Jakob disease. *Lancet*, 337:1441–42.

[Collinge and Rossor, 1996] Collinge, J. and Rossor, M. (1996). A new variant of prion disease. *Lancet*, 347:916–917.

[Colombo et al., 2007] Colombo, M. C., VandeVondele, J., Guidoni, L., Laio, A., and Rothlisberger, U. (2007). QM/MM study of the copper binding sites of prion. *J. Phys. Chem.* in press.

[Donne et al., 1997] Donne, D., Viles, J. H., Groth, D., Mehlhorn, I., and James, T. (1997). Structure of the recombinant full-length hamster prion protein PrP(29–231): The N-terminus is highly flexible. *Proc. Natl. Acad. Sci. USA*, 94:13452–13456.

[Franzini et al., 2003] Franzini, E., Gioia, L. D., Fantucci, P., and Zampella, G. (2003). DFT investigation of copper-peptide complexes related to the octarepeat domain of the prion protein. *Inorg. Chem. Comm.*, 6:650–653.

[Frenkel and Smit, 1996] Frenkel, D. and Smit, B. (1996). *Understanding Molecular Simulation - From Algorithms to Applications*. Academic Press.

[Frigo and Johnson, 2005] Frigo, M. and Johnson, S. G. (2005). The Design and Implementation of FFTW3. *Proceedings of the IEEE*, 93(2):216–231. Online at http://www.fftw.org/fftw-paper-ieee.pdf.

[Furlan et al., 2006] Furlan, S., Guerrieri, F., Penna, G. L., Morante, S., and Rossi, G. C. (2006). Ab initio simulations of Cu binding sites in the

N-terminal region of PrP. In Hansmann, U., Meinke, J., Mohanty, S., and Zimmermann, O., editors, *From Computational Biophysics to Systems Biology*, volume 34 of *NIC series*. John Von Neumann Institute for Computing (NIC). www.fxz-juelich.de/nic.

[Furlan et al., 2007a] Furlan, S., Guerrieri, F., Penna, G. L., Morante, S., and Rossi, G. C. (2007a). Studying the Cu binding sites in the PrP N-terminal region: a test case for ab initio simulations. *Eur. Bioph. J.*, 36(7):841–845.

[Furlan et al., 2007b] Furlan, S., Penna, G. L., Guerrieri, F., Morante, S., and Rossi, G. C. (2007b). Ab initio simulations of Cu binding sites on the N-terminal region of prion protein. *Journal of Biological Inorganical Chemistry*, 12(4):571–583.

[Gabizon et al., 1988] Gabizon, R., McKinley, M. P., Groth, D., and Prusiner, S. B. (1988). Immunoaffinity Purification and Neutralization of Scrapie Prion Infectivity. *Proc. Natl. Acad. Sci. USA*, 85:6617–6621.

[Gaggelli et al., 2006] Gaggelli, E., Kozlowski, H., Valensin, D., and Valensin, G. (2006). Copper Homeostatis and Neurodegenerative Disorders (Alzheimer's, Prion, and Parkinson's Diseases and Amyotrophic Lateral Sclerosis. *Chem. Rev.*, 106:1995–2044.

[Giannozzi et al., 2004] Giannozzi, P., De Angelis, F., and Car, R. (2004). First-principle molecular dynamics with ultrasoft pseudopotentials: Parallel implementation and application to extended bioinorganic systems. *J. Chem. Phys.*, 120(13):5903.

[Govaerts et al., 2004] Govaerts, C., Wille, H., Prusiner, S. B., and Cohen, F. E. (2004). Evidence for assembly of prions with left–handed β-helices into trimers. *Proc. Natl Acad. Sci. USA*, 101:8342–8347.

[GROMACS, 2007] GROMACS (1991–2007). GROMACS, GROningen Machine for Chemical Simulations. www.gromacs.org. Extremely fast classical MD software package, used also in the in the distributed computing project Folding@home.

[Gunnarsson and Lundqvist, 1976] Gunnarsson, O. and Lundqvist, B. I. (1976). Exchange and correlation in atoms, molecules, and solids by the spin-density-functional formalism. *Phys. Rev. B*, 13(10):4274–4298.

[Hamann et al., 1979] Hamann, D., Schlüter, M., and Chiang, C. (1979). Norm-Conserving Pseudopotentials. *Phys. Rev. Lett.*, 43(20):1494.

[Hamann, 1989] Hamann, D. R. (1989). Generalized norm-conserving pseudopotentials. *Phys. Rev. B*, 40(5):2980.

[Hartter and Barnea, 1988] Hartter, D. and Barnea, A. (1988). Evidence for release of copper in the brain: depolarization–induced release of newly taken-up 67 copper. *Synapse*, 2:412–415.

[Herring, 1940] Herring, C. (1940). A New Method for Calculating Wave Functions in Crystals. *Phys. Rev.*, 57:1169.

[Hohenberg and Kohn, 1964] Hohenberg, P. and Kohn, W. (1964). Inhomogeneous Electron Gas. *Phys. Rev.*, 136(3B):B864–B871.

[Hutter et al., 2003] Hutter, G., Heppner, F. L., and Aguzzi, A. (2003). No superoxide dismutase activity of cellular prion protein in vivo. *Biol Chem.*, 384(9):1279–1285.

[Jackson et al., 2001] Jackson, G. S., Murray, I., Hosszu, L. L. P., Gibbs, N., Waltho, J. P., Clarke, A. R., and Collinge, J. (2001). Location and properties ofmetal-binding sites on the human prion protein. *Proc. Natl. Acad. Sci. USA*, 98(15):8531–8535.

[James et al., 1997] James, T. L., Liu, H., Nikolai, B. U., Farr-Jones, S., Zhang, H., and et al. (1997). Solution structure of a 142-residue recombinant prion protein corresponding to the infectious fragment of the scrapie isoform. *Proc. Natl. Acad. Sci. USA*, 94:10086–10091.

[Janak, 1978] Janak, J. (1978). Proof that $\partial E/\partial n_i = \epsilon_i$ in density-functional theory. *Phys. Rev. B*, 18(12):7165.

[Jeffreys and Swirles, 1972] Jeffreys, H. and Swirles, B. (1972). *Methods of Mathematical Physics*. Cambridge University Press, 3rd edition.

[Jones et al., 2005a] Jones, C. E., Klewpatinond, M., Abdelraheim, S. R., Brown, D. R., and Viles, J. H. (2005a). Probing Copper^{2+} Binding to the Prion Protein Using Diamagnetick Nickel^{2+} and ^{1}H NMR: The Unstructured N terminus Facilitates the Coordination of Six Copper^{2+} Ions at Physiological Concentrations. *J. Mol. Biol.*, 346:1393–1407.

[Jones and Gunnarsson, 1989] Jones, R. O. and Gunnarsson, O. (1989). The density functional formalism, its applications and prospects. *Rev. Mod. Phys*, 61(3):689–746.

[Jones et al., 2005b] Jones, S., Batchelor, M., Bhelt, D., Clarke, A. R., Collinge, J., and Jackson, G. S. (2005b). Recombinant prion protein does not possess SOD-1 activity. *Biochem J.*, 392:309–312.

[Klamt et al., 2001] Klamt, F., Dal-Pizzol, F., Conte, D., Frota, J., Walz, R., and et al. (2001). Imbalance of antioxidant defense in mice lacking cellular prion protein. *Free Radic. Biol. Med.*, 30:1137–1144.

[Kleinman and Bylander, 1982] Kleinman, L. and Bylander, D. (1982). Efficacious form for model pseudopotentials. *Phys. Rev. Lett.*, 48(20):1425.

[Kohn and Sham, 1965] Kohn, W. and Sham, L. J. (1965). Self-Consistent Equations Including Exchange and Correlation Effects. *Physical Review*, 140(4A):1133–1138.

[Koopmans, 1934] Koopmans, T. C. (1934). Über die Zuordaung von Wellenfunktionen und Eigenwerten zu den einzelnen Elektronen eines Atoms. *Physica*, 1(2):104–113.

[Kourie et al., 2003] Kourie, J. I., Kenna, B., Tew, D., MF, M. J., Curtain, C. C., Masters, C., Barnham, K., and Cappai, R. (2003). Copper modulation of ion channels of PrP[106-126] mutant prion peptide fragments. *J Membr Biol*, 193:35–45.

[La Penna et al., 2004] La Penna, G., Morante, S., Perico, A., and Rossi, G. C. (2004). Designing generalized statistical ensembles for numerical simulations of biopolymers. *J. Chem. Phys.*, 121(21):10725–10741.

[Levy, 1979] Levy, M. (1979). Universal variational functionals of electron densities, first-order density matrices, and natural spin-orbitals and solution of the v-representability problem. *Proc. Natl. Acad. Sci. USA*, 76(12):6062–6065.

[Lugaresi et al., 1986] Lugaresi, E., Medori, R., Montagna, P., Baruzzi, A., Cortelli, P., Lugaresi, A., Tinuper, P., Zucconi, M., and Gambetti, P.

(1986). Fatal familial insomnia and dysautonomia with selective degeneration of thalamic nuclei. *N Engl J Med.*, 315(16):997–1003.

[Martin and Ortiz, 1997] Martin, R. and Ortiz, G. (1997). Functional theory of extended Coulomb systems. *Phys. Rev. B*, 56(3):1124–1140.

[Millhauser, 2004] Millhauser, G. L. (2004). Copper Binding in the Prion Protein. *Accounts of Chemical Research*, 37(2):79–85.

[Millhauser, 2007] Millhauser, G. L. (2007). Copper and the Prion Protein: Methods, Structures, Function, and Disease. *Annu. Rev. Phys. Chem.*, 58:299–320.

[Miura et al., 2005] Miura, T., Sasaki, S., Toyama, A., and Takeuchi, H. (2005). Copper reduction by the octapeptide repeat region of prion protein: pH dependence and implications in cellular copper uptake. *Biochemistry*, 44:8712–8720.

[Morante et al., 2004] Morante, S., Gonzalez-Iglesias, R., Potrich, C., Meneghini, C., Meyer-Klaucke, W., Menestrina, G., and Gasset, M. (2004). Inter- and Intra-octarepeat Cu(II) Site Geometries in the Prion Protein: IMPLICATIONS IN Cu(II) BINDING COOPERATIVITY AND Cu(II)-MEDIATED ASSEMBLIES. *J. Biol. Chem.*, 279:11753–11759.

[NAMD, 2003] NAMD (2003). NAnoscale Molecular Dynamics. www.ks.uiuc.edu/Research/namd. Classical MD software package, particularly well integrated with the VMD software. Another possible interpretation of the name is Not Another Molecular Dynamics program, which would be a typical computer science joke.

[Nosé, 1984] Nosé, S. (1984). A molecular dynamics method for simulation in the canonical ensemble. *Mol. Phys.*, 52:255–268.

[Palmer et al., 1991] Palmer, M., Dryden, A., Hughes, J., and Collinge, J. (1991). Homozygous prion protein genotype predisposes to sporadic Creutzfeldt-Jakob disease. *Nature*, 352:340–342.

[Pauly and Harris, 1998] Pauly, P. C. and Harris, D. A. (1998). Copper Stimulates Endocytosis of the Prion Protein. *The Journal of Biological Chemistry*, 273(50):33107–33110.

[Pedretti et al., 2004] Pedretti, A., Villa, L., and Vistoli, G. (2004). VEGA - An Open platform to develop chemio-bio-informatics applications, using plug-in architecture and script programming. *JCAMD*, 18:167–173. See also, by the same authors, J. Mol Graph, 21, 47–49 (2002), and Theor. Chem. Acc., 109, 229–232 (2003).

[Perdew and Wang, 1991] Perdew, J. and Wang, Y. (1991). Correlation hole of the spin-polarized electron gas, with exact small-wave-vector and high-density scaling. *Phys. Rev. B*, 44:13298 – 13307.

[Perdew et al., 1996] Perdew, J. P., Burke, K., and Ernzerhof, M. (1996). Generalized Gradient Approximation Made Simple. *Phys. Rev. Lett.*, 77(18):3866–3868. See also: Zhang, Y. and Yang, W., Comment on "Generalized Gradient Approximation Made Simple", Phys. Rev. Lett. 80 (1998) 890 and the reply by Perdew, Burke and Ernzerhof at page 891 of the same issue.

[Phillips and Kleinman, 1959] Phillips, J. and Kleinman, L. (1959). New Method for Calculating Wave Functions in Crystals and Molecules. *Phys. Rev.*, 116(2):287.

[Polchinski, 1984] Polchinski, J. (1984). Renormalization and effective lagrangians. *Nucl. Phys.*, B231:269–295.

[Prusiner, 1998] Prusiner, S. B. (1998). Prions. In *Nobel Lectures*, pages 74–129.

[Pushie and Rauk, 2003] Pushie, M. J. and Rauk, A. (2003). Computational studies of Cu(II)[peptide] binding motifs: Cu[HGGG] and Cu[HG] as models for Cu(II) binding to the prion protein octarepeat region. *J Biol Inorg Chem*, 8:53–65.

[Rappe et al., 1990] Rappe, A. M., Rabe, K. M., Kaxiras, E., and Joannopoulos, J. D. (1990). Optimized pseudopotentials. *Phys. Rev. B*, 41(2):1227.

[Riek et al., 1996] Riek, R., Hornemann, S., Wider, G., Billeter, M., Glockshuber, R., and Wuthrich, K. (1996). NMR structure of the mouse prion protein domain PrP(121-321). *Nature*, 382:180–182.

[Riek et al., 1997] Riek, R., Hornemann, S., Wider, G., Glockshuber, R., and Wuthrich, K. (1997). NMR characterization of the full-length recombinant murine prion protein, mPrP(23-231). *FEBS Lett.*, 413:282–288.

[Sailer et al., 1994] Sailer, A., Büeler, H., Fischer, M., Aguzzi, A., and Weissmann, C. (1994). No propagation of prions in mice devoid of PrP. *Cell*, 77(7):967–968.

[Shaw Jr. and Harrison, 1967] Shaw Jr., R. W. and Harrison, W. A. (1967). Reformulation of the Screened Heine-Abarenkov Model Potential. *Phys. Rev.*, 163(3):604.

[Sigel and Martin, 1981] Sigel, H. and Martin, R. B. (1981). Coordinating Properties of the Amide Bond. Stability and Structure of Metal Ion Complexes of Peptides and Related Ligands. *Chem. Rev.*, 82:385–426.

[Smith, 1998] Smith, D. R. (1998). Copper 1996. *Coord. Chem. Rev.*, 172:457–573.

[Soto, 2004] Soto, C. (2004). Diagnosing prion diseases: needs, challenges and hopes. *Nature Reviews Microbiology*, 2:808–819.

[Stöckel et al., 1998] Stöckel, J., Safar, J., Wallace, A. C., Cohen, F. E., and Prusiner, S. B. (1998). Prion Protein Selectively Binds Copper(II) Ions. *Biochemistry*, 37:7185–7193.

[Tassone et al., 1994] Tassone, F., Mauri, F., and Car, R. (1994). Acceleration schemes for ab initio molecular-dynamics simulations and electronic-structure calculations. *Phys. Rev. B*, 50(15):10561–10573.

[TCDB] TCDB. Tcdb, transport classification database. www.tcdb.org. Extremely useful database on transport proteins, mantained by Prof Milton H. Saier's group at the Division of Biological Sciences, University of California San Diego.

[Topp and Hopfield, 1973] Topp, W. C. and Hopfield, J. J. (1973). Chemically motivated pseudopotential for sodium. *Phys. Rev. B*, 7(4):1295.

[U. Rothlisberger, 2007] U. Rothlisberger (2007). http://lcbcpc21.epfl.ch/Research/research.html. Homepage of Prof Röthlisberger's group at the Laboratory of Computational Chemistry and Biochemistry at the Swiss Federal Institute of Technology.

[Vanderbilt, 1985] Vanderbilt, D. (1985). Optimally smooth norm-conserving pseudopotentials. *Phys. Rev. B*, 32(12):8412.

[Vanderbilt, 1990] Vanderbilt, D. (1990). Soft self-consistent pseudopotentials in a generalized eigenvalue formalism. *Phys. Rev. B*, 41(11):7892.

[von Barth and Gelatt, 1980] von Barth, U. and Gelatt, C. D. (1980). Validity of the frozen-core approximation and pseudopotential theory for cohesive energy calculations. *Phys. Rev. B*, 21(6):2222–2228.

[von Barth and Hedin, 1972] von Barth, U. and Hedin, L. (1972). A local exchange-correlation potential for the spin polarized case: I. *J. Phys. C*, 5:1629–1642.

[Walter et al., 2006] Walter, E. D., Chattopadhyay, M., and Millhauser, G. L. (2006). The Affinity of Copper Binding to the Prion Protein Octarepeat Domain: Evidence for Negative Cooperativity. *Biochemistry*, 45:13083–13092.

[Will et al., 1996] Will, R. G., Ironside, J. W., Zeidler, M., Cousens, S. N., Estibeiro, K., Alperovitch, A., Poser, S., Pocchiari, M., Hofman, A., and Smith, P. G. (1996). A new variant of Creutzfeldt-Jakob disease in the UK. *Lancet*, 347:921–925.

[Wille et al., 2002] Wille, H., Michelitsch, M. D., Guenebaut, V., Supattapone, S., Serban, A., and et al. (2002). Structural studies of the scrapie prion protein by electron crystallography. *Proc. Natl. Acad. Sci. USA*, 99:3563–3568.

[Wopfner et al., 1999] Wopfner, F., Weidenhofer, G., Schneider, R., von Brunn, A., Gilch, S., and et al. (1999). Analysis of 27 mammalian and 9 avian PrP revelas high conservation of flexible regions of the prion protein. *J. Mol. Biol.*, 289:1163–1178.

[Yanagihara et al., 2002] Yanagihara, C., Yasuda, M., Maeda, K., Miyoshi, K., and Nishimura, Y. (2002). Rapidly progressive dementia syndrome

associated with a novel four extra repeat mutation in the prion protein gene. *J. Neurol. Neurosurg. Psychiatry*, 72:788–791.

[Young, 2001] Young, D. (2001). *Computational Chemistry: A Practical Guide for Applying Techniques to Real World Problems.* John Wiley & Sons, New York, USA.

[Zahn et al., 2000] Zahn, R., Liu, A., Luhrs, T., Riek, R., von Schroetter, C., and et al. (2000). NMR solution structure of the human prion protein. *Proc. Natl. Acad. Sci. USA*, 97:145–150.

[Zwicker, 1975] Zwicker, R. (1975). Trial Functions in pseudopotential theory. *Phys. Rev. B*, 12(12):5502.